Synthesis and Characterization of Multi-Component (Fe-Ni-Si) Oxide Surface and Its Application in Removing Organic Dyes from Water

by

Syed Abdul Monim

SUBMITTED IN PARTIAL FULFILLMENT OF THE REQUIREMENT FOR THE DEGREE OF MASTER OF PHILOSOPHY (M. PHIL.) IN CHEMISTRY

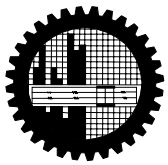

Department of Chemistry

BANGLADESH UNIVERSITY OF ENGINEERING AND TECHNOLOGY

Dhaka-1000, Bangladesh

2010.

Declaration

It is hereby declared that this thesis or any part of it has not been submitted elsewhere for the award of any degree or diploma.

Signature of the Candidate

Syed Abdul Monim

Name of the Candidate

Dedicated to

Freedom fighters
&
All of my inner hearted adored friends

CONTENTS

LIST OF FIGURES

LIST OF TABLE

Acknowledgement

I would like to express my gratitude and sincere thanks to my supervisor Professor Dr. Al-Nakib Chowdhury who played an influential part in the completion of this thesis. His guidance, words of wisdom and ever-present tendency to help have certainly been invaluable all through this thesis. Given my background, chemistry was not especially my cup of tea. He played an instrumental role in the development of this novel idea and guided me every time when there was a problem. He certainly is one of the most important people for me here, to transform a greenhorn mechanical engineer into a matured, motivated, independent, research driven and extremely inquisitive environmental engineer. I might go on to a different field in the future, but the initial development is the toughest part.

I would also like to acknowledge the entire department of Chemistry of Bangladesh University of Engineering and Technology which helped me to get an overall knowledge about the field, which is imperative in doing research dealing with a real world problem. The completion of this research in its present shape would not have been possible without support of Professor Dr. Md. Mominul Islam, Assistant Professor, Department of Chemistry, BUET, Mr. Neamul Hayet Khansur, Chungju University, Korea and Mrs. Nurtaj Begum. I also would like to take this opportunity to thank Professor Dr. Md. Manwarul Islam, Professor Dr. Md. Rafiq Ullah, Professor Dr. Md. Nazrul Islam, Mrs. Danisha Tabassum, Professor Dr. Syed Shamsul Alam, Mr. S. M. Akteruzzaman, Mrs. Samira Saymoma, Mr. Bin Yeamin, Mr. Ariful Hoque, Mr. Rafiqul Bari, Mr. Mohibul Islam, Mr. Mobinul Islam, Mr. Sharan Roy, Mr. Iqbal Mahmud, Mr. Shubhasish Bhadra, Mr. Syed Rahin Ahmed, Mr. Al-Mamun, Mr. Afsar, Mr. Arup, Mr. Mostafa Kamal Masud, Mr. Mamun, Mr. Muyed Sultan, Mr. Jahirul Islam all of whom played a very important role in the completion of this thesis. I would like to mention a special note of thanks to Mr. Md. Zahurul Alam

for spending his time to teach me how to use the various analytical instruments. I would also like to thank all staffs of Chemistry department in BUET and SUST for their technical support. My thanks are also to my friends all around the world.

I would like to finish by thanking my parents and sister, who are responsible for my being in this position. Their patience, confidence and advice have been invaluable all through my life.

S. A. Monim
Author

Abstract

In the present study, iron-nickel-silicon mixed oxide nano surface was synthesized by sol-gel method. The nanoparticles thus obtained were characterized by means of EDX, XRD and SEM techniques. Elemental analysis exhibited the presence of iron, nickel, silicon and oxygen elements in the mixed oxide with a composition of $Fe_{0.78}Ni_{0.76}Si_{0.46}O_3$. The results showed that the iron-nickel-silicon mixed oxide nanoparticles were successfully synthesized. The average crystallite size was calculated from the XRD data to be approximately 18 nm. The specific surface area of this multi-component nano oxide was found to be 78.30 m^2g^{-1}. The point zero charge of this surface was observed to be at pH 9.80. The adsorption property of mixed oxide for removal of organic cationic (Methylene Blue abbreviated as MB) and anionic (Orange Green abbreviated as OG) dyes were assessed with various parameters including effect of pH, contact time, initial dye concentration, temperature and dose of mixed oxide. The adsorbent was tested for removal of dyes from synthetic solution. The maximum adsorption capacity of nano mixed (Fe-Ni-Si) oxide for both MB and OG dyes at pH 7. Kinetic study showed that both MB and OG followed pseudo-second-order kinetics equation with the constant 30.09×10^{-2} $gmol^{-1}min^{-1}$ for MB and 8.0×10^{-2} $gmol^{-1}min^{-1}$ for OG at room temperature. The free energy, ΔG°, was negative which proves that the adsorption was spontaneous. The enthalpy change, ΔH° was positive for MB and negative for OG which indicates that adsorption processes were endothermic and exothermic in nature, respectively. Adsorption isotherm was interpreted by Langmuir equation from the obtained data and maximum adsorption capacity of oxide monolayer for MB dye was 30.09×10^{-4} $molg^{-1}$. With the increase of adsorbent dose the percentage of dye removal was increased but amount adsorbed of dyes per gram adsorbent was decreased. The catalytic property was examined by photodegradation of MB and OG.

Chapter 1

INTRODUCTION

1.1 Background and present state of the problem

The recently rejuvenated multi-component oxide materials are attractive in application e.g. adsorbent, catalysts, fine optics, strong magnet, semiconductors, piezoelectrics, superconductors, refractories, nuclear fuels etc. [1-4]. A number of chemical synthesis techniques, such as the precursor compound methods, the co-precipitation method, the sol-gel method, the solvent evaporation, the hydrothermal and the emulsion methods are known for the preparation of the mixed oxide [5]. Among the methods, the sol-gel method has been extensively used due to their ease, low cost and ability to control the particle size and shape [6]. Mixed metal oxides that have high surface area, high conductivity, electrochemical storability and pseudo capacitive behavior are of interest [7]. In catalysis, purification and separation processes, alloy or multi-component system is usually effective than single component [8-9]. Dyes from the effluents of textile industries are a group of hazardous chemicals as well as important sources of water pollution. Organic dyes undergo chemical as well as biological change in the aquatic system, consume dissolved oxygen and thus directly disturb the aquatic eco-system and mutagenic to human [10]. So, effective research on degradation of dye component is an important issue. Removal of dyes may be achieved via adsorption and degradation process. Adsorption or degradation may be carried out using adsorbent/catalyst like metal oxide or nano composites [11]. Thus, in this research work, synthesis of a multi-component oxide surface, *viz* Fe oxide/ Ni oxide/ Si oxide by sol-gel method and its use as an adsorbent for organic dyes are planned to be carried out.

1.2 Materials Today

Materials science is one of the oldest forms of engineering and applied science. The field has now broadened to include every class of materials; as because materials have been imperative to human civilization. And now in the twentieth

century materials not just one, but many have become the most important single factor on which the advance of technology and industry depends. Despite the amazing variety of modern day of materials, the search still goes on for materials to meet new and critical service requirements not only in an advance technology area such as aerospace, but in the manufacture of industrial and consumer products as well. Also, superior materials are needed to meet higher quality and reliability standard, epitomizes by long term product warranties and the demand for safe products. Finally, the search goes on constantly for new and superior materials to lower costs. The study of metal oxides is a significant part of materials science with their diverse application including adsorptive abilities. They even also have so many other potential applications like as catalyst, semiconductor, alternative cathode materials, pH sensing materials, capacitors, coating materials, pigments and so on. Among these so many function its adsorption behaviors have been particularly established here in this paper; where metal mixed oxide surface can be a vital adsorbent for removing organic dyes (cationic and anionic) [12].

1.3 Different types of materials

1.3.1 Metals

Metals are crystalline solid materials consist of metal atoms distributed in a definite pattern resulting from their close packing. The types of close packing arrangement depend upon the size and electronic configuration of the atoms involved in the formation of crystal lattice. Since the metal atoms are all in direct contact with one another in the lattice and their valence electrons are in identical energy states, it is believed that the electrons are free to migrate between atoms. Metal atoms have an excess of low energy orbital vacancies. These vacancies enable valence electrons to move from near a certain nucleus to near any other nucleus where their position remains indistinguishable from the first.

Thus, metals may be pictured as a collection of positive atomic cores embedded in a fluid or sea of electrons. For this fluid of electrons, metals are good conductors of electricity and heat. Metals have metallic luster; they are malleable, ductile and high melting points. Metals have simple crystal lattices since metallic bonding envisages closest packing of atoms-one layer above another. Metals may have any system of seven common crystal systems. Fe, Cu, Al, Ag, Au etc are the most common metals which are very useful to us.

1.3.2 Semiconductors

Semiconductors are special kind of materials which have the properties of semi conductivity is an electrical property of materials. A relatively small group of elements and compounds have an important electrical property, semi conduction in which they are neither good electrical conductors nor good electrical insulators. Instead, their ability to conduct electricity is intermediate. Si, Ge, impure ZnO, impure NiO are some examples of semiconductors.

In a semiconductor element, the energies of the valence electrons, which bind the crystal together, lie in the highest filled energy band, called the valence band. The empty band above called the conduction band and is separated from the valence band by an energy gap. The magnitude of the energy gap or the width of the forbidden energy zone is characteristic of the lattice alone and varies widely for different crystals.

Semiconductors are of two kinds such as

(i) Intrinsic semiconductor
(ii) Extrinsic semiconductor

(i) Intrinsic semiconductors: If a pure, elemental substance shows the semiconducting properties, it is called intrinsic semiconductor. Pure Si, Ge shows these semiconducting properties. Semi conduction results from the thermal promotion of electrons from a filled valence band to an empty conduction band.

(ii) Extrinsic semiconductors: Extrinsic semi conduction result from impurity additions known as dopant, and the process of adding these components is called doping. These types of semiconductors are extrinsic semiconductors. At room temperature the conductivity of semiconductors results from electrons and holes introduced by impurities in the crystal. Extrinsic semiconductors are of two kinds such as p-type extrinsic semiconductor and n-type extrinsic semiconductor.

p-type extrinsic semiconductors: The p-type semiconductor is obtained when the impurity atoms have fewer valence electrons than the silicon or germanium atoms of the original crystal. When a trivalent element such as B, Al, Ga, is substituted for Si atom, the structure will be locally incomplete and the impurity atom will acquire an extra electron from a nearly bond in the lattice to approximate the tetrahedral cloud distribution of the lattice. This creates a positive hole localized near the impurity, which will attempt to neutralize itself by taking an electron from another neighboring bond [13].

n-type semiconductors: They n-type semiconductor arises from substitution of impurity atoms having more valence electrons than Si or Ge atoms. Elements such as P, As, Sb, and Bi have five valence electrons. When such an element is substituted for a silicon atom, four of its five electrons will enter the inter-atomic bonds, but the fifth electron will be only slightly attracted by the excess of the positive charge on the nucleus. Thermal agitation even at room temperature is sufficient to transfer this electron to the conduction band. Since conductivity is due to the motion of electrons in the conduction band, this semiconductor is called n-type and the impurity is called the donor. Titanium dioxide or titania is a non-stoichiometric transition metal oxide and behaves as n-type semiconductor [14].

There are three naturally occurring crystal phases of titanium dioxide: rutile, anatase, and brookhite. Most of the electrochemical and photocatalytic work to

date have been performed on rutile or anatase, or a mixture of the two. Both rutile and anatase have tetragonal unit cells, and both structures contain slightly distorted TiO_6 octahedral. Rutile is thermodynamically more stable than anatase at room temperature; the free energy change for antatase to rutile is –5.4 kJ/mol [14].

The absorption and reflection properties of rutile have been studied extensively. At 4K, the short wavelength absorption edge for rutile is 410 nm (bandgap energy = 3.05 eV) [15, 16]. The lowest energy electronic absorption at 3.05 eV is an indirect transition. On the other hand, the bandgap of anatase is reported as 3.2 eV [17]. The absorption coefficients for both crystal phases are reported as ~10^5 cm^{-1} at 340 nm [18].

1.4 Nanomaterials

Nanotechnology is expected to be the basis of many of the main technological innovations of the 21st century. Research and development in this field is growing rapidly throughout the world. A major output of this activity is the development of new materials in the nanometer scale, including manoparticles. A unique aspect of nanotechnology is the vastly increased ratio of the surface area to volume present in many nanoscale materials which opens new possibilities in surface-based science, such as catalysis. A number of physical phenomena become noticeably pronounced as the size of the system decreases. These include statistical mechanical effects, as well as quantum mechanical effects, for example the “the quantum size effect” where the electronic properties of solids are altered with great reductions in particle size. This effect does not come into play by going from macro dimension. However, it becomes dominant when the nanometer size range is reached.

Materials reduced to the nanoscale can suddenly show very different properties compared to what they exhibit on a macroscale, enabling unique application. For instance, opaque substances become transparent (copper); inert materials become catalyst (platinum); stable materials turn combustible (aluminum); solids turn into liquids at room temperature (gold); insulators become conductors (silicon). Materials such as gold, which is chemically inert at normal scales, can serve as a potent chemical catalyst at nanoscales. Much of the fascination with nanotechnology exhibits at the nanoscale.

A nanoparticle (which historically has included nanopowder, nanocluster and nanocrystal) is a small particle with at least one dimension less than 100 nm. This definition can be fleshed out further in order to remove ambiguity from future nano nomenclature. A nanoparticle is an amorphous or semicrystalline zero dimensional (0D) nano structure with at least one dimension between 10 and 100 nm and a relatively large (≥15%) size dispersion [19].

1.5 Oxide materials

An oxide is a chemical compound containing at least one oxygen atom as well as at least one other element. Most of the Earth's crust consists of oxides. Oxides result when elements are oxidized by oxygen in air. Virtually, all elements burn into atmospheric oxygen. In the presence of water and oxygen (or simply air), some elements - lithium, sodium, potassium, rubidium, cesium, strontium and barium - react rapidly, even dangerously to give the hydroxides. In part for this reason, alkali and alkaline earth metals are not found in nature in their metallic, i.e., native, form. The surface of most metals consists of oxides and hydroxides in the presence of air. A well known example is aluminum foil, which is coated with a thin film of aluminum oxide that passivity the metal, slowing further corrosion. Due to its electro negativity, oxygen forms chemical bonds with almost all elements to give the corresponding oxides. So-called noble metals (common examples: gold, platinum) resist direct chemical

combination with oxygen, and substances like gold (III) oxide must be generated by indirect routes.

Inorganic oxides are one of the most important materials for science and technology. Especially transition metal oxides have characteristics surface. It has drawn great attention to researchers. Metal oxide has been used as catalyst, sensor, and adsorbent for removal of toxic chemical, electrode material as well as used in electro chromic device and solar cell etc. Nowadays nano metal oxide is one of the promising materials for scientists. The applications of nano oxide particles are increasing day by day. The most commonly used transition metal oxides are titania, manganese oxide, zinc oxide, cobalt oxide, nickel oxide, iron oxide etc [11].

1.6 Types of Oxide materials

The oxide catalysts are mainly classified into three groups:

(a) Semiconductor oxides

These are the oxides of transition metal, for example, NiO, ZnO, MnO_2, TiO_2, Cr_2O_3 etc. The catalytic activity is mainly due to lattice defect and oxidation state of the metal ion. The important reactions that are catalyzed by semiconductor oxides include oxidation (both complete and partial), dehydrogenation, desulphurization of hydrocarbon etc.

(b) Insulator oxides

This group includes Al_2O_3, SiO_2 and MgO etc. The catalytic activity is mainly due to acid-base properties of these oxides. The important reactions that are catalyzed by insulator oxides are alkylation of aromatic hydrocarbons, dehydration of alcohol etc.

(c) Mixed oxide

Mixed metal oxide is a binary or more mixture of metal oxides. It is a new type of material. These oxides could be used as surface material. Mixed systems have the potential for exhibiting chemical properties that differ notably from those of the corresponding single component oxides. The incorporation of one metal oxide are to other oxide may change the band gap energy of host metal oxide. Mixed metal oxides widely used as catalyst, adsorbent, sensors, oxidant, and electrode material. It is also used for the removal of toxic chemicals from the environment.

Most mixed oxides are made of at least two oxide phases. Better catalytic activity is observed with the mixed oxide catalysts according to the following mechanisms: stabilization, control of redox properties, creation of acidity and basicity, combination of more than two functions to evolve acid oxidation and acid-base bi-functional catalysts. For examples,

• V-P oxides for selective oxidation of butane to malefic anhydride.

• Bi-Mo oxides for selective oxidation of propene to acrolene.

• Perovskite oxides ($LnCoO_3$, $LaCoO_3$, $LnMnO_3$ etc.) for hydrogenation of alkenes [20].

1.7 Nickel(II) Oxide

Nickel(II) oxide is the chemical compound with the formula NiO. It is notable as being the only well characterized oxide of nickel (although nickel(III) oxide, Ni_2O_3 and NiO_2 have been claimed[r]. The mineralogical form of NiO, bunsenite, is very rare. It is classified as a basic metal oxide [21]. Several million kilograms are produced in varying quality annually, mainly as an intermediate in the production of nickel alloys. NiO has a variety of specialized applications and generally

applications distinguish between "chemical", which is relatively pure material for specialty applications, and "metallurgical grade", which is mainly used for the production of alloys. It is used in the ceramic industry to make frits, ferrites, and porcelain glazes. The sintered oxide is used to produce nickel steel alloys. Charles Édouard Guillaume won the 1920 Nobel Prize in Physics for his work on nickel steel alloys which he called invar and elinvar. NiO was also a component in the Nickel-iron battery, also known as the Edison Battery, and is a component in fuel cells. It is the precursor to many nickel salts, for use as specialty chemicals and catalysts. More recently, NiO was used to make the NiCd rechargeable batteries found in many electronic devices until the development of the environmentally superior Lithium Ion battery [22].

Structure

NiO adopts the NaCl structure, with octahedral Ni(II) and O^{2-} sites. The conceptually simple structure is commonly known as the rock salt structure. Like many other binary metal oxides, NiO is often non-stoichiometric, meaning that the Ni:O ratio deviates from 1:1. In nickel oxide this non-stoichiometry is accompanied by a color change, with the stoichiometrically correct NiO being green and the non-stoichiometric NiO being black [23].

1.8 Iron(III) Oxide

Iron(III) oxide is the inorganic compound with the formula Fe_2O_3. It is of one of the three main oxides of iron, the other two being iron(II) oxide (FeO), which is rare, and iron(II,III) oxide (Fe_3O_4), which also occurs naturally as the mineral magnetite. As the mineral known as hematite, Fe_2O_3 is the main source of the iron for the steel industry. Fe_2O_3 is paramagnetic, reddish brown, and readily attacked by acids. Rust is often called iron(III) oxide, and to some extent, this label is useful, because rust shares several properties and has a similar

composition. To a chemist, rust is considered an ill-defined material, described as hydrated ferric oxide [24].

Alpha phase

α-Fe_2O_3 has the rhombohedral, corundum (α-Al_2O_3) structure and is the most common form. It occurs naturally as the mineral hematite which is mined as the main ore of iron. It is antiferromagnetic below ~260 K (Morin transition temperature), and weak ferromagnetic between 260 K and 950 K Neel temperature.

Beta phase

Cubic face centered, metastable, at temperatures above 500 °C converts to alpha phase. It can be prepared by reduction of hematite by carbon, pyrolysis of iron(III) chloride solution, or thermal decomposition of iron(III) sulfate.

Gamma phase

Cubic, metastable, converts to the alpha phase at high temperatures. Occurs naturally as the mineral maghemite and Ferromagnetic. Ultra fine particles, smaller than 10 nanometers, are superparamagnetic. Can be prepared by thermal dehydratation of gamma iron(III) oxide-hydroxide, careful oxidation of iron(II,III) oxide. The ultrafine particles can be prepared by thermal decomposition of iron(III) oxalate [25].

1.9 Silicon Oxide

The chemical compound silicon dioxide, also known as silica (from the Latin s*ilex*), is an oxide of silicon with a chemical formula of SiO_2 and has been known for its hardness since antiquity. Silica is most commonly found in nature as sand

or quartz, as well as in the cell walls of diatoms. Silica is the most abundant mineral in the Earth's crust. Silica is manufactured in several forms including fused quartz, crystal, fumed silica (or pyrogenic silica, trademarked Aerosil or Cab-O-Sil), colloidal silica, silica gel, and aero gel. In addition, silica nanosprings are produced by the vapor-liquid-solid method at temperatures as low as room temperature [26-27].

Crystal structure

Tetrahedral structural unit of silica (SiO_4), the basic building block of the most ideal glass was former. In the vast majority of silicates, the Si atom shows tetrahedral coordination, with 4 oxygen atoms surrounding a central Si atom. The most common example is seen in the quartz crystalline form of silica SiO_2. In each of the most thermodynamically stable crystalline forms of silica, on average, all 4 of the vertices (or oxygen atoms) of the SiO_4 tetrahedra are shared with others, yielding the net chemical formula: SiO_2. The amorphous structure of glassy silica (SiO_2) is in two-dimensions. No long-range order is present; however there is local ordering with respect to the tetrahedral arrangement of oxygen (O) atoms around the silicon (Si) atoms. Note that a fourth oxygen atom is bonded to each silicon atom, either behind the plane of the screen or in front of it; these atoms are omitted for clarity. Relation between refractive index and density for some SiO_2 forms. For example, in the unit cell of alpha-quartz, the central tetrahedron shares all 4 of its corner O atoms, the 2 face-centered tetrahedra share 2 of their corner O atoms, and the 4 edge-centered terahedra share just one of their O atoms with other SiO_4 tetrahedra. This leaves a net average of 12 out of 24 total vertices for that portion of the 7 SiO_4 tetrahedra which are considered to be a part of the unit cell for silica [28].

1.10 Synthesis techniques of metal oxide and mixed metal oxides

Supported metal oxide and mixed metal oxide are usually prepared by the following methods:

(i) Precipitation.

(ii) Co-precipitation.

(iii) Incipient wet impregnation.

(iv) Deposition.

(v) Grafting.

(vi) Sol-gel method.

(vii) Precipitation-deposition.

(viii) Selective removal.

1.10.1 Precipitation Method

Hydroxide or carbonate of the desired metal [29] is precipitated out from solution by using a precipitating agent. The hydroxides or carbonates are decomposed by heating to the oxides, which are, reduced to the metal when required on to a suspension of the support. In all precipitations it is essential to carefully control all the details of the process including [30]:

i) The order and rate of addition of one solution into the other.

(ii) The mixing procedure.

(iii) The pH and variation of pH during the process.

(iv) The maturation process.

Precipitation involves two distinct processes, namely nucleation and growth. Nucleation requires that the system is far from equilibrium. Growth of the new phase takes place in conditions which gradually approach the equilibrium state.

Many procedures are used for precipitation. One simple method is to add drop-wise the solution containing the active component to the precipitating solution, or vice versa. There is little difference between those inverse procedures. In both cases high super saturation can be produced locally, leading, if the solubility constant is low, to fine precipitates. If not, redissolution takes place at the beginning of the process, when agitation disperses the precipitate in the liquid. In both cases, concentrations change continuously throughout the precipitation process resulting in an inhomogeneous product being formed, at least with respect to texture. Any precipitation process is situated somewhere between two extremes. Either the solutions are contacted instantaneously (only an ideal situation as, in all cases, diffusion has to take place), the super saturation decreasing continuously, or the super saturation is maintained constant during the whole precipitation process.

Instantaneous precipitation is achieved by two methods. The first consists in pouring continuously, in constant proportion, both solutions into a vessel under constant and vigorous stirring. The second consists in mixing the solutions through specially designed mixing nozzles. The latter method ensures a better uniformity in composition and texture of the Precipitate.

1.10.2 Co-precipitation Method

This method involves the addition of a precipitation agent leading to the formation of a mixture of metal compound and the support, both previously in solution. This method is traditionally associated with nickel alumina catalyst used mostly in the hydrogenation of unsaturated fatty oils [30]. At a defined

temperature the precipitating agent is OH^- ions that convert the active metal salts to a mixture of metal hydroxide. After drying, the decomposed and reduced to get a co-precipitated supported catalyst [31]. This method offers a better surface in terms of homogeneity, though some of the active component may be embedded within the carrier and hence not available. This method is especially employed for the preparation of mixed oxide catalyst.

1.10.3 Sol-gel method

Sol-gel preparation, which involves the formation of a sol followed by formation of a gel, typically uses either colloidal dispersions or inorganic precursors as the starting material. However, it is important to realize that sol-gel preparation can be done with a wide variety of precursors. With an alkoxide (M(OR),) as a precursor, sol-gel chemistry can be described in terms of two classes of reactions:

Hydrolysis: $MOR + H_2O = MOH + ROH$

Condensation: $MOH + ROM = MOM + ROH$

or $MOH + HOM = MOM + H_2O$

Despite its oversimplification, this description of sol-gel chemistry identifies two key ideas. First, a gel forms because of the condensation of partially hydrolyzed species into a three-dimensional polymeric network. Second, any factors that affect either or both of these reactions are likely to impact on the properties of the gel. In fact, it is the control of many of these factors, generally referred to as sol-gel parameters that separate sol-gel preparation from other methods. A representative but not exhaustive list of these parameters includes type of precursor, type of solvent, water content, acid or base content, precursor concentration, and temperature. These parameters affect the structure of the initial gel and, in turn, the properties of the material at all subsequent processing steps [32].

A gel, a solid matrix encapsulating a solvent, needs to be dried to remove the solvent. The time between the formation of a gel and its drying, known as aging, is also an important parameter. As Scherer pointed out, a gel is not static during aging but can continue to undergo hydrolysis and condensation. Furthermore, syneresis, which is the expulsion of solvent due to gel shrinkage, and coarsening, which is the dissolution and reprecipitation of particles, can occur. These phenomena can affect both the chemical and structural properties of the gel after its initial formation. One other parameter that affects a sol-gel product is the drying condition. Conventional evaporative drying, such as heating a gel in an oven, induces capillary pressure associated with the liquid-vapor interface within a pore. In a sample with a distribution of pore sizes, the resultant differential capillary pressure often collapses the porous network during drying. The dried sample, known as a xerogel, thus often has a surface area and pore volume that is too low to be of catalytic interest. There are several ways to minimize the deleterious effect of conventional drying, and xerogels with high surface areas and pore volumes can be prepared with care. One other approach is that of Kistler, who used supercritical drying to bypass the problem of differential capillary pressure. The resultant materials, known as aerogels, have high surface area, porous structure, and low density. In a way drying can be viewed as part of the overall aging process because the material can, and often does, undergo physical and chemical changes during this stage [33].

Let us return to the issue of control and see how it is relevant to the preparation of catalytic materials. In the preparation of single-component materials, sol-gel preparation can achieve very high purity because of the quality of available precursors. Furthermore, the textural properties of the product, most notably surface area and pore size distribution, can be tailored. However, we believe the area in which sol-gel preparation is going to make the biggest impact is multi-component systems. We see the following specific advantages: (i) the ability to control structure and composition at a molecular level, (ii) the ability to introduce several components in a single step, (iii) the ability to impose kinetic constraints

on a system and thereby stabilize metastable phases, and (iv) the ability to fine tune the activation behavior of a sample and thereby trace the genesis of active species [32]. Finally, with either single-component or multi-component systems, sol-gel preparation allows different product forms to be made. As we shall see, one particular interesting class of materials is inorganic membranes that can perform both catalytic and separation function.

1.11 Characterization of metal oxide and mixed Oxide material

Metal and mixed metal oxide characterization is necessary to establish understanding and control of metal and mixed metal oxides synthesis and application. Characterization is done by using a variety of different techniques, mainly drawn from metal oxide materials. Common techniques are Electron Microscopy [TEM, SEM], Atomic Force Microscopy [AFM], Dynamic Light Scattering [DLS], X-ray Photoelectron Spectroscopy [XPS], powder X-ray Diffractometry [XRD], Energy Dispersion X-ray (EDX) spectroscopy and Fourier Transform Infrared Spectroscopy. Whilst the theory has been known for over a century, the technology for Nanoparticle Tracking Analysis (NTA) allow a direct tracking of the Brownian motion and this method therefore allow the sizing of individual nanoparticles of metal oxide in solution [34].

1.12 Surface Morphology

Scientists have taken to naming their particles after the real world shapes that they might represent. Nanospheres [35], Nanoreefs [36], nanoboxs [37], microsphere [35] and more have appeared in the literature. These morphologies sometimes arise spontaneously as an effect of a templating or directing agent present in the synthesis such as micellular emulsions or anodized alumina pores, or form the innate crysllographic growth patterns of the materials themselves [38]. Some of these morphologies may serve a purpose, such as

long carbon nanotubes being used to bridge an electrical junction, or just a scientific curiosity like the stars shown at left.

1.13 Importance of dye removing

Water is absolutely essential to animals and plants in order for their survival. Human beings use water for drinking, bathing, washing, culinary purpose, transportation, industrial and agricultural activities etc [39]. The day to day human activities and industrial revolution have influenced the flow and storage of water and the quality of available fresh water. Many industries like textile, refineries, chemical, plastic and food processing plants produce wastewater characterized by a perceptible content of organics [40]. Significant amounts of chemically different dyes are used in various industries such as textile, pesticide, paint, solvent, pharmaceuticals, paper, pulp and petroleum etc [41-42].

Textile and other industrial dyes have become major environmental contaminants in many countries including Bangladesh owing to their nonbiodegradability and toxicity [43-45]. Several of these dyes are stable and resist photodegradation by sunlight, oxidation by molecular oxygen O_2, and decomposition by common acids and bases.

The textile industry plays a part in the economy of several countries around the world [46]. A typical textile dyeing process consists of resizing, scouring, bleaching, dyeing, finishing and drying operations. Dyeing is a fundamental operation during textile fiber processing. The dyeing process consumes large quantities of water for dyeing, fixing and washing and produce large volume of wastewater [9, 47]. Over the last decades, the increasing demand for dyes by the textile industries has shown a high pollutant potential. It is estimated that around 10-15% of the dyes are lost in the effluent during the dyeing processes [48].

The effluent generated from the textile processing industries are considered to be a very complex and inconsistent mixture of many pollutants, such as, mixture of heavy metal ions (e.g., Cr, Al, Cu etc.), suspended solids, dissolved solids, inorganic salts, dispersing agents, dyestuffs, and other toxic organic pollutants including poly vinyl alcohol, starches, various surfactants, organic-chlorine based pesticides, biocides as well as acidic and alkaline contaminants.

Effluents discharged from textile and dyeing industries are characterized by low BOD, high COD and variation of pH in the range of 2-12 [9, 40, 46, 47, 48-50]. Color is usually the first contaminant to be recognized in wastewater; a very small amount of dye in water (10-20mg/L) is also highly visible and affects water transparency and the gas solubility of water bodies. The discharge of these colored dye effluent as wastewater in the ecosystem is a damaging source of esthetic pollution, eutrophication, and interruption in many natural processes (e.g., photosynthesis, respiration) and perturbations in aquatic life. These dyes in the strongly absorb sunlight, which decreases the intensity of light absorbed by water plants and phytoplankton, reducing photosynthesis and the oxygenation of water reservoirs [46, 48, 51, 52]. Dyes often contain elements such as nitrogen, Chlorine or sulfur. The oxidation product of these molecules may be more toxic than the parent molecule [49]. Because of these unbearable problems created by the discharge of dyes as effluent, it requires clear concepts about dye and its undesirable impact and a quick search for the remedy of these problems.

1.14 Dye

Dyes are organic colorants that can be firmly fixed to the fabrics and other supporting materials used in textile, food and other industries for imparting different shades of colors [50, 53-55]. All colored compounds are not dyes. A substance is referred to as a dye when it bears the following criteria [53-59] -

1. It must have a desired color to match the object to be dyed.

2. It must be capable of being fixed to the fabrics or supports directly or indirectly with the help of certain reagents called mordant.

3. When fixed to the supports, the color must be fast to light and resistant to soap and water and to a certain extent to dilute acids and alkalis.

1.15 Classification of dyes

Dyes can be classified as anionic, cationic and nonionic according to their dissociation in an aqueous solution. According to the application they can be classified as bellow [60] –

1. Acid dyes: Acid dyes are anionic compounds that are mainly used for dyeing nitrogen containing fabrics like wool, polyamide, and silk and modified acryl. Most acid dyes are azo, anthraquinone or triarylmethane.

2. Reactive dyes: Dyes with reactive groups that form covalent bonds with OH^-, NH^- or HS^- groups in fibers are known as reactive dyes. The reactive group is often a heterocyclic aromatic ring substituted with chloride or fluoride (e.g., diclorotriazine).

3. Metal complex dyes: These are strong complexes of one metal atom (usually Cr, Cu, Co or Ni) and one or two dye molecules, respectively 1:1 and 1:2 metal complex dyes.

4. Basic dyes: Basic dyes are cationic compounds that are used for dyeing acid group containing fibers, usually synthetic fibers like modified polyacryl.

5. Pigment dyes: These insoluble, nonionic compounds or insoluble salts retain their crystalline or particulate structure throughout their application.

6. Sulfur dyes: Sulfur dyes are complex polymeric aromatics with heterocyclic S-containing rings.

7. Solvent dyes: Solvent dyes are nonionic dyes that are used for dyeing substrates in which they dissolve (e.g., plastics, varnish, ink, waxes and fats).

8. Food dyes: Food dyes are usually used in foods, soft drinks, medicines etc. These dyes should be used in such quantity that would not cause any health hazard to human being. These dyes are prepared from coal tar such as tartrazine, sunset yellow, carmoisine, green-S, allura red, caramel aqua marine etc.

9. Organic Ionic dyes: Methylene blue (MB) and orange green (OG) are the typical organic ionic dyes. MB is cationic in nature while OG is an anionic one. Molecular weight of MB and OG are 355.89 and 452.38. λ_{max} of MB and OG are 664 nm and 477 nm respectively. There chemical structures are shown in Figure 1.1

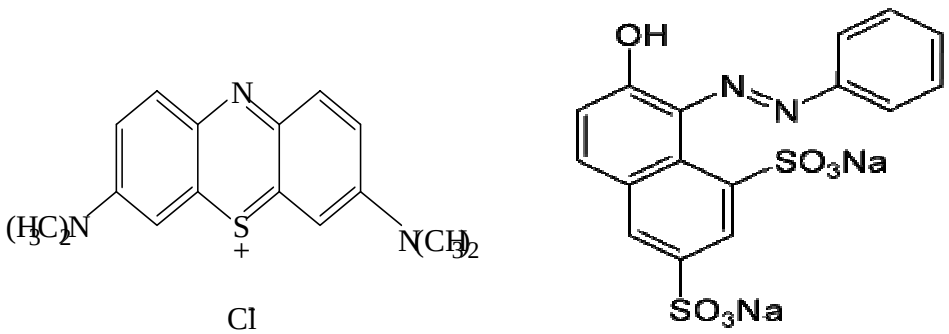

(a) (b)

Figure 1.1: Chemical structure of (a) MB and (b) OG.

Our research interest was to remove MB and OG in water solution.

1.16 Color in compounds and its sensation

If a substance absorbs visible light, it appears to have a color, if not it appears white [61]. So in order for a compound to be colored light absorbing system (chromophore) must be present in it. Various theories have been put forward to establish a relationship between color and constitution. Some important theories are Witt's theory, quinoid theory, resonance theory, molecular orbital theory.

Witt's theory:

According to Otto N. Witt (1876) all colored compounds contain unsaturated groups, which are responsible for exhibiting color and he called these groups as chromophores [55]. A compound containing a chromophore is called chromogen. The most effective are shown in Figure 1.2:

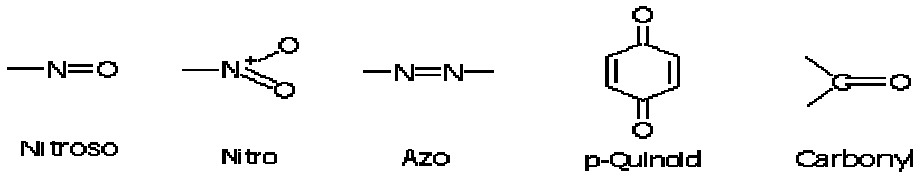

Figure 1.2: Structures of some effective chromophores.

On the other hand, there are some groups whose presence in a chromogen, modify the color of chromogen but it cannot impart color to it, are called auxochromes. Auxochromes are either acidic or basic and usually salt forming groups, such on $-NH_2$,-OH etc. or solubilizing radicals –COOH, SO_2H. Since, auxochromic groups are capable of forming salts with acidic or basic groups of the fiber; they help the chromogen to fix permanently to the fiber. Therefore if a chromogen has one or more auxochromes, the resulting substance is called a dye i.e.

Dye = chromogen + auxochrome (1)

There are two types of chromophores-

1. Independent chromophores: when a single chromophore is sufficient to impart color to the compound. For example, azo groups (-N═N-), nitroso group (-NO) etc.

2. Dependent chromophores: when more than one chromophore is required to produce color in the chromogen. For example, >C═C< group etc.

A bathochromic effect (red shift) and a hypsochromic effect (blue shift) are the shifting of the absorption band to the longer and shorter wavelengths, respectively. A hyperchromic effect and hypochromic effect are those which respectively increases and decreases the intensity of absorption.

Quinonoid theory:

The notable points on this theory [62] are –

1. Dyes are either weak acid or base.

2. While in solution it (Dye) undergoes ionization as

$$\text{H-Dye} \longleftrightarrow H^+ + Dye^- \qquad (2)$$

3. The unionized H-Dye molecule and the anion dye are tautomeric forms of the dye.

4. One tautomeric form possesses the quinonoid structural unit and is called the

quinonoid form.

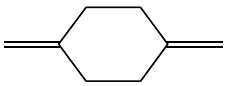

It has a deep color. The other form has a less intense coloring group, say, -N═N- and or simply benzene ring and is called the benzenoid form. This form has light color or no color.

5.The change of the dye is accompanied by a change in the pH of the solution.To illustrate the Quinonoid theory, Methyl orange, an acidic azo dye, has been taken as an example in Figure 1.3:

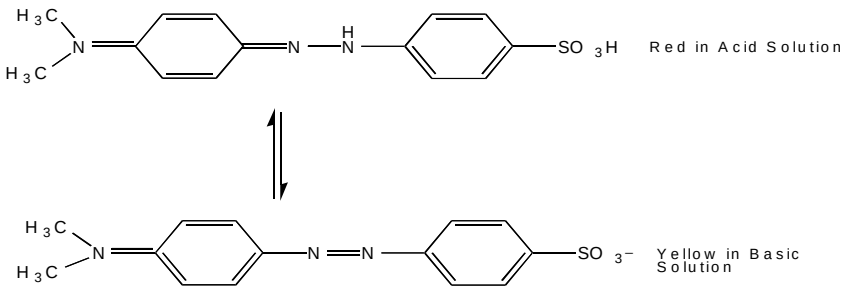

Figure 1.3: Illustration of Quinonoid theory

Molecular orbital approach to color

In molecular orbital (MO) theory, an atom or molecule is excited when one electron is transferred from a bonding to an anti-bonding orbital. Electronic transitions, however, can occur in different ways. A transition in which a bonding σ-electron is excited to an anti-bonding σ-orbital is referred to as a σ to σ* transition. In the same way, Π to Π* represents the transition of a bonding Π-electron to an antibonding Π-orbital. An n to Π* transition represents the transition of one electron of a lone pair, i.e., a non-bonding pair electron of electrons, to an anti-bonding Π-orbital (Figure 1.4).

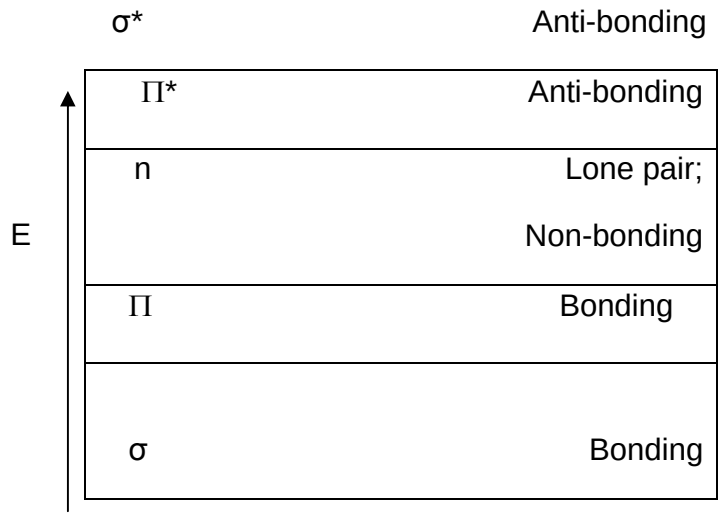

Figure 1.4: Schematic representation of different transitions

This type of transition occurs with compounds containing double bonds involving hetero-atoms, e.g., >C=O, >C=N-, >C=S, etc., and may be represented as follows:

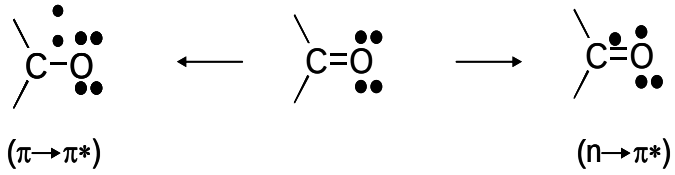

The transitions are brought about by the absorption of different amounts of energy. Of the large number of possibilities, only the following transitions are allowed, and their general order of energy difference is:

$$\sigma \longrightarrow \sigma^* > n \longrightarrow \sigma^* > \pi \longrightarrow \pi^* > n \longrightarrow \pi^*$$

Since the energy difference between the highest occupied Π-orbital level and lowest unoccupied level is smaller than any other electronic transition, the

longest wavelength in the absorption spectrum corresponds to this transition, and the shorter wavelengths correspond to the other transitions. Calculation and experimental work has shown that as conjugation increases, the energy difference between the highest occupied and lowest unoccupied Π-orbital decreases (V.B. theory). Thus, as conjugation increases, the maximum in the absorption band shifts to the longer wavelength, and when it reaches the visible region, complementary color will appear in the compound. We see the color complementary to that which is absorbed [60-63].

Table 1.1: Clarification of absorbed color and its complementary color.

Light absorbed		**Color observed**
Wavelengt (nm)	Color of absorbed light	
400	Violet	Greenish Yellow
425	Indigo blue	Yellow
450	Blue	Orange
490	Blue-green	Red
510	Green	Purple
530	Yellow-Green	Violet
550	Yellow	Indigo-blue
590	Orange	Blue
640	Red	Bluish-Green
730	Purple	Green

Whereas, benzene is a symmetrical molecule and consequently has no associated transition dipole, some of its bending vibrational modes distort its

shape to affect absorption. Introduction of substituents into the benzene ring destroys its symmetry and thereby gives rise to increased intensity of absorption, and by extending of conjugation, increases the wavelengths of the absorption band.

1.17 Harmful impact of dye pollutants

The color produced by minute amount of organic dyes in water is considered to be very important, because, the color in water is aesthetically unpleasant [64]. Disposal of this colored water into receiving water can be toxic to aquatic life. They upset the biological activity in water bodies. They also pose a problem because they may be mutagenic, carcinogenic and can cause sever damage to human beings, such as, dysfunction of kidney, reproductive system, liver, brain and central nervous system [65, 66]. The most acutely toxic dyes for algae are cationic, basic dyes. The most acutely toxic dyes for fish are basic dyes, especially those with a triphenylmethane structure. Fish also seem to be relatively sensitive to many acid dyes [57]. The chance of human mortality due to acute dyestuff toxicity is probably very low. However, acute sensitization reactions by humans to dyestuffs often occur. Especially some disperse dyestuffs have been found to cause allergic reactions, i.e. eczema or contact dermatitis [58]. Reduction of azo dyes, i.e. cleavage of the dyes azo linkage(s), leads to formation of aromatic amines. The acute toxic hazard of aromatic amines is carcinogenesis, especially bladder cancer.

1.18 Dye treatment techniques

Various physical, chemical and biological treatment techniques can be employed to remove color from dye containing wastewaters [40-42, 45, 49, 50, 52,60]. Physico-chemical techniques include membrane filtration,

coagulation/flocculation, precipitation, flotation, adsorption, ion exchange, ion pair extraction, ultrasonic mineralization, electrolysis, advanced oxidation (chlorination, bleaching, ozonation, Fenton oxidation and photocatalytic oxidation) and chemical reduction. Biological techniques include bacterial and fungal biosorption and biodegradation in aerobic, anaerobic, anoxic or combined anaerobic/aerobic treatment processes.

1.19 Adsorption:

Adsorption is a surface phenomenon exhibited by the surfaces of liquids or solids due to the exceptional characteristics of their surfaces from the bulk matter. Formally adsorption may be defined as a process in which the concentration of a chemical species is greater in the surface than in the bulk resulting from inelastic collision suffered by molecules on the surface. The species that is adsorbed is called adsorbate and the material of the surface is called adsorbent. Adsorption strictly refers to accumulation of adsorbate on the surface only due to residual field of force [67, 68]. The reverse process of adsorption, i.e. removal of adsorbed species is termed desorption.

1.20 Types of Adsorption

Adsorption may be sub-divided into two categories:

(a) Physisorption.

(b) Chemisorption.

1.20.1 Physisorption

Physisorption occurs when non-balanced physical forces appear at the boundary of the phases and adsorbed species is attached to the surface by weekly Van der Waals force. Physisorption is characterized by,

(i) Low heat of adsorption (10-40 KJ/mol).

(ii) Non specific.

(iii) Mono or multi-layer.

(iv) Rapid, non activated and reversible.

(v) Significant at low temperature.

(vi) No electron transfer.

1.20.2 Chemisorption

Adsorption, which results from chemical bond formation (strong interaction) between the adsorbent and the adsorbate in a monolayer on the surface, is called chemisorption [69].

Chemisorption is characterized by,

(i) More heat of adsorption (80-400 KJ/mol, sometimes endothermic).

(ii) Very specific for active site of heterogeneous catalyst.

(iii) Mono-layer only.

(iv) Effective over a wide range of temperature.

(v) Slow, activated and irreversible.

(vi) Electron transfer between adsorbate and surface.

1.21 Adsorption Isotherms

The variation of surface coverage (Θ) with equilibrium pressure (or concentration in the case of solution) at a given temperature is called adsorption isotherm. According to IUPAC classification [70], there are six different types of adsorption isotherm as shown in the Figure 1.5:

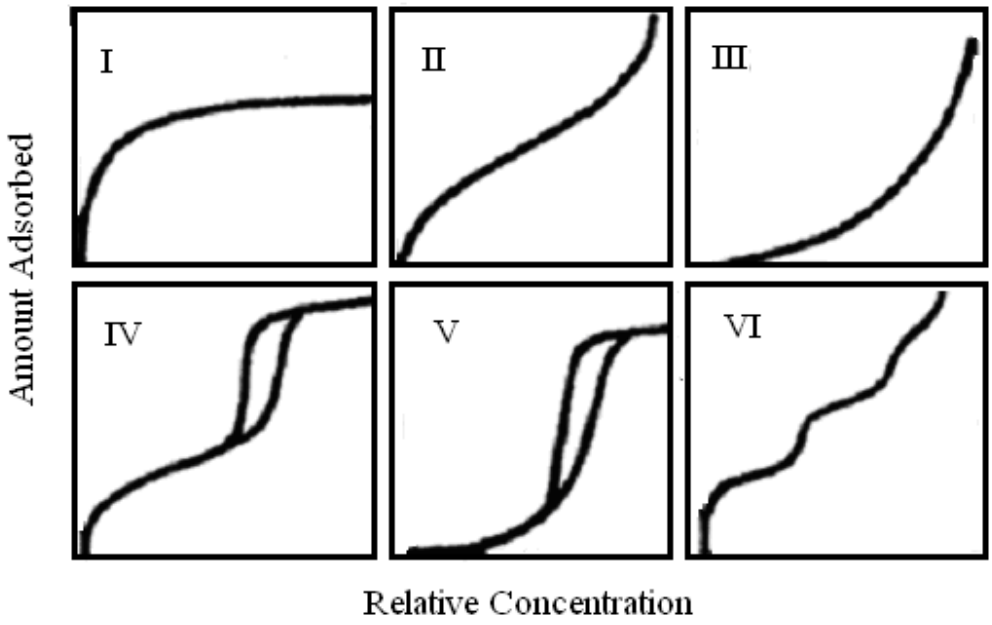

Figure 1.5: IUPAC Classification of adsorption isotherms.

(a) Type 1: This shape of the isotherm is characterized by the asymptotic approach of monolayer of adsorbate on the surface.

(b) Type 2: This is the most common type of isotherm corresponding to multi-layer formation on a surface of high adsorption potential.

(c) Type 3: This pattern of isotherm is comparatively uncommon, corresponding to multi-layer formation on the solid.

(d) Type 4 & 5: These are analogous to type 2 & 3 on porous adsorbents where the adsorption is limited by the volume of mesopores, causing the adsorption to

level off at a pressure less than saturation pressure of adsorbate (P_0). They reflect capillary condensation and may show hysteresis effect.

IUPAC classification considers adsorption at sub critical temperature, but adsorption at near critical and super critical temperature was not considered. Hence this classification is incomplete. Considering the adsorption at near or super critical temperature a new classification [71] is proposed as shown in the Figure 1.6.

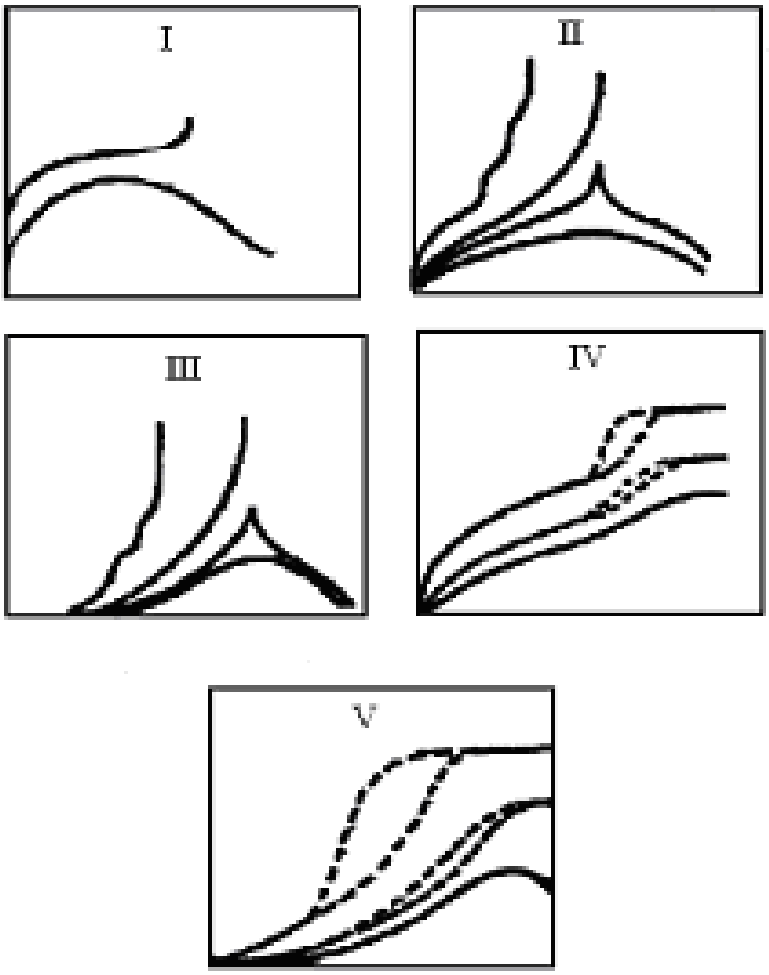

Figure 1.6: A new classification for adsorption isotherms.

1.22 Model of Adsorption Isotherms

Several theoretical models were proposed in order to explain the experimental adsorption isotherms:

(a) Langmuir isotherm.

(b) Freundlich isotherm.

(c) BET isotherm.

(d) Temkin isotherms etc.

Characteristics feature of Langmuir isotherm equation [72]:

(i) Adsorption is limited to monolayer formation.

(ii) In the case of physisorption, this equation satisfactorily explains adsorption behavior only at low surface coverage and at low adsorbate pressure.

(iii) In the case of chemisorption which is associated with monolayer coverage Langmuir equation is quite consistent.

Langmuir derived the following equation (a) to explain the experimental adsorption isotherm,

$$\Theta = aC_e/(1+aC_e) \quad \ldots\ldots\ldots\ldots\ldots\ldots\ldots\ldots\ldots\ldots \quad (1)$$

The fraction of the surface of the surface covered by the adsobate can be expressed as,

$$\Theta = q/q_m \quad \ldots\ldots\ldots\ldots\ldots\ldots\ldots\ldots\ldots\ldots \quad (2)$$

From eqn. (1) and (2)

$$q/q_m = aC_e/(1+aC_e) \quad \ldots\ldots\ldots\ldots\ldots\ldots\ldots\ldots\ldots\ldots \quad (3)$$

Where, x/m = q = the amount of adsorbate adsorbed at eqm. Conctration, (C_e) in mol g^{-1}

K′ = q_m = monolayer capacity in mol g^{-1}

a = K = adsorption constant (eqm. constant for adsorption process) in L mol^{-1}

From eqn. (3), we have,

$C_e/(x/m) = C_e/K' + 1/KK'$ ……..(4)

From plot of $C_e/(x/m)$ vs C_e ,

Slope = 1/K′

K′ = 1/slope =monolayer capacity,

And, intercept = 1/KK

K = 1/(intercept * K′) = equilibrium constant = a

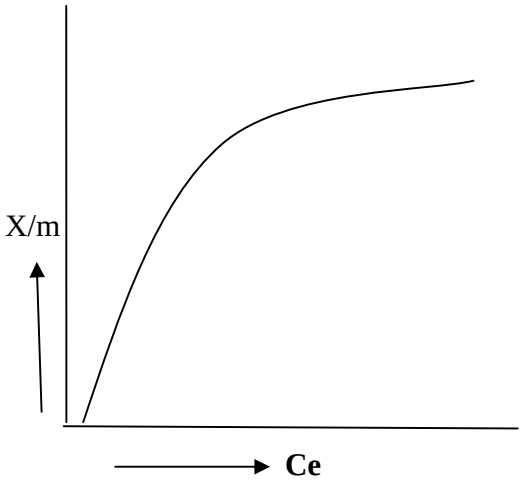

Figure 1.7a: Langmuir plot of X/m vs Eq^m concentration (Ce)

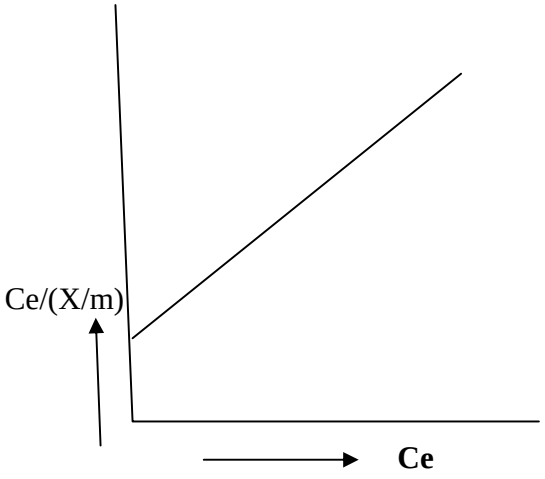

Figure. 1.7b: Langmuir-Hinshelwood plot of Ce/(X/m) vs Ce

1.23 Photochemistry

Photochemistry is concerned with the interaction of light quantum and a molecule and the subsequent chemical and physical changes which result from this interaction. The study of photochemistry includes the entire phenomenon associated with the absorption and emission of radiation by chemical system. It includes phenomena such as fluorescence and phosphorescence, luminescence chemical reaction, photo-stimulated reactions such as photographic, photosynthetic and photolytic reactions of various kinds.

Absorption of light: A photochemical reaction takes place by the absorption of electromagnetic radiation by a molecule. According to Planck's quantum theory, absorption of energy is quantized and is given by E=hv where, h is the Planck's constant and v is the frequency of the absorbed radiation. Planck's equation can also be written as E=hc/λ where, c is the velocity of light and λ is the wave length of the absorbed radiation.

Spectrum: A plot of absorbance or transmittance or reflectance as a measure of intensity of radiation against the wavelength or frequency or wave number of the radiation absorbed or transmitted or reflected by the substances.

Emission and absorption spectrum: The intensity of emission is directly proportional to the concentration of the analyte in the solution being aspirated. The absorption spectrum is dependent on the absorption capability of light by analyte species.

Consequences of the Absorption of Light: As light is a radiant energy, absorption of light means absorption of energy. The changes that might be produced by the absorbed energy may be as follows:

Excitation: The internal energy of the molecules or atoms may be raised in specific amounts i.e. are raised from ground state to excited states. (Quantum transition)

Dissociation: The molecule breaks down to form smaller molecules, atom or free radicals.

Luminescence: When the substance, absorbing the light does not undergo photochemical reaction. The substance is then said to show luminescence. The emission of light in the visible region of the spectrum is attributed to the return of one or more outer electrons of the excited molecules or atoms to the normal position as result of collisions with other atoms or molecules.

Fluorescence: In the fluorescence process a molecule is first excited to higher singlet state and if the life time of the excited state is less than 10^{-6} second, it undergoes non radiative vibrational deactivation in the excited singlet state and finally turns back to the ground singlet sate with the emission of photon having longer wavelength than that absorbed in the initial photon absorption process. Fluorescence stops just after the removal of the exciting light source.

Phosphorescence: In the phosphorescence process a molecule is first excited to upper singlet state by the absorption of photon of a certain wavelength. The molecule then undergoes nonradiative vibrational deactivation in the upper singlet state as well as intersystem crossing to the comparatively stable excited triplet state from which it turns back to the ground singlet state with the emission of photon of longer wavelegth. Since excited triplet state has considerable lifetime, the molecule may continue emission of light even after the removal of the exciting light source.

Chemiluminescence: This is the phenomenon of emission of light as a result of certain chemical reactions. The glow of fireflies due to the aerial oxidation of luciferon (a protein) in the presence of enzyme luciferase is an example of chemiluminescence [73].

1.24 Theoretical aspects of experimental techniques

1.24.1 SEM Technique

The scanning electron microscope (SEM) uses a finely focused beam of electrons to scan over the area of interest. The beam-specimen interaction is a complex phenomenon. The electrons actually penetrate into the sample surface, ionizing the sample and cause the release of electrons from the sample. These electrons are detected and amplified into a SEM image that consists of Back Scattered Electrons and Secondary Electrons. Since the electron beam has a specific energy and the sample a specific atomic structure, different image will be collected from different samples, even if they have the same geometric appearance [74].

1.24.2 Elemental analysis

EDX is a micro analytical technique that uses the characteristic spectrum of X-ray emitted by the specimen after excitation by high-energy electrons to obtain information about its elemental composition. An electron beam strikes the surface of the sample. The energy of the beam is 120 keV. This causes X-rays to be emitted. The energy of the X-rays emitted depends on the material under examination. The X-rays are generated in the whole section. The detector used in EDX is the Lithium drifted Silicon detector. This detector must be operated at liquid nitrogen temperatures. When an X-ray strikes the detector, it will generate a photoelectron within the body of the Si. As this photoelectron travels through the Si, it generates electron-hole pairs. The electrons and holes are attracted to opposite ends of the detector with the aid of a strong electric field. The size of the current pulse thus generated depends on the number of electron-hole pairs created, which in turn depends on the energy of the incoming X-ray, which depends on the composition of the sample. Thus, an X-ray spectrum can be acquired giving information on the elemental composition of the material under

examination. By moving the electron beam across the material an image of each element in the sample can be acquired.

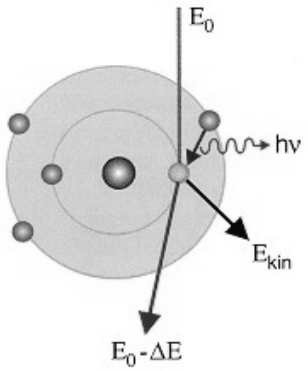

Figure 1.8: Emission of X-ray due to the collision of electron beam with the surface of the solid.

If an electron beam strikes the surface X-rays (hv) were emitted, which energy depends on the elemental composition of the sample and Vice versa the energy of the electrons is reduced. Analysis of the X-rays is called EDX [74].

1.24.3 X-Ray Diffraction

The X-ray diffraction (XRD) provides substantial information on the crystal structure. This method is applied for the investigation of orderly arrangements of atoms or molecules through the interaction of electromagnetic radiation to give interface effects with structures comparable in size to the wavelength of the radiation. Studies on the crystal structures developed based on methods using single crystals after the discovery of X-ray diffraction by crystals made by the Von Laue [59]. Now a days XRD is used not only for the determination of crystal structure but also chemical analysis, such as chain conformations and packing for polymers, for stress measurements and for the measurement of phase equilibria and the measurement of particle size, for the determination of

the orientation of the crystal and the ensemble of orientations in a polycrystalline material.

X-rays are the electromagnetic radiation whose wavelength is in the neighborhood of 1^{o} A. The wave length of an X-ray is thus of the same order of magnitude as the lattice constant of crystals, and it is this which makes X-rays so useful in structures analysis of crystals whenever X-ray are incident on a crystal surface they are reflected. The reflection abides by the celebrated Bragg's law as given below:

$$2d\ Sin\theta = n\lambda$$

Where, d is distance between crystal planes, θ is the incident angle, λ is the wave length of X-ray and n is a positive integer. The diffracted X-ray may be detected by their action on photographic films or plates or by means of a radiation counter or electronic equipment feeding data to a computer [75].

1.24.5 Principle of Absorption Spectroscopy

The greater the number of molecules capable of absorbing light of a given wavelength; the greater will be the extent of light absorption. Furthermore, the more effective a molecule is in absorbing light of a given wavelength, the greater will be the extent of light absorption. From these guiding ideas, the following empirical expression, known as the Beer-Lambert law, which is the basis of spectrometric methods of chemical analysis, may be formulated:

$$A = \log (I_0/I) = \varepsilon cl \text{ (for a given wavelength)} \qquad (1)$$

where, I_0 = Intensity of the light incident upon the sample cell.

I = Intensity of the light having the sample cell.

c = Molar concentration of solute.

l = Thickness of sample cell (cm).

ε = Molar absorption coefficient.

A = Absorbance.

The Molar absorption coefficient (ε) is a property of the molecule undergoing an electronic transition and related to transition probability and is not a function of the variable parameters involved in preparing a solution. The value of e indicates how intense a given transition is and totally an intrinsic property of the molecule, i.e.

$\varepsilon > 10^4$ is high intensity absorption.

$\varepsilon < 10^3$ is low intensity absorption.

ε = 100 to 1000 is forbidden transition.

1.25 Characterization of Surface Properties by Adsorption Methods

Adsorption methods [76] may be used to provide information about the total surface area of a catalyst, the surface area of the phase carrying the active sites, or possibly even the type and number of active sites. The interaction between the adsorbate and the adsorbent may be chemical (chemisorption) or physical (physisorption) in nature and ideally should be a surface-specific interaction. It is necessary to be aware, however, that in some cases the interaction between the adsorbate and the adsorbent can lead to a chemical reaction in which more than just the surface layer of the adsorbent is involved. For example, when using oxidizing compounds as adsorbates (O_2 or N_2O) with metals such as copper or nickel or sulfides, sub-surface oxidation may occur.

Physical adsorption is used in the BET method to determine total surface areas [77]. Many catalysts comprise an active component deposited on a support. In order to investigate relationships between catalytic properties and the amount of

active surface it is necessary to have a means of determining the surface area of the phase carrying the active sites (active phase) in the presence of the support. One has to resort to phenomena specific to the active phase. Chemisorption on the active phase is commonly used for this purpose.

Because of its intrinsically specific nature, chemisorption has an irreplaceable role. It should be recognized, however, that well defined thermodynamic equilibrium physisorption is much more difficult to achieve by chemisorption than with physisorption. Moreover, it does not obey simple kinetics. Empiricism permits the derivation of procedures which give reproducible results, and yield values which are proportional to the true surface area within certain limits. But the real coefficient of proportionality is actually unknown. Different procedures are used, according to UIC nature of the active phase/support system to be characterized, and depending on the choice of adsorbate. Provided standard, reproducible procedures are used, invaluable information can be obtained.

A wide variety of adsorbates has been used, the choice depending on the nature of the surface to be examined and the type of information being pursued; e.g. for metals, H_2, CO,O_2 and N_2O; for sulfides, NO, CO, O_2, H_2S and organo-sulfur compounds; for oxides, NH_3, CO_2 and various organic compounds.

With simple probe molecules, such as H_2, information about the number of surface metal atoms is readily obtained by using adsorption measurements. However, even with such simple probe molecules further information about the heterogeneity of a surface may be obtained by performing temperature-programmed desorption measurements. With probe molecules which are chemically more specific (e.g. NH_3 and organic amines, H_2S and organic sulfides) it may be possible to obtain information about the number and nature of specific types of surface sites, for example, the number and strength of Lewis or Bronsted acid sites on oxides, zeolites or sulfides.

The use of more than one technique can provide important additional information about the nature of sites on a particular solid surface. For example, infrared spectroscopy may be used in conjunction with quantitative chemisorption measurements of CO to determine the type of binding of CO and hence the nature and number of the active sites. The combination of chemisorption and ESR spectroscopy permits the characterization of the electronic properties of the surface. Care should be taken when using adsorption with microporous solids, as new effects may arise. Specific literature should be consulted in this case**.**

1.26 Determination of Specific Surface Area by Adsorption Measurements

Adsorption measurements have a variety of uses and applications, but perhaps the most important from our point of view is in determining the surface areas of catalysts. Provided the rate of transport of reactants to the surface, and product away from the surface, is faster than the catalyzed reaction, then the observed rate should be proportional to the surface area of the active phase of the catalyst. Adsorption measurement [78] can be performed by two ways,

(1) Gas adsorption measurement.

(2) Dye adsorption measurement.

The surface area of a catalyst could then be determined by either BET or Langmuir adsorption equation depending on which is appropriate for given data.

1.26.1 Gas Adsorption Measurements

Gas adsorption is accompanied by adsorption of a gas or vapour onto a bare solid surface.The total surface area of the catalyst can determined by adsorption of relatively inert gases like Ar, N_2 etc. at near their condensation temperature, as at such condition adsorption is non specific and physical in nature. If the

catalysts are not susceptible to poisoning by H_2, O_2, CO, NO gases, the specific surface area, i.e. the surface area due to active metal component can be determined by chemisorption of these gases.

1.26.2 Dye Adsorption Measurements

Dye adsorption technique involves the adsorption of dye molecules from solution onto a solid surface, in particular, dyes such as methylene blue. The method of adsorption of methylene blue in liquid phase for specific surface area determination has been adopted widely for various natural solids: activated carbon, charcoal, silica.

1.27 Point of Zero Charge

The pH where the net total particle charge is zero is called the point of zero charge (PZC), which is one of the most important parameters used to describe variable-charge surfaces. The PZC of the oxide may be the most important parameter since it is the pH around which strong buffering effect is observed [80]. The buffering effect is seen through the plateau on a pH final (pH after oxide addition) vs. pH initial graph.

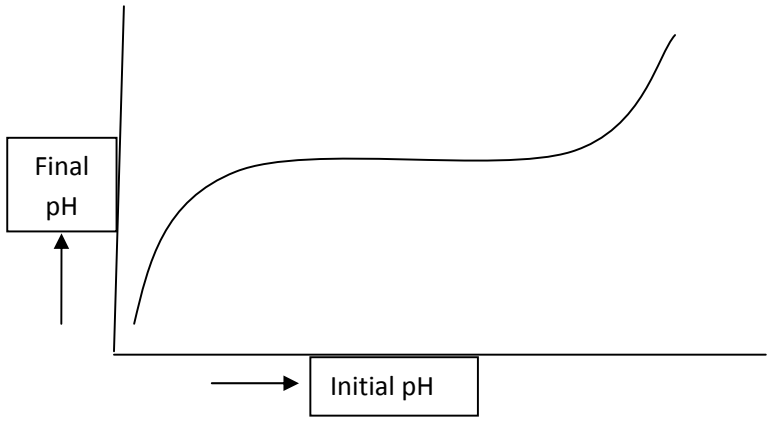

Figure 1.9: The plateau on a pH final (pH after oxide addition) vs. pH initial graph.

The oxide surface becomes protonated (deprotonated) when the initial pH is below (above) the afore-mentioned plateau region [80]. Oxide ions are strong bases [81]. Thus, in aqueous solutions, they become neutralized by water to form hydroxyl groups. The hydroxyl groups on the surface of an amphoteric oxide then become protonated or deprotonated, which leads the solution pH increasing or decreasing [80]. In other words, as oxides in an acidic (basic) pH become protonated (deprotonated) the solution, which supplies (consumes) protons, becomes more basic (acidic) [80]. This general concept is shown in the diagram (Figure 1.10).

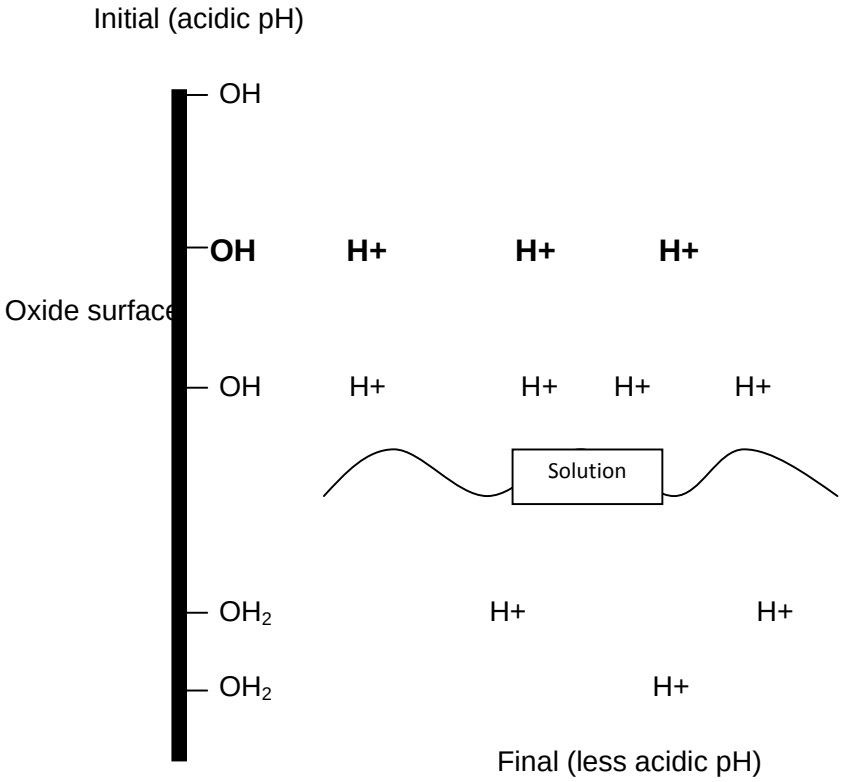

Fig. 1.10: A visual representation of a pH shift.

In solution, when the pH is greater than the PZC, the surface of the oxide is negatively charged and deprotonated. When the pH is less than the PZC, the surface of the oxide is positively charged and protonated. So oxides that are places in solutions with a pH greater than its PZC will absorb cations and oxides

contacted with a solution with a pH less than its PZC will absorb anions. Two important points are to be noted here,

1. The surface charge is equal to the fraction of positively charged sites minus the fraction of negatively charged sites [82].

2. The electrical double layer consists of a layer of charge on the oxide's particle surface and another layer of opposite charge in the surrounding solution [83].

1.28 Methods for the Determination of Point of Zero Charge (PZC)

There are several methods [84] namely:

(1) Potentiometric titration.

(2) Mass titration.

(3) Ion adsorption.

(4) Electrophroretic mobility.

1.28.1 Mass Titration

It was originally developed for pure metal oxides [85-87] and later extended so that it can be used also for contaminated samples [43/50m]. The principle of the method is simple; one needs to be added subsequent portions of metal oxide powder to the water or aqueous electrolyte solution, which might be acidified or may contain a base. The pH of the system is changed gradually and approaches a constant value, which is the PZC in the case of pure oxide. If the sample is contaminated, i.e. if it contains a certain portion of acid or base, the final pH is higher or lower than PZC, depending on the type and amount of the acid or base in the powder.

1.29 Literature survey and aim of the present work

Preparation of new mixed metal oxides of both industrial and synthetic importance has become a routine work in advanced material laboratories. Much work has been directed in the synthesis and characterization of metal oxide and mixed metal oxides type semiconductor photo catalyst and adsorbent as they have effective capability to destroy toxic and hazardous organic substances.

Michael J. Hudson et al have performed an excellent piece of work [88] on the preparation and characterization of mesophorous, high-surface-area zirconium(IV) oxide. They prepared high-surface-area zirconium(IV) oxide by incorporation of cationic quaternary ammonium surfactants in the hydrous oxide and subsequent calcinations of the inorganic/organic intermediate. The surfactants are incorporated by cation exchange at a pH above the isoelectric point of the hydrous oxide. After calcinations to 723 K and above, the ordering is a linear function of the chain length. Scaffolding, rather than a templating, mechanism is invoked to explain this ordering. Calcination of the materials to 723–973 K results in the formation of a mesoporous zirconium(IV) oxide.

An ingenious piece of research was conducted by **Maria Flytzani-Stephanopoulos** [89] on nanostructured cerium oxide “ecocatalysts”. Various techniques can be used to prepare nanocrystalline cerium oxide. For large scale production, several precipitation and gelation techniques are suitable. Ceria doped with rare-earth oxides or zirconia can be easily prepared by a coprecipitation (CP) method using ammonium carbonate as the precipitant. This involves mixing an aqueous solution of cerium(III) nitrate and other metal nitrates in desired proportions with $(NH4)_2CO_3$ at 60–70°C, keeping a constant pH value of 8, and aging the precipitate at 60–70°C for 1 h. After aging, the precipitate is filtered and washed with distilled water several times, then it is dried at 100–120°C and calcined in air at several hundred degrees Celsius for

10 h at a heating rate of 2°C/min. This method typically produces a well-crystallized material with needlelike crystals.

Point of zero charge (PZC) of metal oxide catalyst is an important parameter in preparation of the catalyst, since most of the metal oxide catalysts are amphoteric in nature. **John R. Regalbuto and coworkers** [90] determined surface charging parameters in aqueous solution by the method of equilibrium pH at high oxide loading. They determined PZC of alpha-alumina, gama-alumina, theta- alumina and silica by this method. 500 ml pH solutions ranging from 0 to 13 with increments of approximately 0.5 were prepared. The ionic strength of all the solutions was kept constant. After the oxide addition the solutions were placed on a shaker. Final pH increasing was recorded. The initial pH versus the final pH was plotted to show the PZC.

Chip Appel and coworkers [91] determined the PZC in soil and, minerals (kaolinite and synthetic goethite) collected from Puerto Rico an oxisol and ultisol using three methods:

(1) Potentiometric titration measuring the adsorption of H^+ and OH^- on amphoteric surfaces in solutions of varying ionic strength,

(2) Direct assessment of surface charges via non-specific ion adsorption as a function of pH and ionic strength and

(3) Electroacoustic mobility of reversible particles as it varies with pH and ionic strength.

Their studies revel that the PZC values, determined by first two methods, for Kaolinite are 2.7-3.2 and that of synthetic goethite is 7.4-8.2. The PZC for soil range from 3.9 to 4.4 for oxisol and 2.3-3.7 for the ultisol The PZC, determined by electroacoustic mobility, of Kaolinite is 3.8-4.1 and that of synthetic goethite is 8.1-8.2, furthermore the values found for oxisol is 3.4-3.5 and that of ultisol 2.6-2.7. **Parker et al** [92] have proposed several methods for the determination of

the PZC in soils and other materials dominated by variable surface-charge colloids. In soils researchers have generally relied on potentometric titration, which masses changes in surface potential with changes in activities of H^+ and OH^-, to determine the point of zero salt effect (PZSE) or point of zero net proton charge (PZNPC). They have also used non-specific ion adsorption, which measures changes in the electrostatic adsorption of a cation and anion with changes in the activities of H^+ and OH^-, to find the point of zero net charge (PZNC)

Another method for determining of the PZC is Mass Titration method, originally developed for pure metal oxides by **J.S. Noh et al** [93] and later extended by **S. Zalac** [94] for contaminated samples. The principle of this method is simple; one needs to add subsequent portions of metal oxide powder to the water or an aqueous electrolyte solution, which might be acidified or may contain a base. The pH of the system changes gradually and approaches a constant value, which is the point of zero charge in the case of pure oxide. If the sample is contaminated, i.e. if it contains a certain portion of acid or base, the final pH is higher or lower than PZC, depending on the type and amount of the acid or base in the powder. In the case of contamination, one needs to perform an acid-base titration of the concentrated suspension and the inflexion point provides the information on the PZC, and on the fraction of impurities in the powder. The advantage of mass titration is that one does need to perform blank titration; instead one simply adds metal oxide powder to the electrolyte aqueous solution of known pH [95].

M. Kosmulski determined the PZC of TiO_2 by means of potentiometric titration of by means of electrokinetic methods [96]. He used a set of 138 PZC of titanium dioxide was to explore the effect of the crystalline structure on the PZC. The average and median PZC at pH 5.6 and 5.8, respectively, was found when the entire data set was taken into account. The PZC of anatase (31 entries,

average and median 5.9 and 6, respectively) is slightly higher than that of rutile (49 entries, average and median 5.4 and 5.5, respectively), and the difference between the polymorphs corresponds to half of a standard deviation in each set of PZC.

From the early days of using bone charcoal for decolorization of sugar solution and other foods, to today's thousand of applications, the adsorption phenomenon has become a useful tool for purification and separation technologies [97-98]. Adsorption phenomena are operative in most natural, physical, biological and chemical systems and adsorption operations employing solids such as activated carbon, alumina, silica gel and zeolite are so far used widely in industrial applications and for purification of waters and wastewater [99-101].

A large specific surface area is preferable for providing large adsorption capacity. As a result, presently, a great deal of attention has been focused on the search for new materials with better adsorption capacity [102-104]. In catalysis, alloys or multicomponent system often perform better than its pure or single component [8-9]. Like catalysis, adsorption is also a surface property. Thus, employment of a binary or multicomponent surface for adsorption seems to be interesting to be investigated.

Cobalt oxide like other transition metal oxides has attracted much attention due to its potential application in many fields and its distinctive structure and properties [105-106]. Nano-size substances were found to be superior to bulk ones in battery applications improving the toughness of ceramics, increasing the density of magnetic recording and improving performance as a catalyst. There are the preparation of pure nano-sized substances is very important not only for the study of their properties but also for their application.

Materials based on cobalt oxides have attracted a great interest in view of their technological and fundamental scientific importance [107-109]. **Kobayashi *et***

al., [107] have reported that in the presence of CO and H_2 thin film of Co_3O_4 shows reversible change in the Vis-near IR absorption band. This phenomenon can be applied in the fabrication of solid-state gas sensors. Thin films of Co_3O_4 have been reported to change color from brown to light yellow when Li^+ ions are inserted [108]. The reversible change of optical properties of Co_3O_4 under an external stimulus can be used to fabricate electrochromic devices [109]. Such a broad perspective of utilization has increased the importance of synthesizing cobalt oxide nanocomposites.

Ting and Zexaing [110] successfully fabricated Metal oxide nanostructures (CuO, Co_3O_4, ZnO and α-Fe_2O_3) by a simple and efficient method: heating the appropriate metals in air at low temperatures ranging from 200 to 400^oC. The chemical composition, morphology and crystallinity of the nanostructures have been characterized by micro-Raman spectroscopy, X-ray diffraction, scanning electron microscopy and transmission electron microscopy.

Systematic synthesis of mixed-metal oxides in NiO-Co_3O_4, NiO-MoO_3, and NiO-CuO systems via liquid-feed flame spray pyrolysis (LF-FSP) was studied by **AZURDIA Jose A., MCCRUM Andrew and LAINE Richard M.** [111]. The LF-FSP process is a general aerosol combustion synthesis route to a wide range of lightly agglomerated oxide nanopowders. The materials reported here were produced by aerosolizing ethanol solutions of propionate and ammonium molybdate precursors synthesized by reacting the metal nitrate with propionic acid.

Mixed metal oxide system produced via the sol-gel method are of particular interest also because the opportunity exists for generating materials intermixed at atomic level. Such systems have the potential for exhibiting chemical properties that differ notably from those of the corresponding single component oxides. Synthesis and characterization of several mixed metal oxides with unique properties has been reported in the literature [112-114]

The present study would be conducted to evaluate the process characteristics in terms of the mode of the multi-component (Fe-Ni-Si) oxide material synthesis and characterization, its surface behavior and applications in removing organic dyes from aqueous solution. In doing so, the possible outcome of this research work might be:

1. To establish a simplistic process for the synthesis of a multi-component metal oxide surface.
2. To compare the removal capacity of organic dyes between the multi-component and single oxide surfaces.
3. To determine the surface area for evaluating the adsorption capacity of this material.
4. To measure the point of zero charge (PZC) of this adsorbent.
5. Batch experiments to remove organic dyes from effluents by measuring various parameters such as effect of pH and adsorbent dose, concentration effect, thermodynamic, kinetic and isotherm study.
6. Kinetic study of photo catalytic degradation of organic dye.

Chapter 2

EXPERIMENTAL

2.1 Materials and Probes

2.1.1 Chemicals

The chemicals and reagents used in this work are listed below. These are analytical grade and used without further purification except aniline which was distilled twice prior to use. Doubly distilled water was used as solvent to prepare most of the solution of this work.

(i) Iron nitrate [Uni-chem, China]
(ii) Nickel nitrate [Merck, India]
(iii) Sodium carbonate [Merck, India]
(iv) Sodium Silicate [Merck, India]
(v) Hydrochloric acid (32%) [E. Merck, Germany]
(vi) Sodium hydroxide [E. Merck, Germany]
(vii) Sodium chloride [Uni-chem, China]
(viii) Methylene blue [E. Merck, Germany]
(ix) Orange Green [E. Merck, Germany]

2.1.2 Instruments

Analysis of the samples performed in this work employed the following devices:

(i) UV-visible spectrophotometer [UV-1601 PC, Shimadzu, Japan]
(ii) Scanning electron microscope [Philips XL30, Holland]
(iii) X-ray diffractometer [Philips, Expert Pro, Holland]
(iv) pH meter [Hanna, pH 209, India]
(v) Centrifuge machine [Hermle, 2200 A, Germany]
(vi) Shaker machine [Heidolph Unimex 1010]
(vii) 100 mesh sieve [Endecotls test sieves limited, England]
(viii) Digital balance, [FR-200, Japan]
(ix) Furnace [DK, Chino, England]
(x) Microburette [China]

2.2 Preparation of Metal Oxide and Mixed Oxide material

Iron (III) and Ni(II)- based ternary oxide material was prepared *in situ* in a reactor which involve the simultaneous generation of hydrous ferric oxide (FeOOH), hydrous nickel oxide and silica gel. A mixture containing sodium silicate (Na_2SiO_3) and sodium carbonate (Na_2CO_3) was kept under stirring. After that, the iron (III) nitrates and nickel (II) nitrite solution was added in the former mixture under stirred condition to yield Fe-Ni-Si oxide at an appropriate pH. The Fe-Ni-Si slurry was then allowed to age for a few hours. The slurry was then be washed and separated by filtration. Finally, the dewatered solid was dried at a temperature of 200 °C for 3 hours in an oven. The iron(III), nickel(II) and silicon single oxide was prepared following the above method.

2.3 Characterization of synthesized materials

2.3.1 X-ray Diffraction

Iron oxides, nickel oxides, silicon oxides and iron-nickel-silicon mixed oxide materials were analyzed for their X-ray diffraction pattern in the powder state. For this purpose, the samples were prepared as the procedure described in section 2.2. The powder samples were pressed in a square aluminum sample holder (40 mm $\times$ 40 mm) with a 1 mm deep rectangular hole (20 mm $\times$ 15 mm) and pressed against an optical smooth glass plate. The upper surface of the sample was labeled in the plane with its sample holder. The sample holder was then placed in the diffractometer.

2.3.2 Surface Morphology

Iron oxides, nickel oxides, silicon oxides and iron-nickel-silicon mixed oxide samples were dispersed on a conducting steel plate. Iron oxides, nickel oxides, silica oxides and iron-nickel-silica mixed oxide thus prepared following the methods described in section 2.2 were examined for their surface morphology.

For this purpose, scanning electron microscopy technique was adopted. The dried powder iron oxides, nickel oxides, silicon oxides and iron-nickel-silicon mixed oxide samples were dispersed on a conducting carbon glued strip. The sample-loaded strip was then mounted to a chamber that evacuated to ~ 10^{-3} to 10^{-4} torr and then a very thin gold layer (~ few nanometers thick) were sputtered on the sample to ensure the conductivity of the sample surface. The sample was then placed in the main SEM chamber to view its surface. The system was computer interfaced and thus provides recording of the surface images in the computer file for its use as hard copy.

2.3.3 Electron Diffraction X-ray (EDX) Spectra

Elemental analysis of the synthesized iron oxides, nickel oxides, silicon oxides and iron-nickel-silicon mixed oxide materials was performed by EDX spectra. The dried powders of iron oxide, nickel oxide, silicon oxide and iron-nickel-silicon mixed oxide were dispersed on a 1cm × 1cm conducting steel plate. The still plates were then placed on a conducting carbon glued strip and a very thin gold layer was sputtered on the sample to ensure the conductivity of the sample surface. The sample was then placed in the main SEM chamber integrated with the EDX machine.

2.4 Removal of MB and OG dye using synthesized materials

2.4.1 Preparation of dye solution

A. Stock MB Solution

It was prepared by dissolving 0.036g solid MB to 500 mL double distilled water. In this way, 2.02×10^{-4} M MB solution was prepared which was used as stock MB solution.

B. Dilution of MB stock solution

Now with help of this stock solution, some solution such as 5×10^{-5}M, 1×10^{-5}M etc. were prepared by dilution method.

C. Stock OG Solution

It was prepared by dissolving 0.046g solid OG to 500 mL double distilled water. In this way, 2.03×10^{-4} M OG solution was prepared which was used as stock OG solution.

D. Dilution of OG stock solution

Now with help of this stock solution, some solution such as 5×10^{-5}M, 1×10^{-5}M etc. were prepared by using the formula by dilution method.

2.4.2 Determination of Concentration of Dye

The UV-Vis spectral analysis of the sample solutions employed a double beam spectrophotometer. UV-Vis spectroscopic analysis for the adsorption and degradation studies involved the aqueous solution of different pH. The references in these cases were the corresponding aqueous solutions that used for preparing the adsorbate solutions. The determination of the amount of dye adsorbed by a substrate was done by spectroscopy in the visible region.

2.4.2 Adsorption (Batch) Process

In this process initially dye solution (without adding adsorbent) was determined by UV-Visible spectrophotometer. Then required amount of adsorbent was added in 50 mL of specific concentration of dye solution. This solution was shaken for required time at room and different temperature. Then the suspension was centrifuged. After that dye from the above solution was again determined using UV-Visible spectrophotometer. The pH was adjusted as the required condition. Difference between two data showed the adsorpitivity of the adsorbent.

2. 4.3 Spectrum of MB

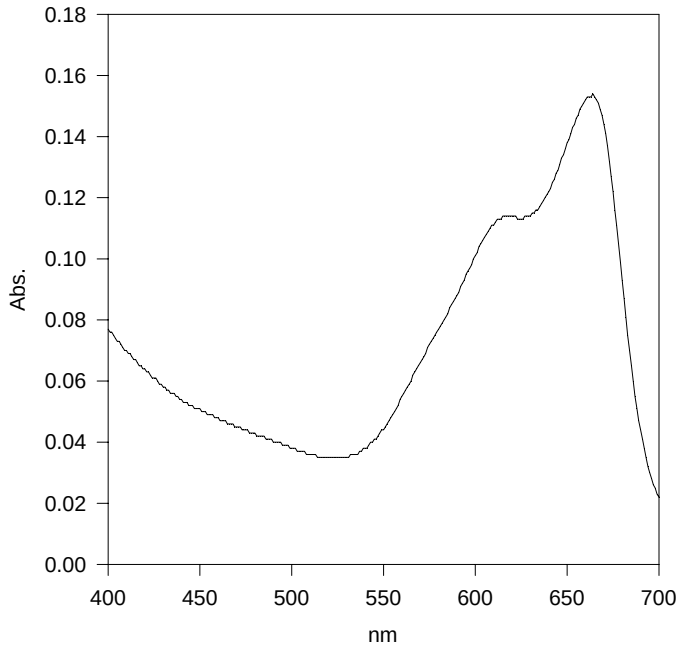

Figure 2.1: Spectrum of an aqueous solution of MB

2.4.4 Spectrum of OG

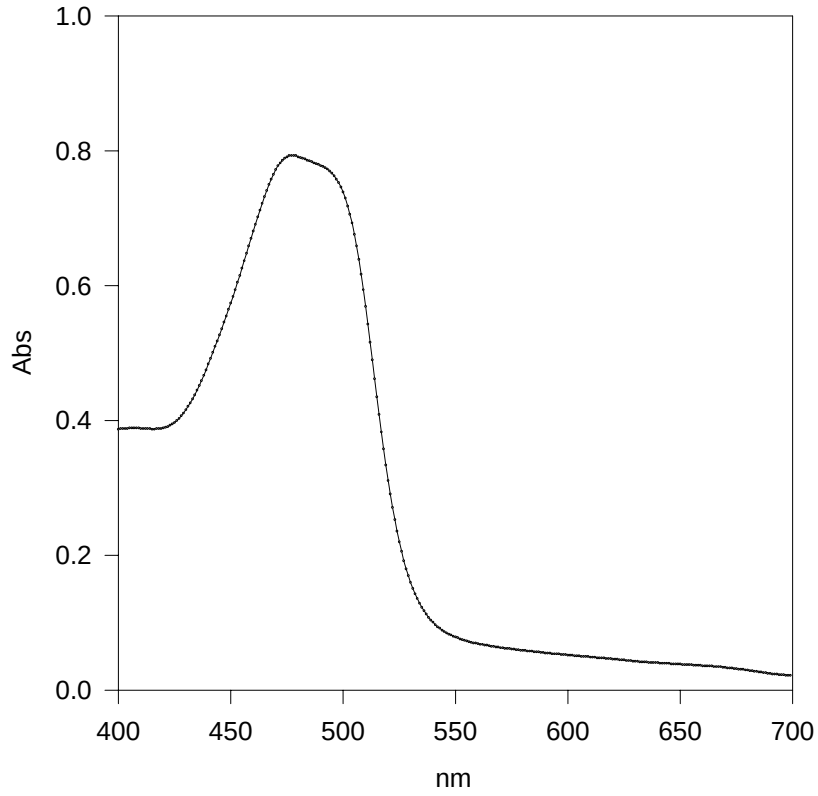

Figure 2.2: Spectrum of an aqueous solution of OG

2.4.5 Determination of molar absorption co-efficient (ε) of MB

Table 2.1: Absorbance of MB solution at different concentrations

Reference: Water λ_{max} for MB Solution: 664 nm

Temperature: 34°C pH: 6.92

Run No	Concentration of MB (M)	Absorbance
1	1×10^{-6}	0.07
2	2×10^{-6}	0.14
3	4×10^{-6}	0.28
4	6×10^{-6}	0.43
5	8×10^{-6}	0.58
6	10×10^{-6}	0.74

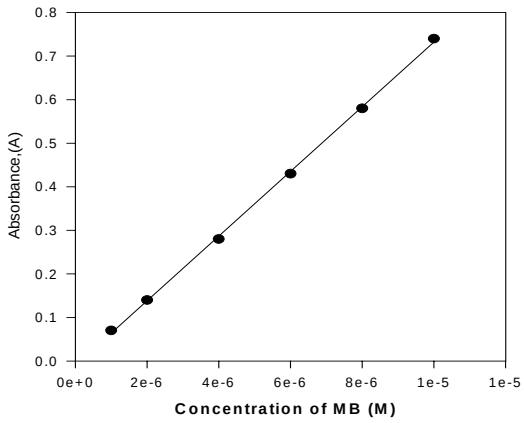

Figure 2.3: Beer-Lambert plot for the determination of molar extinction co-efficient of MB

Result: The molar absorption co-efficient (ε) is 74246 L $mol^{-1}cm^{-1}$.

2.4.6 Determination of molar absorption co-efficient (ε) of OG

Table 2.2: Absorbance of OG solution at different concentrations

Reference: Water λ_{max} for MB Solution: 477 nm

Temperature: 29°C pH: 6.55

Run No	Concentration of OG (M)	Absorbance
1	1×10^{-5}	0.14
2	2×10^{-5}	0.28
3	4×10^{-5}	0.57
4	6×10^{-5}	0.68
5	8×10^{-5}	1.14
6	10×10^{-5}	1.42

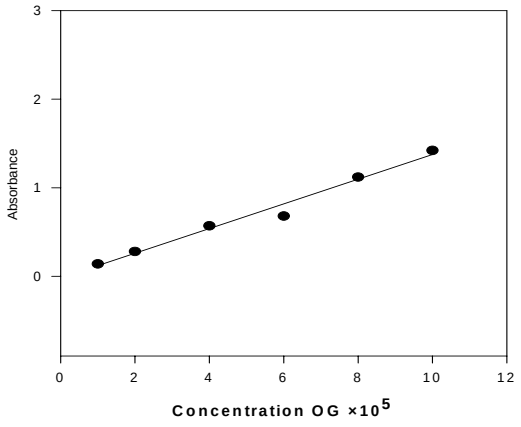

Figure 2.4: Beer-Lambert plot for the determination of molar extinction co-efficient of OG

Result: The molar absorption co-efficient (ε) is 13920 L $mol^{-1}cm^{-1}$.

2.4.7 Effect of pH on the spectral behavior of MB

Table 2.3: Absorbance of MB solutions at different pH of the medium

Reference: Water Temperature: 33°C

λ_{max} for MB Solution: 664 nm

Run No	Conc. Of MB (M) $\times 10^5$	pH	Instant Abs.	Abs. after 24 hours
1	1.00	5.35	0.694	0.694
2	1.00	6.92	0.694	0.694
3	1.00	9.24	0.694	0.694

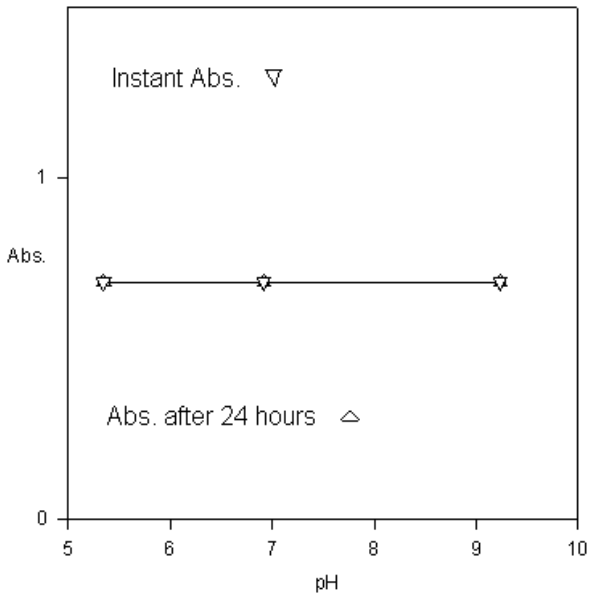

Figure 2.5: A plot of pH versus Absorbance for determination of stability of MB solution

Result: MB solution is stable for 24 hours.

2.4.8 Effect of pH on the spectral behavior of OG

Table2.4: Absorbance of OG solutions at different pH of the medium

Reference: Water Temperature: 33°C

λ_{max} for OG Solution: 477 nm

Run No	Conc. of OG (M) $\times 10^5$	pH	Instant Abs.	Abs. after 24 hours
1	1.00	4.95	0.71	0.71
2	1.00	6.55	0.71	0.71
3	1.00	8.75	0.71	0.71

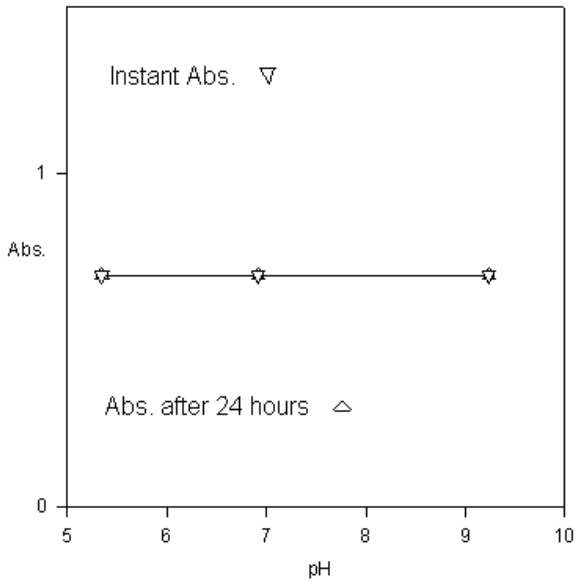

Figure 2.6: A plot of pH versus Absorbance for determination of stability of MB solution

Result: OG solution is stable for 24 hours.

2.5 Photochemical reactor designing

The Photocatalytic reactors were designed in an easier and inexpensive manner. Batch reactors were designed for the photodegradation study. For UV degradation study, three 10 W UV tube lights were placed parallel on the top inside of a wooden box. The walls, inside the box were covered with aluminum foil to ensure the maximum light to fall on the reaction vessel by reflection. Pyrex beaker (150 mL) was used as reaction vessel, which along with the reacting solution was placed 10 cm below the tube light on a magnetic stirrer. The reaction vessel was placed 10 cm below the light source on the same type magnetic stirrer. Fan was used for cooling the solution and light source in both cases. Figure 2.7 shows photos of the reactors and dark room used for the present studies.

(a) **(b)**

Figure 2.7: Photos of reactors (a) UV degradation starting. (b) UV degradation ending

2.6 Determination of Specific Surface Area of synthesized material

Dye adsorption technique involves the adsorption of dye molecules from solution onto a solid surface, in particular, dyes such as MB. The method of adsorption of MB in liquid phase for specific surface area determination has been adopted widely for various natural solids: activated carbon, charcoal, silica.In aqueous solution MB is a cationic dye which adsorbs to negatively charged catalyst surface. The MB molecule has a rectangular shape with dimensions of approximately (17A° x 7.6A° x 3.25A°). This molecule may attach to the catalyst surface in various orientations, so the area covered by one MB molecule may vary;(1) if molecule lies on its largest face on the surface under study, the covered area is about 130 $(A^o)^2$ per molecule, (2) if molecule is tilted (65-70^o) with respect to the surface under study, the covered area is about 66 $(A^o)^2$ per molecule and (3) if the longest is oriented perpendicular to the surface, the covered area is about 24.7 $(A^o)^2$ per molecule. MB is chosen in this study because of its strong adsorption onto solid and recognized usefulness in characterization of catalyst. Also in aqueous solution it shows distinct absorption band near uv-visible region (400-800 nm) of the electromagnetic radiation with absorption maxima at 664 nm.

2.6.1 Calculation of Amount Adsorbed on per gram of Adsorbate (X/m):

$X/m = (C_0 - C_{eq}) \times V \times M/(1000 \times 0.01)$ mol g^{-1}

Where, C_0 = Conc. of dye solution before addition of adsorbate

C_{eq} = Conc. of dye solution at equilibrium (after addition of adsorbate)

V = Volume of solution of each bottle

M = Molecular weight of dye

m = amount of adsorbate (catalyst)

2.6.2 Calculation of surface area

The adsorption technique is characterized by high bonding energy (ionic coloumbian attraction - chemisorption) and it is generally limited to a monolayer formation. Thus the Langmuir adsorption isotherm can be applicable in determining the specific surface area of the catalyst.

The linear form of the Langmuir adsorption equation is,

$[C_e]/(X/m) = [C_e]/K' + 1/K\,K'$

Where,

C_e = Concentration of dye solution at equilibrium (after addition of adsorbate)

X = Amount adsorbed on per gram of adsorbent

m= Amount of adsorbent

K' = Monolayer capacity

K = Adsorption coefficient

Plot of $[C_e]/(X/m)$ vs $[C_e]$ yields a straight line; from the slope we can get the amount of dye adsorbed to form a monolayer of adsorbate on the catalyst.

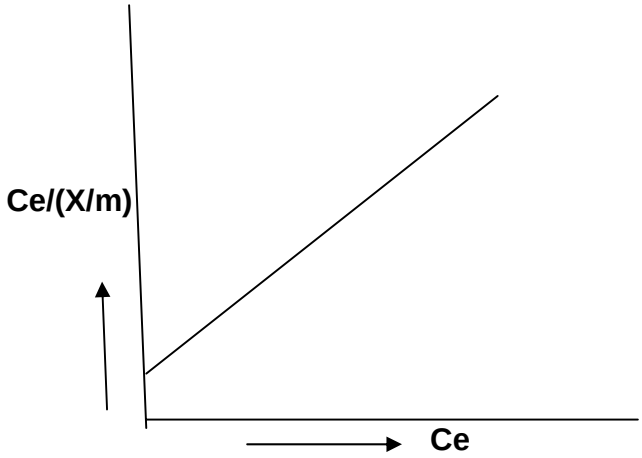

Figure 2.8: Langmuir-Hinshelwood plot of Ce/(X/m) vs Ce

The surface area (As) of the catalysts can then be calculated from the equation

$$As = K' \times N_a \times A \times 10^{-20}\ m^2\ g^{-1}$$

Where,

N_a = Avodagadro number,

A = Cross sectional area of the adsorbate.

2.7 Determination of (pH_{PZC}) of iron-nickel-silicon mixed oxide

The point of zero charge, pH_{PZC}, of solid substance (pH_{PZC}) means the pH at which the positive and negative charge in the surface is equal. To determine the point of zero charge of iron-nickel-silica mixed oxide the experiment was done in the following way:

Exactly 1.0 g of iron-nickel-silicon mixed oxide was taken in four different reagent bottles. Then 1×10^{-1} M NaCl solution was added to each bottle. The sample solution was agitated for 24.0 hours at low speed in a shaker. Then the suspensions were observed in each bottle. Two bottles of them were titrated directly with 0.065 M HCl and 0.065 M NaOH using microburette (± 0.01 mL). The pH values were noted carefully after addition of each drop of titrant (acid and alkali). Contents of other two bottles were filtered with sintered crucible and the supernatant thus obtained were titrated with 0.065 M HCl acid and 0.065 M NaOH. The experiments were carried out in the same way for the 1×10^{-2} M and 1×10^{-3} M NaCl solutions.

Chapter 3

RESULTS & DISCUSSION

3.1 Characterization of Synthesized Nano Materials

Iron oxide, Nickel oxide, silica oxide and Iron-Nickel-Silicon mixed oxide were prepared by sol-gel method. The above four nano oxides are characterized by Energy-dispersive X-ray spectroscopy (EDX), Scanning Electron Microscopy (SEM), X-Ray Diffraction (XRD), Specific Surface area (SSA) and Point Zero Charge (pH_{PZC}). EDX provided the information about chemical composition [11]. The nano oxide materials were characterized in terms of their particle size and morphology by SEM [11]. In XRD analysis, the crystalline structure and particle size were found [115]. The overall surface charge of materials and the specific surface area were given by acid-base titration and dye adsorption method, respectively [90].

3.1.1 EDX Spectral Analysis of Nano Mixed (Fe-Ni-Si) Oxide

Energy-dispersive X-ray spectroscopy (EDS or EDX) is an analytical technique [1] used for the elemental analysis or chemical characterization of a sample. It is one of the variants of X-ray fluorescence spectroscopy which relies on the investigation of a sample through interactions between electromagnetic radiation and matter, analyzing X-rays emitted by the matter in response to being hit with charged particles. Its characterization capabilities are due in large part to the fundamental principle that each element has a unique atomic structure allowing X-rays that are characteristic of an element's atomic structure to be identified uniquely from one another.

To stimulate the emission of characteristic X-rays from a specimen, a high-energy beam of charged particles such as electrons or protons, or a beam of X-rays, is focused into the sample being studied. At rest, an atom within the sample contains ground state (or unexcited) electrons in discrete energy levels or electron shells bound to the nucleus. The incident beam may excite an electron in an inner shell, ejecting it from the shell while creating an electron hole where the electron was. An electron from an outer, higher-energy shell then fills the hole, and the difference in energy between the higher-energy shell and the lower energy shell may be released in the form of

an X-ray. The number and energy of the X-rays emitted from a specimen can be measured by an energy-dispersive spectrometer. As the energy of the X-rays is characteristic of the difference in energy between the two shells, and of the atomic structure of the element from which they were emitted, this allows the elemental composition of the specimen to be measured [116].

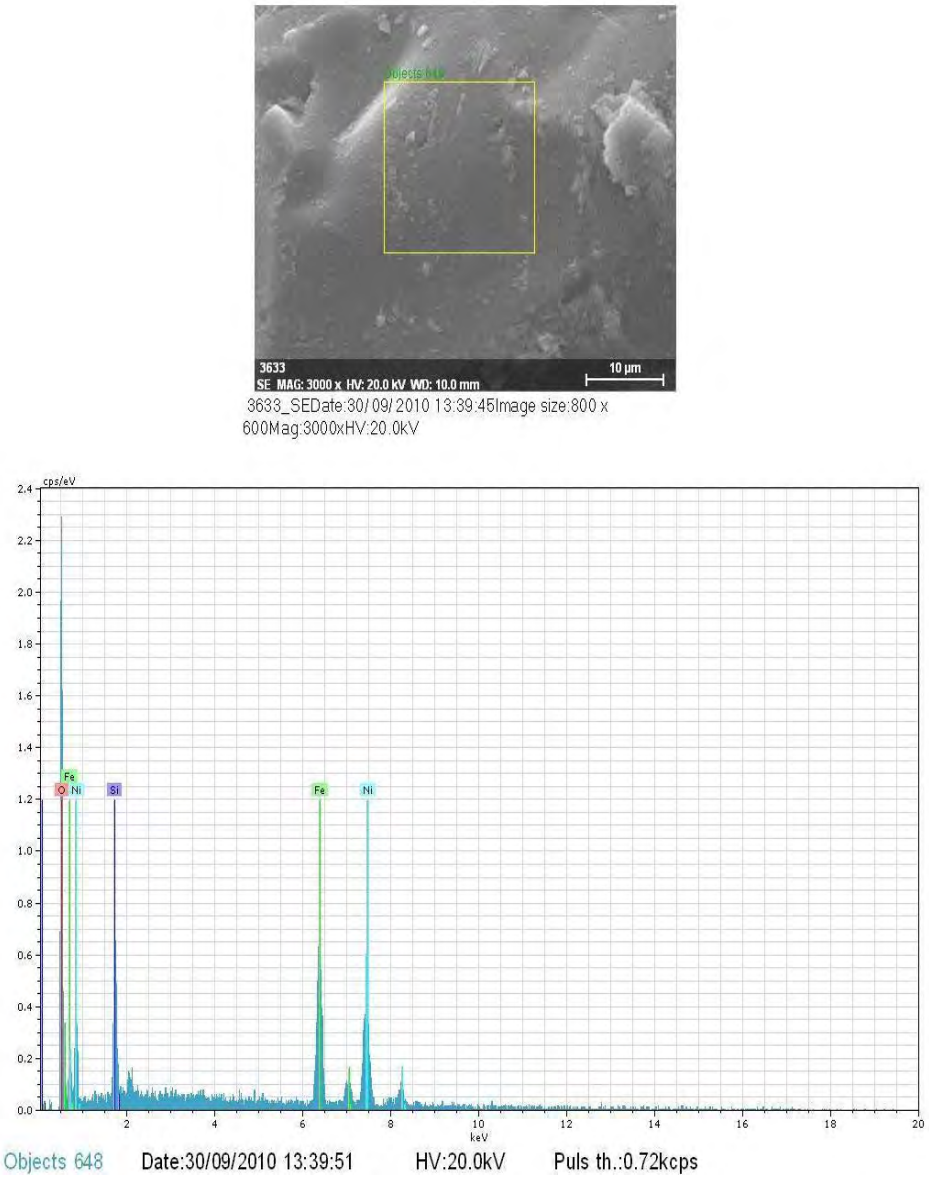

Figure 3.1.1.1: EDX spectrum of the Nano Mixed (Fe-Ni-Si) oxide.

Elemental analysis of the prepared solid Mixed (Fe-Ni-Si) was performed by employing EDX method. For this purpose, the sample was used that employed for SEM analysis which has been described in section 2.3.4. The pattern of the EDX spectrum is presented in Figure 3.1.1.1 The peaks observed at 6.34 and 0.72 keV for K and L lines respectively of the iron element; at 7.56 and 0.82 keV for K and L lines of the nickel element; at 1.8 keV for k series of the element of silica and 0.52 keV for k lines of the oxygen element. The percentage of Fe, Ni, Si and O were determined from the intensity of the lines ans the results are summarized further in Table 3.1.1.1

Table 3.1.1.1: Elemental composition of as prepared mixed (Fe-Ni-Si) oxide

Iron (%)	Nickel (%)	Silica (%)	Oxygen (%)	Tentative Chemical formula
29.08	30.06	8.93	31.94	$Fe_{0.78}$ $Ni_{0.76}Si_{0.46}O_3$

Thus, from the chemical composition obtained from the EDX spectrum, it can be calculated that the prepared nano mixed (Fe-Ni-Si) oxide is $Fe_{0.78}$ $Ni_{0.76}Si_{0.46}O_3$ and no other phases are present.

3.1.2 X-ray Diffraction

X-ray scattering techniques are a family of non-destructive analytical techniques which reveal information about the crystallographic structure, chemical composition, and physical properties of materials and thin films. These techniques are based on observing the scattered intensity of an X-ray beam hitting a sample as a function of incident and scattered angle, polarization, and wavelength or energy [115].

X-ray diffraction yields the atomic structure of materials and is based on the elastic scattering of X-rays from the electron clouds of the individual atoms in the system. The most comprehensive description of scattering from crystals is given by the dynamical theory of diffraction. Single-crystal X-ray diffraction

is a technique used to solve the complete structure of crystalline materials, ranging from simple inorganic solids to complex macromolecules, such as proteins. Powder diffraction (XRD) is a technique used to characterize the crystallographic structure, crystallite size (grain size), and preferred orientation in polycrystalline or powdered solid samples. Powder diffraction is commonly used to identify unknown substances, by comparing diffraction data against a database maintained by the International Centre for Diffraction Data. It may also be used to characterize heterogeneous solid mixtures to determine relative abundance of crystalline compounds and, when coupled with lattice refinement techniques, such as Rietveld refinement, can provide structural information on unknown materials. Powder diffraction is also a common method for determining strains in crystalline materials. An effect of the finite crystallite sizes is seen as a broadening of the peaks in an X-ray diffraction as is explained by the Scherrer Equation [2].

The XRD pattern of iron oxide, nickel Oxide, silicon oxide and iron-nickel-silicon mixed oxide in listed Figure 3.1.2.1 to 3.1.2.4. The scattering pattern as a function of Bragg angle, 2θ at λ=0.154nm for the studied samples powder are present in those figure.

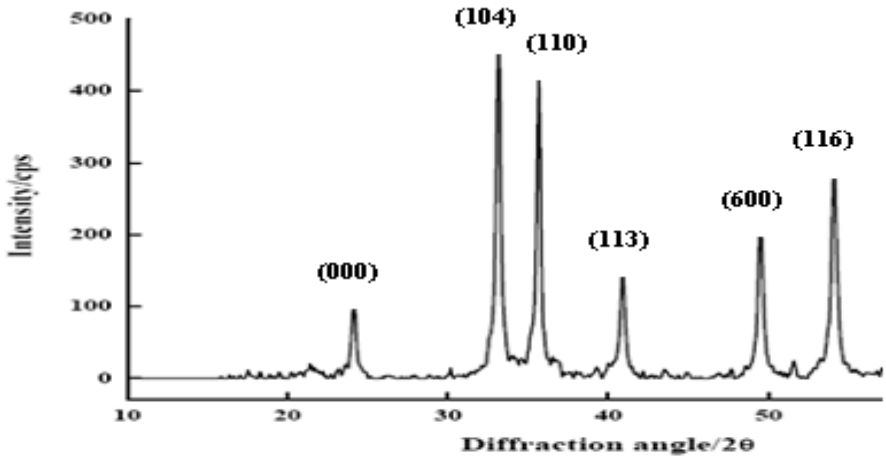

Figure 3.1.2.1: XRD pattern of Iron Oxide

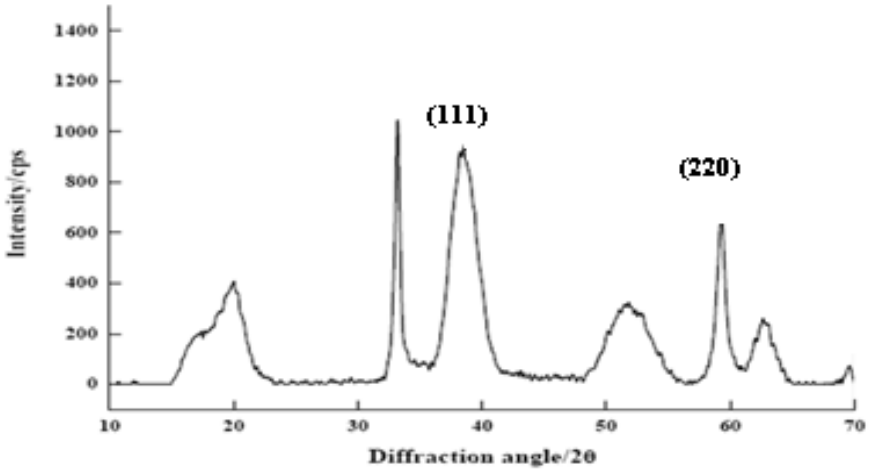

Figure 3.1.2.2: XRD pattern of Nickel Oxide

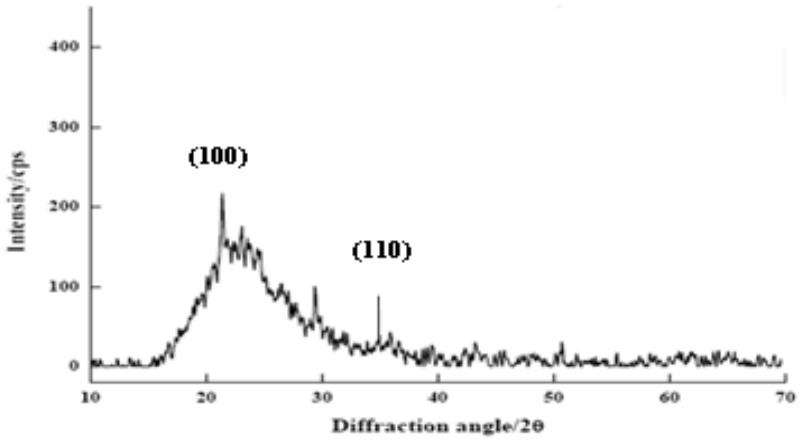

Figure 3.1.2.3: XRD pattern of Silicon Oxide

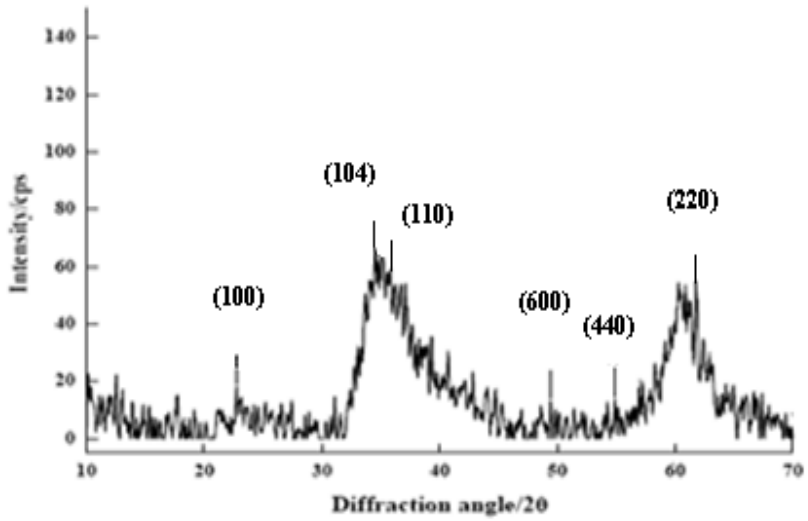

Figure 3.1.2.4: XRD pattern of Iron-Nickel-Silica Mixed Oxide

Figure 3.1.2.1 shows the XRD results of the reference sample. The content of our results matches with JCPDS (Joint Committee on Powder Diffraction Standard) card 730603 on Annes A indentifying the sample to be α-Fe_2O_3.

Figure 3.1.2.2 exhibits the XRD results of Nickel Oxide, the recognize Miller Indice (h, k, l) lattice plane peaks are observed at 111 (37.2°) and 220 (59.250°) which are matches with JCPDS card 40835.

Figure 3.1.2.3, the XRD pattern of Silica Oxide displays the characteristic peaks 100 (20.4°) and 110 (35.8°) which are similar to the JCPDS card 110252.

The XRD pattern of Iron-Nickel- Silica Mixed oxide is illustrated in Figure 3.1.2.4. The distinguishing lattice plane peaks are present in 100 (23.7°), 104(34.8°), 110(35.8°), 448 (36.8°), 600(49.5°), 440 (59.4°) and 220 (62.6°). The peaks 100 and 110 are counterpart of JCPDS card 110252; 600, 440 and 448 are match with JCPDS card 361216; 104 is match with JCPDS card

730603; the peak 220 are similar to JCPDS card 40835. The Miller Indice (h, k, l) lattice planes of Iron, Nickel and Silica single oxide are present in Mixed (Fe-Ni-Si) oxide with partial deviation of 2θ angle of the plane. The XRD pattern shows the evidence which is perfectly synthesized our desired mixed (Fe-Ni-Si) oxide.

Crystallite size of Single and Multi-component Oxide

The finite crystallite sizes is found of as a broadening of the peaks in an X-ray diffraction as is explained by the Scherrer Equation [6]. The Scherrer Equation is

$$D_p = \frac{0.94\lambda}{\beta_{1/2}\cos\theta}$$

Where, θ = Bragg angle,

λ=0.154nm = wave length of X-ray

$\beta_{1/2}$ =Full Width Half- maxima (FWHM),

D_p = crystallite size of particle

For using Scherrer Equation the crystallite size of these materials are obtained. The particle size of, iron-nickel-silicon mixed oxide, iron oxide, nickel oxide and silicon oxide is 18, 24, 26 and 37 nanometer, respectively.

3.1.3 Scanning Electron Microscopy

The scanning electron microscope (SEM) is a type of electron microscope that images the sample surface by scanning it with a high-energy beam of electrons in a raster scan pattern [6]. The electrons interact with the atoms that make up the sample producing signals that contain information about the sample's surface topography, composition and other properties such as

electrical conductivity. A wide range of magnifications is possible, from about 10 times (about equivalent to that of a powerful hand-lens) to more than 500,000 times, about 250 times the magnification limit of the best light microscopes. The iron oxide (Figure 3.1.3.2 d-e), nickel oxide (Figure 3.1.3.3 f-g), silica oxide (Figure 3.1.3.4 h-i) and mixed (Fe-Ni-Si) oxide (Figure 3.1.3.1 a-c) samples obtained were layered over steel plate for its SEM analysis. All the images display well-dispersed nanoparticles, however, with different morphologies and varying uniformity [11].

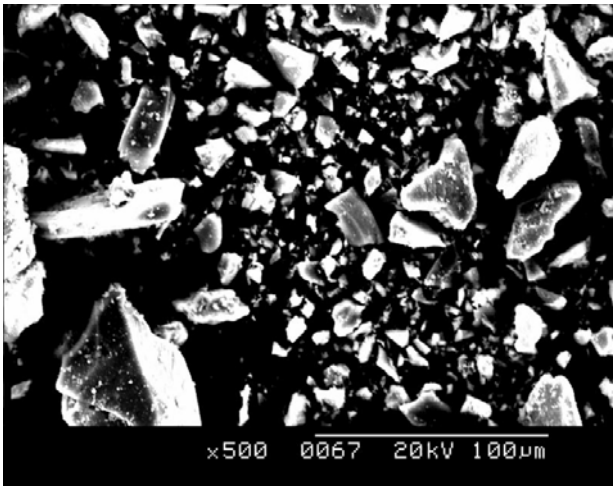

(a)

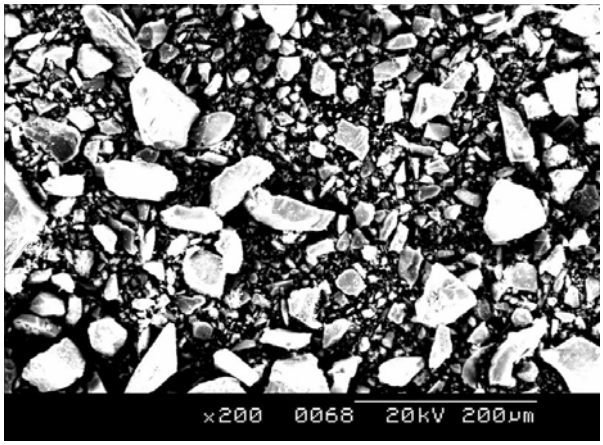

(b)

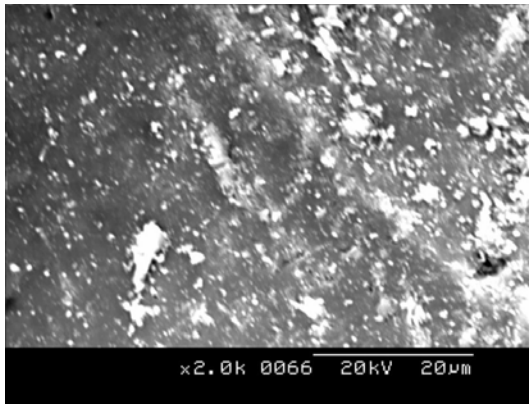

(c)

Figure 3.1.3.1(a-c): SEM micrograph of Mixed (Fe-Ni-Si) Oxide at different pixels.

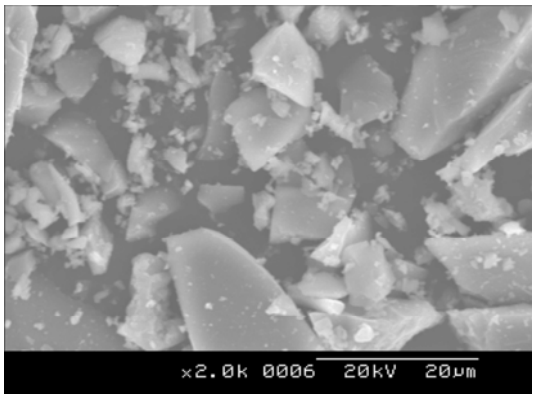

(d)

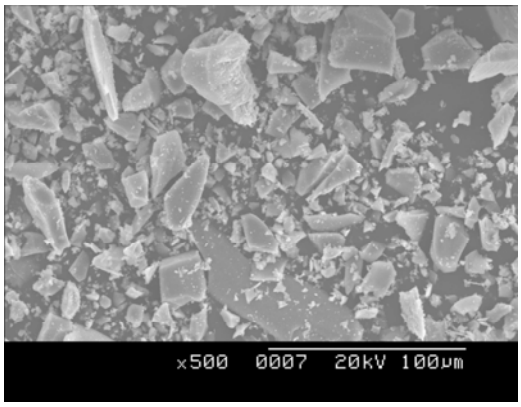

(e)

Figure 3.1.3.2 (d-e): SEM micrograph of Iron Oxide at different pixels

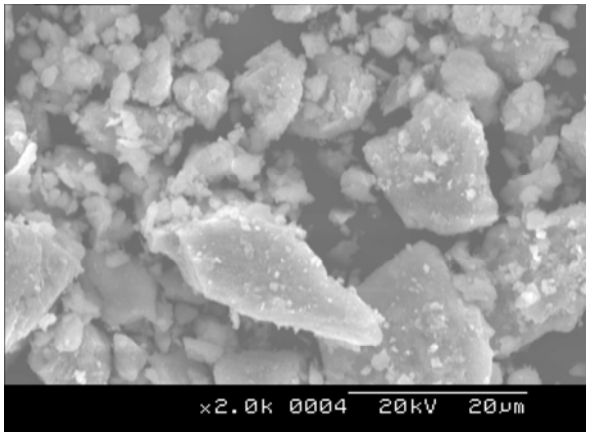

(f)

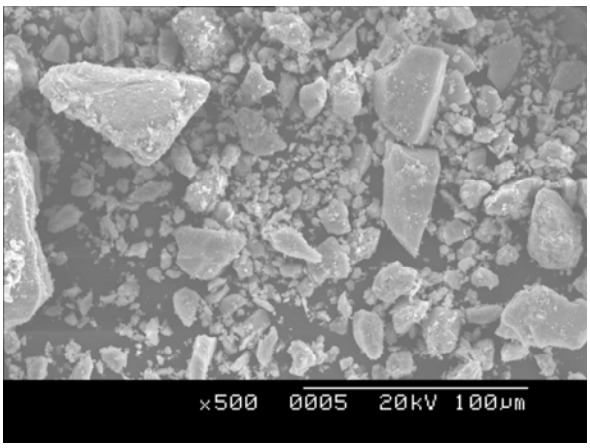

(g)

Figure3.1.3.3 (f-g): SEM micrograph of Nickel Oxide at different pixels.

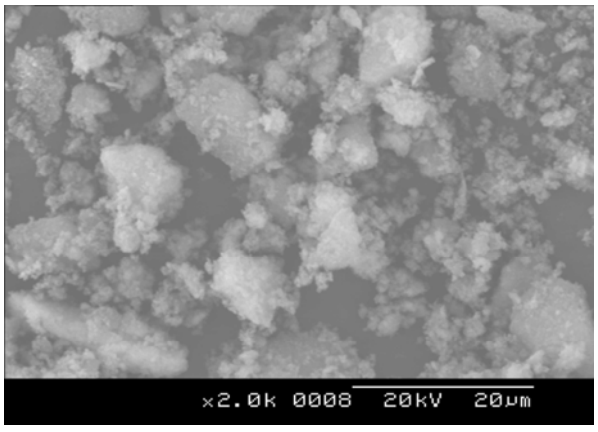

(h)

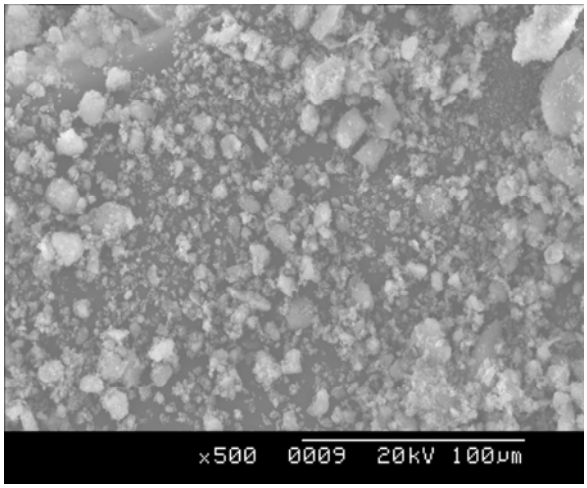

(i)

Figure 3.1.3.4 (h-i): SEM micrograph of Silica Oxide at different pixels

The average particle size distribution measured from SEM may be in higher range (10 nm to 100 nm) than the crystallite size measured from XRD. This is expected as the XRD measurement a mean of the actual crystallite size. Albeit, the particles were found to be highly crystallite according to the X-ray diffraction studies but from the SEM images a thin amorphous layer surrounding each particle was observed [117].

3.1.4 Determination of Specific Surface Area of Nano Mixed (Fe-Ni-Si) Oxide by Dye (MB) adsorption method

Table 3.1.4.1: Data for the calculation of surface area

Amount of Nano Mixed (Fe-Ni-Si) Oxide: 0.01g

Shaking Time: 120 min

Temperature: 31°C

Volume of each solution: 50 mL

Molar absorption co-efficient: 74246 $mol^{-1}cm^{-1}$

pH of the solution : 6.92

Run No	Initial conc. of MB×10^6 q_0 ($molL^{-1}$)	Abs.	Equilibrium conc. of MB ×10^6 q_e ($molL^{-1}$)	Adsorbed conc. of MB×10^6 q_m ($molL^{-1}$)	Amount Adsorbed of MB×10^6 q_m/m ($molg^{-1}$)	$q_e/(q_m/m)$ ×10^3
1	10	0.111	1.50	8.50	42.50	35
2	12	0.178	2.40	9.60	48.50	49
3	14	0.193	2.90	11.10	55.50	52
4	16	0.267	3.60	13.40	67.00	56
5	18	0.297	4.00	14.00	70.00	57
6	20	0.349	4.70	15.30	76.50	61
7	22	0.453	6.10	15.90	79.50	76
8	24	0.587	7.90	16.10	80.50	98
9	26	0.731	9.85	16.15	80.75	122

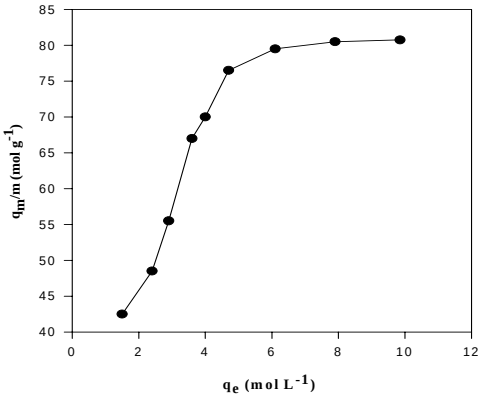

Figure 3.1.4.1: Langmuir plot of q_m/m versus q_e for adsorption of MB onto mixed oxide

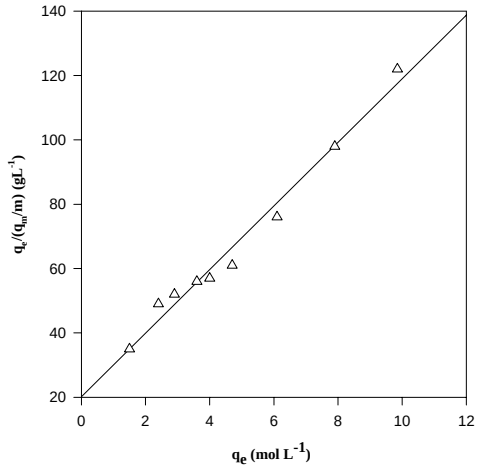

Figure 3.1.4.2: Langmuir-Hinshelwood plot of $q_e/(q_m/m)$ vs q_e

The adsorption of MB onto Nano Mixed (Fe-Ni-Si) Oxide follows Langmuir – Hinshelwood isotherm at pH6.92 at room temperature (R^2= 0.98). From the Langmuir-Hinshelwood plot of $q_e/(q_m/m)$ vs q_e, it has been found monolayer capacity K' = 1×10^{-4}mol g^{-1} from slope and adsorption constant K = 2.0125×10^{-2} $Lmol^{-1}$from the intercept. Then the specific surface area of the Nano Mixed (Fe-Ni-Si) Oxide was calculated. The specific surface area of Nano Mixed (Fe-Ni-Si) Oxide follows at pH6.92 at room temperature (R^2= 0.98) is 78.30 m^2g^{-1}.

3.1.5 Determination of point of zero charge (pH_{PZC}) of mixed (Fe-Ni-Si) oxide

The point of zero charge of solids substances (pH_{PZC}) means the pH at which the positive and negative charge in the surface are equal. pH_{PZC} has been determined by simple acid-base titration. It is described in section 2.4.5. The pH metric titration curves for three different concentration of NaCl solution which is shown in Table 3.1.5.1 - 3.1.5.3 and Figure. 3.1.5.1 -3.1.5.3. The data are given in Table 3.1.5.4. The net titration curves corresponding to three different ionic strengths are shown in Figure 3.1.5.4. The pH_{PZC} has been found to be 9.80. If the pH of the bulk higher than pH_{PZC} surface becomes negative and the lowering of the pH of the bulk than pH_{PZC} surface becomes positive.

Optimize data for pHpzc

Amount of mixed oxide: 1 g

Volume of NaCl solution taken: 50mL

Strength of NaCl: 1×10^{-1}M, 1×10^{-2}M and 1×10^{-3}M

Rate of agitation: 215 rpm

Time of agitation: 24 hours

Strength of HCl and NaOH solution: 0.065M

Table 3.1.5.1: pH metric titration of nano mixed (Fe-Ni-Si) oxide material with 1×10^{-1}M NaCl

Volume of HCl (mL)	pH of the solution		Volume of NaOH	pH of the solution	
	Suspension	Filtrate		Suspension	Filtrate
0.0	9.38	9.18	0.00	9.36	9.21
0.5	9.01	8.81	0.50	9.56	9.42
1.0	8.79	8.64	1.0	9.72	9.61
1.5	8.64	8.46	1.5	9.83	9.73
2.0	8.50	8.26	2.0	9.91	9.83
2.5	8.38	8.11	2.5	9.97	9.91
3.0	8.26	7.99	3.0	10.02	9.97
3.5	8.15	7.89	3.5	10.06	10.01
4.0	8.04	7.76	4.0	10.10	10.06
4.5	7.92	7.62	4.5	10.14	10.12
5.0	7.84	7.51	5.0	10.18	10.17
5.5	7.76	7.37	5.5	10.22	10.23
6.0	7.69	7.22	6.0	10.26	10.29
6.5	7.62	7.14	6.5	10.29	10.37
7.0	7.55	7.05	7.0	10.33	10.41
7.5	7.50	6.99	7.5	10.37	10.46
8.0	7.43	6.92	8.0	10.40	10.50
8.5	7.37	6.83	8.5	10.43	10.54
9.0	7.31	6.75	9.0	10.46	10.58
9.5	7.26	6.67	9.5	10.49	10.61
10.0	7.19	6.59	10.0	10.52	10.63
10.5	7.13	6.49	10.5	10.55	10.66
11.0	7.07	6.41	11.0	10.58	10.68

11.5	7.01	6.38	11.5	10.60	10.70
12.0	6.94	6.31	12.0	10.62	10.72
12.5	6.86	6.21	12.5	10.64	10.74
13.0	6.78	6.14	13.0	10.66	10.76
13.5	6.72	6.07	13.5	10.67	10.77
14.0	6.66	6.00	14.0	10.68	10.78
14.5	6.59	5.94	14.5	10.69	10.79
15.0	6.51	5.88	15.0	10.69	10.79
15.5	6.44	5.82	15.5	10.70	10.80
16.0	6.32	5.78	16.0	10.70	10.80
16.5	6.23	5.74	16.5	10.71	10.81
17.0	6.15	5.70	17.0	10.71	10.81
17.5	6.10	5.68	17.5	10.72	10.82
18.0	6.04	5.66	18.0	10.72	10.82
18.5	5.98	5.64	18.5	10.72	10.82
19.0	5.93	5.62	19.0	10.73	10.83
20.0	5.90	5.60	20.0	10.73	10.83
20.5	5.88	5.61	20.5	10.74	10.85
21.0	5.86	5.60	21.0	10.74	10.86
21.5	5.85	5.59	21.5	10.75	10.87
22.0	5.84	5.58	22.0	10.75	10.87
22.5	5.83	5.56	22.5	10.76	10.87
23.0	5.83	5.55	23.0	10.76	10.88

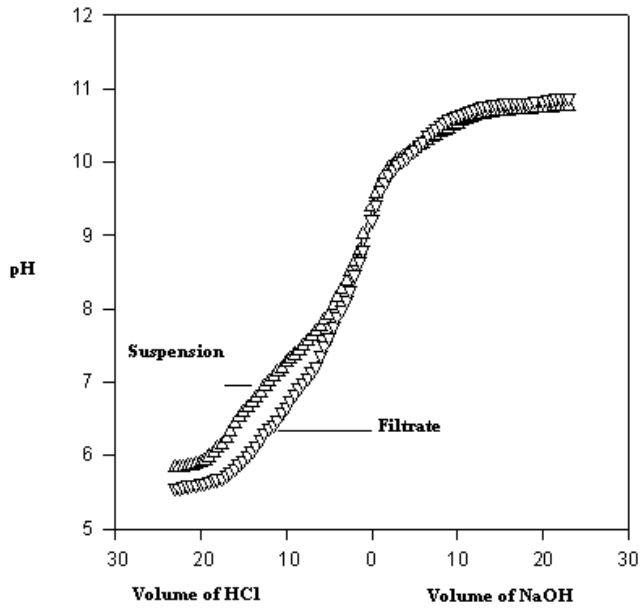

Figure 3.1.5.1: pH metric titration curves for nano mixed (Fe-Ni-Si) oxide with 1×10^{-1}M NaCl

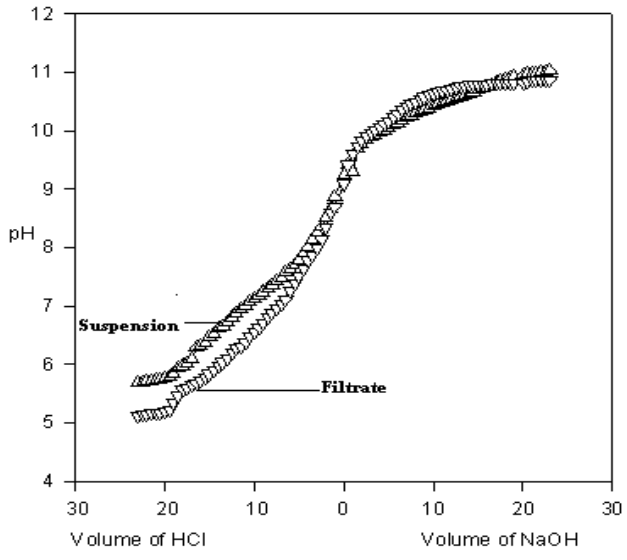

Figure 3.1.5.2: pH metric titration curves for nano mixed (Fe-Ni-Si) oxide with 1.10×10^{-2} NaCl.

Table 3.1.5.2: pH metric titration of nano mixed (Fe-Ni-Si) oxide material with 1×10^{-2}M NaCl

Volume of HCl (mL)	pH of the solution		Volume of NaOH	pH of the solution	
	Suspension	Filtrate		Suspension	Filtrate
0.0	9.25	9.09	0.00	9.27	9.08
0.5	8.87	8.70	0.50	9.43	9.32
1.0	8.66	8.59	1.0	9.30	9.51
1.5	8.51	8.35	1.5	9.70	9.63
2.0	8.37	8.15	2.0	9.78	9.73
2.5	8.25	8.00	2.5	9.84	9.81
3.0	8.13	7.88	3.0	9.91	9.87
3.5	8.02	7.78	3.5	9.93	9.91
4.0	7.91	7.65	4.0	9.97	9.96
4.5	7.79	7.51	4.5	10.01	10.02
5.0	7.71	7.40	5.0	10.05	10.07
5.5	7.63	7.27	5.5	10.10	10.03
6.0	7.57	7.12	6.0	10.14	10.19
6.5	7.49	7.04	6.5	10.18	10.27
7.0	7.43	6.95	7.0	10.22	10.31
7.5	7.36	6.89	7.5	10.26	10.36
8.0	7.30	6.81	8.0	10.30	10.40
8.5	7.24	6.72	8.5	10.33	10.44
9.0	7.18	6.64	9.0	10.36	10.48
9.5	7.13	6.56	9.5	10.39	10.41
10.0	7.07	6.49	10.0	10.42	10.43
10.5	7.01	6.39	10.5	10.45	10.56
11.0	6.94	6.31	11.0	10.48	10.58
11.5	6.88	6.28	11.5	10.51	10.60

12.0	6.81	6.21	12.0	10.54	10.62
12.5	6.73	6.11	12.5	10.56	10.64
13.0	6.65	6.04	13.0	10.58	10.66
13.5	6.62	5.97	13.5	10.61	10.67
14.0	6.53	5.90	14.0	10.64	10.68
14.5	6.46	5.84	14.5	10.67	10.69
15.0	6.38	5.78	15.0	10.70	10.69
15.5	6.31	5.72	15.5	10.73	10.70
16.0	6.29	5.68	16.0	10.76	10.70
16.5	6.10	5.64	16.5	10.79	10.71
17.0	6.02	5.60	17.0	10.82	10.71
17.5	5.98	5.58	17.5	10.85	10.72
18.0	5.93	5.46	18.0	10.88	10.72
18.5	5.85	5.34	18.5	10.91	10.72
19.0	5.80	5.22	19.0	10.94	10.73
20.0	5.77	5.20	20.0	10.97	10.73
20.5	5.75	5.18	20.5	10.98	10.75
21.0	5.73	5.17	21.0	10.98	10.76
21.5	5.72	5.16	21.5	10.99	10.77
22.0	5.71	5.15	22.0	11.01	10.77
22.5	5.70	5.14	22.5	11.02	10.77
23.0	5.70	5.13	23.0	10.03	10.78

Table 3.1.5.3: pH metric titration of nano mixed (Fe-Ni-Si) oxide material with 1×10^{-3}M NaCl

Volume of HCl (mL)	pH of the solution		Volume of NaOH	pH of the solution	
	Suspension	Filtrate		Suspension	Filtrate
0.0	9.11	8.95	0.00	9.09	8.97
0.5	8.77	8.57	0.50	9.56	9.42
1.0	8.55	8.42	1.0	9.72	9.61
1.5	8.40	8.22	1.5	9.83	9.73
2.0	8.26	8.04	2.0	9.91	9.83
2.5	8.14	7.87	2.5	9.97	9.91
3.0	8.03	7.75	3.0	10.02	9.97
3.5	7.91	7.62	3.5	10.06	10.01
4.0	7.80	7.54	4.0	10.10	10.06
4.5	7.68	7.40	4.5	10.14	10.12
5.0	7.60	7.29	5.0	10.18	10.17
5.5	7.52	7.15	5.5	10.22	10.23
6.0	7.45	7.02	6.0	10.26	10.29
6.5	7.38	6.90	6.5	10.29	10.37
7.0	7.31	6.80	7.0	10.33	10.41
7.5	7.26	6.77	7.5	10.37	10.46
8.0	7.19	6.80	8.0	10.40	10.50
8.5	7.13	6.61	8.5	10.43	10.54
9.0	7.07	6.53	9.0	10.46	10.58
9.5	7.02	6.45	9.5	10.49	10.61
10.0	6.96	6.37	10.0	10.52	10.63
10.5	6.91	6.22	10.5	10.55	10.66
11.0	6.83	6.19	11.0	10.58	10.68
11.5	6.77	6.16	11.5	10.60	10.70

12.0	6.70	6.09	12.0	10.62	10.72
12.5	6.62	5.99	12.5	10.64	10.74
13.0	6.54	5.90	13.0	10.66	10.76
13.5	6.48	5.85	13.5	10.67	10.77
14.0	6.42	5.78	14.0	10.68	10.78
14.5	6.35	5.72	14.5	10.69	10.79
15.0	6.27	5.63	15.0	10.69	10.79
15.5	6.20	5.62	15.5	10.70	10.80
16.0	6.08	5.56	16.0	10.70	10.80
16.5	5.99	5.52	16.5	10.71	10.81
17.0	5.91	5.50	17.0	10.71	10.81
17.5	5.86	5.46	17.5	10.72	10.82
18.0	5.82	5.42	18.0	10.72	10.82
18.5	5.78	5.40	18.5	10.72	10.82
19.0	5.74	5.38	19.0	10.73	10.83
20.0	5.70	5.35	20.0	10.73	10.83
20.5	5.66	5.32	20.5	10.74	10.85
21.0	5.63	5.29	21.0	10.74	10.86
21.5	5.60	5.26	21.5	10.75	10.87
22.0	5.57	5.24	22.0	10.75	10.87
22.5	5.54	5.22	22.5	10.76	10.87
23.0	5.51	5.21	23.0	10.76	10.88

Table 3.1.5.4: Data for net titration of nano mixed (Fe-Ni-Si) Oxide.

Strength of NaCl	ΔV of HCl	pH	ΔV of NaOH	pH
1×10^{-1}	0.5	8.64	0.5	9.83
	1.0	8.26	2.0	10.58
	1.5	7.76	8.0	10.74
	2.5	6.59	9.5	10.76
	5.5	5.88		
1×10^{-2}	0.5	8.37	0.5	9.91
	1.0	8.13	1.5	10.56
	1.5	7.63	2.0	10.64
	3.5	7.07	3.5	10.73
	4.0	6.94		
	4.5	6.64		
	5.0	6.31		
	6.0	5.72		
1×10^{-3}	4.0	5.99	0.5	9.83
	6.0	6.63	1.0	10.37
			1.5	10.45
			2.5	10.66
			3.0	10.68
			4.0	10.70
			8.5	10.74
			9.5	10.76

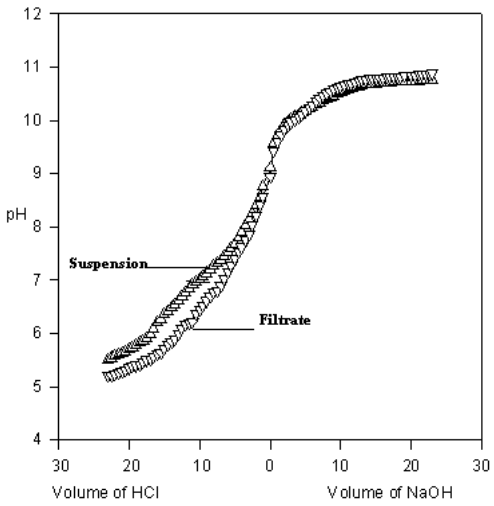

Figure 3.1.5.3: pH metric titration curves for nano mixed (Fe-Ni-Si) oxide with 1.10×10^{-3} M NaCl.

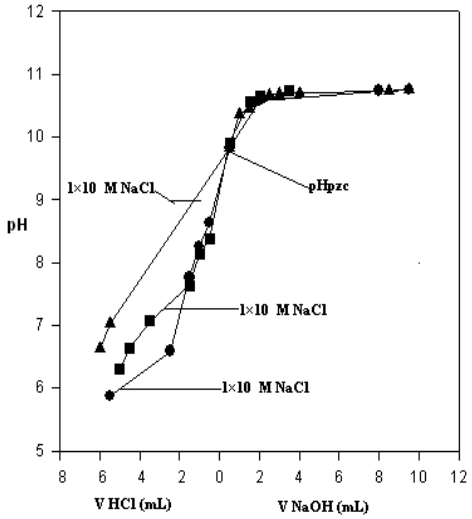

Figure 3.1.5.4: Net titration curves for nano mixed (Fe-Ni-Si) oxide in the presence of different concentrations of NaCl. These curves intersect at pHpzc.

Result: From figure 3.1.5.4, the point of zero charge of nano mixed (Fe-Ni-Si) oxide was found to be 9.80.

3.2 Removal of organic dyes (MB and OG) using batch experiment

The comparative studies of the removal capacity of the dyes between the multi-component (Fe-Ni-Si) and single oxide nanoparticle surface were employed by batch experiment and the effect of concentration of dye, pH, temperature, mixed oxide doses, contact time using synthetic solution were also conducted onto multi-component (Fe-Ni-Si) adsorption by batch experiment. The catalytic property of multi-component (Fe-Ni-Si) oxide nanoparticle was examined.

3.2.1Comperative study of the removal of dyes between the multi-component (Fe-Ni-Si) and single oxide nanoparticle surface

Table 3.2.1.1: Comparative study of the removal capacity of MB dye between multi-component (Fe-Ni-Si) and single oxide nanoparticle surface

Temperature: 34°C Shaking Time: 15 min

Shaking Speed: 4.5 rpm Volume of the MB solution: 50mL

Amount of Adsorbent: 0.05g Centrifuge Time: 10 min (2500 rpm)

Run No	Oxide Surface	Initial conc. of MB×10^5 q_0 ($molL^{-1}$)	Abs.	Equilibrium conc. of MB×10^5 q_e ($molL^{-1}$)	Adsorbed conc. of MB×10^5 q_m ($molL^{-1}$)	Amount Adsorbed of MB×10^5 q_m/m ($molg^{-1}$)
1	Mixed (Fe-Ni-Si) oxide	3.2	0.736	1.0	2.2	2.2
2	Silicon oxide	3.2	1.936	2.6	0.6	0.6
3	Iron Oxide	3.2	2.228	3.0	0.2	0.2
4	Nickel Oxide	3.2	2.358	3.1	0.1	0.1

Table 3.2.1.2: Comparative study of the removal capacity of OG dye between multi-component (Fe-Ni-Si) and single oxide nanoparticle surface

Temperature: 34°C Shaking Time: 15 min

Shaking Speed: 4.5 rpm Amount of Adsorbent: 0.05g

Volume of the MB solution: 50mL Centrifuge Time: 10 min (2500 rpm)

Run No	Oxide Surface	Initial conc. of OG×10^5 q_0 ($molL^{-1}$)	Abs.	Equilibrium conc. of OG×10^5 q_e ($molL^{-1}$)	Adsorbed conc. of OG×10^5 q_m ($molL^{-1}$)	Amount Adsorbed of OG×10^5 q_m/m ($molg^{-1}$)
1	Mixed (Fe-Ni-Si) oxide	5.10	0.531	3.80	1.30	1.30
2	Silicon oxide	5.10	0.598	4.30	0.80	0.80
3	Iron Oxide	5.10	0.685	4.90	0.20	0.20
4	Nickel Oxide	5.10	0.69	4.95	0.15	0.15

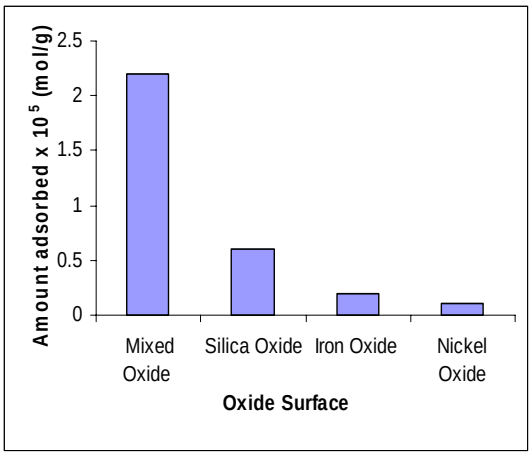

Figure 3.2.1.1: Amount adsorbed of MB dye by different oxide

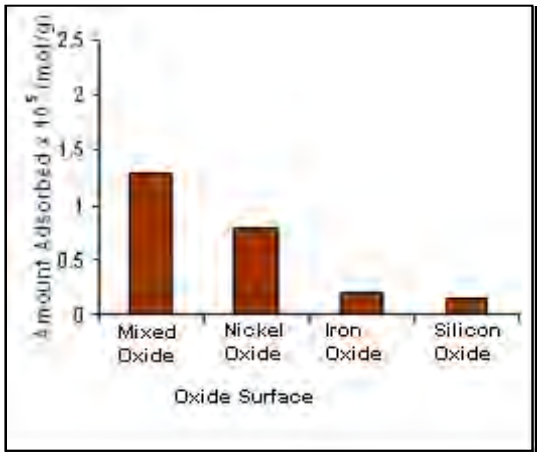

Figure 3.2.1.2: Amount adsorbed of OG dye by different oxide

In figure 3.21.1 and 3.2.1.2, it has been observed that multi-component (Fe-Ni-Si) oxide nanoparticle was showed the highest removal capacity both cationic (MB) and anionic (OG) dye from its single oxide. It was effective

adsorbent for both anionic and cationic dye. The details adsorption properties of multi-component (Fe-Ni-Si) oxide nanoparticle would be successfully characterized in this research work.

3.2.2 Effect of pH on MB and OG uptake

Table 3.2.2.1: Data for the pH on adsorption behavior of MB by nano mixed (Fe-Ni-Si) oxide adsorbent.

Reference: Water — Amount of mixed oxide: 0.05g

λ_{max} for MB solution: 664nm — Temperature: 32°C

Volume of the solution: 50mL — Shaking time: 15 min

Molar adsorption co-efficient: 74246 $Lmol^{-1}cm^{-1}$

Run No	Initial conc. of MB×10^5 q_0 ($molL^{-1}$)	pH	Abs	Equilibrium conc. of MB×10^5 q_e ($molL^{-1}$)	Adsorbed conc. of MB×10^5 q_m ($molL^{-1}$)	Amount Adsorbed of MB×10^5 q_m/m ($molg^{-1}$)
1	4.50	5.35	0.48	0.65	3.85	3.85
2	4.50	6.92	0.36	0.48	4.02	4.02
3	4.50	9.24	0.43	0.58	3.92	3.92

Table 3.2.2.2: Data for the pH on adsorption behavior of OG by Nano Mixed (Fe-Ni-Si) Oxide adsorbent.

Reference: Water Amount of mixed oxide: 0.05g

λ_{max} for OG solution: 477nm Temperature: 32°C

Volume of the solution: 50mL Shaking time: 15 min

Molar adsorption co-efficient: 13920 $Lmol^{-1}cm^{-1}$

Run No	Initial Conc. of OG×10^5 q_0 ($molL^{-1}$)	pH	Abs.	Equilibrium Conc. of OG ×10^5 q_m ($molL^{-1}$)	Adsorbed Conc. of OG×10^5 q_m ($molL^{-1}$)	Amount Adsorbed of OG×10^5 q_m/m ($molg^{-1}$)
1	5.00	4.95	0.44	3.16	1.84	1.84
2	5.00	6.55	0.41	2.95	2.05	2.05
3	5.00	8.75	0.49	3.12	1.48	1.48

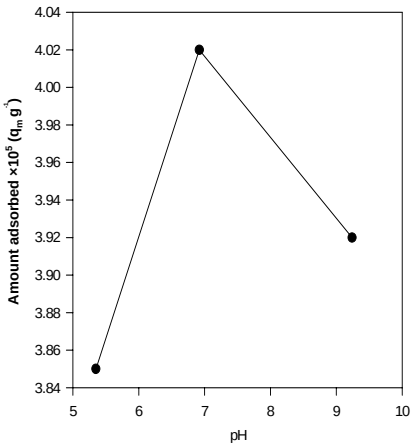

Figure 3.2.2.1: Effect of pH of MB adsorption

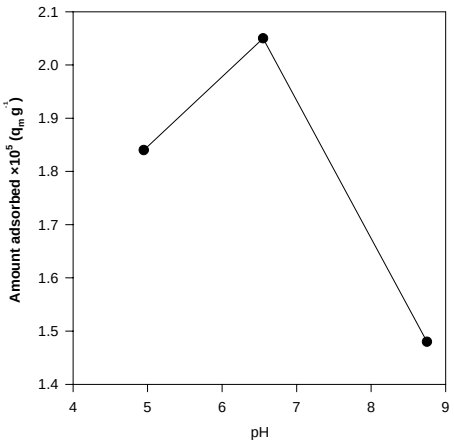

Figure 3.2.2.2: Effect of pH of OG adsorption

The pH of the system exerts profound influence on the adsorptive uptake of adsorbate molecules presumably due to its influence on the surface properties of the adsorbent and ionization or dissociation on the adsorbate molecule. Despite of the importance of pH, pH control is not easily maintained. Figure 3.2.2.1-2 shows the variations on the removal of dyes from synthetic solution at different pH. From the figure it is evident that the amount of adsorbed MB and OG dye per gram adsobent is the highest at neutral pH. The amount of adsorbed of cationic dye (MB) per gram adsorbent is low in acidic condition. On the other hand, the lower amount adsorbed of anionic dye (OG) is observed in basic condition. This indicates the strong force of interaction between the dyes and mixed (Fe-Ni-Si) oxide that, either H^+ or OH^- ions could influence the adsorption capacity [118].

3.2.3 Effect of contact time and kinetic study

Table 3.2.3.1: Data for the contact time on adsorption behavior of MB by nano mixed (Fe-Ni-Si) oxide adsorbent.

Reference: Water — Amount of mixed oxide: 0.05g

λ_{max} for MB solution: 664nm — Temperature: 31°C

Volume of the solution: 50mL — pH: 6.92

Run No	Initial conc. of MB×10^5 q_0(molL^{-1})	Time t (min)	Abs.	Equilibrium conc. of MB ×10^5 q_e (molL^{-1})	Adsorbed conc. of MB×10^5 q_m(molL^{-1})	Amount Adsorbed of MB×10^5 q_m/m (molg^{-1})
1	5.00	15	0.784	1.05	3.95	3.95
2	5.00	30	0.373	0.50	4.50	4.50
3	5.00	60	0.273	0.37	4.63	4.63
4	5.00	90	0.182	0.25	4.75	4.75
5	5.00	120	0.180	0.23	4.77	4.77

Table 3.2.3.2: Data for the contact time on adsorption behavior of OG by nano mixed (Fe-Ni-Si) oxide adsorbent.

Reference: Water | Amount of mixed oxide: 0.05g

λ_{max} for OG solution: 477nm | Temperature: 31°C

Volume of the solution: 50mL | pH: 6.55

Run No	Initial conc. of OG×10^5 q_0 ($molL^{-1}$)	Time (min)	Abs.	Equilibrium conc. of OG ×10^5 q_e ($molL^{-1}$)	Adsorbed conc. of OG ×10^5 q_m ($molL^{-1}$)	Amount Adsorbed of OG ×10^5 q_m/m ($molg^{-1}$)
1	5.00	15	0.531	3.81	1.19	1.19
2	5.00	30	0.461	3.31	1.69	1.69
3	5.00	60	0.436	3.13	1.87	1.87
4	5.00	90	0.415	2.99	2.01	2.01
5	5.00	120	0.41	2.94	2.06	2.06

Kinetic models applied to the adsorption MB and OG onto nano mixed (Fe-Ni-Si) oxide

Several steps can be used to examine the controlling mechanism of adsorption process such as chemical reaction, diffusion control and mass transfer, kinetic data are used to test experimental data from the adsorption of MB and OG onto nano mixed (Fe-Ni-Si) oxide is required for selecting optimum operating conditions for the full-scale batch process. The kinetic parameters, which are helpful for the prediction of adsorption rate, give information designing and modeling the adsorption process. Thus the kinetics of MB and OG adsorption onto Nano Mixed (Fe-Ni-Si) oxide were analysis using pseudo-first order [40], pseudo-second order [42], intraparticle diffusion [46] kinetic models. The conformity between experimental data and model predicted values was expressed by the co-relation coefficients (r^2, values

closed to equal to 1). The relative higher values are the applicable model to the kinetics of dye adsorption onto mixed (Fe-Ni-Si) oxide. The required derived data for these kinetics models is listed below in Table 3.2.3.3.

Table 3.2.3.3: Derived data for various kinetic model of adsorption of MB and OG onto Fe-Ni-Si mixed oxide.

Dye	Time (min)	$t^{1/2}$	Adsobed amount at time (t) $\times 10^5$ q_t (molg^{-1})	Amount adsobed at equilibrium at time (et) $\times 10^5$ q_z (molg^{-1})	$\ln(q_{et} - q_t)$ $\times 10^5$	$t/q_t \times 10^{-5}$
MB	15	3.87	3.95	4.77	-11.71	3.80
	30	5.48	4.50		-12.82	6.67
	60	7.75	4.63		-13.47	12.91
	90	9.49	4.75		-15.42	18.94
	120	10.45	4.77		-	25.15
OG	15	3.87	1.19	2.06	-11.65	12.6
	30	5.48	1.69		-12.51	17.8
	60	7.75	1.87		-13.17	32.1
	90	9.49	2.01		-14.51	44.8
	120	10.45	2.06		-	58.3

Pseudo-first- Order equation

The adsorption kinetic data (Table 3.2.3.3) were described by the Lagergren pseudo-first- Order model [9], which is the earliest known equation describing the adsorption rate based on the adsorption capacity. The first order rate equation is generally express as follows:

$$\ln (q_{et}-q_t) = \ln q_{et} - k_1 t \qquad (1)$$

Where q_{et} and q_t are the adsorption capacity at equilibrium and at time t, respectively ($molg^{-1}$), k_1 is rate constant of pseudo-first- order adsorption ($Lmol^{-1}$).

In order to obtain the rate constants, the values of $\ln(q_{et}-q_t)$ were linearly correlated with t by plot of $\ln(q_{et}-q_t)$ versus t to give a linear relationship from k_1 and predicted qet can be determined from the slope and intercept of the plot, respectively [Figure 3.2.3.1-2(a)]. The variation in rate should be proportional to the first power and concentration for strict surface adsorption. However, the relationship between initial solute concentration and rate of adsorption will not be linear when pore diffusion limits the adsorption process.

Figure 3.2.3.1-2 (b) shows that the pseudo-first-order equation fits well for the first 30 min both MB and OG adsorption process and thereafter the data deviate from theory. Thus, the model represents the initial stages where rapid adsorption occurs well but cannot be applied for the entire adsorption process. Furthermore, the correlation co-efficient r^2 are relatively low (Table 3.2.3.3). This shows that the adsorption of MB and OG onto Nano Mixed (Fe-Ni-Si) oxide cannot be applied and the reaction mechanism is not a first order reaction.

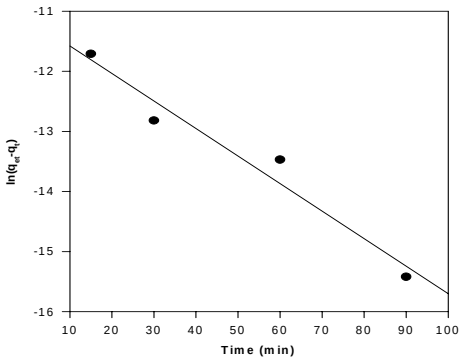

(a)

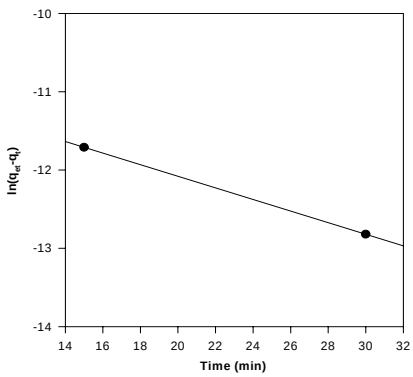

(b)

Figure 3.2.3.1: Pseudo first order kinetics for MB adsorption onto nano mixed oxide **(a)** entire process **(b)** first 30 min

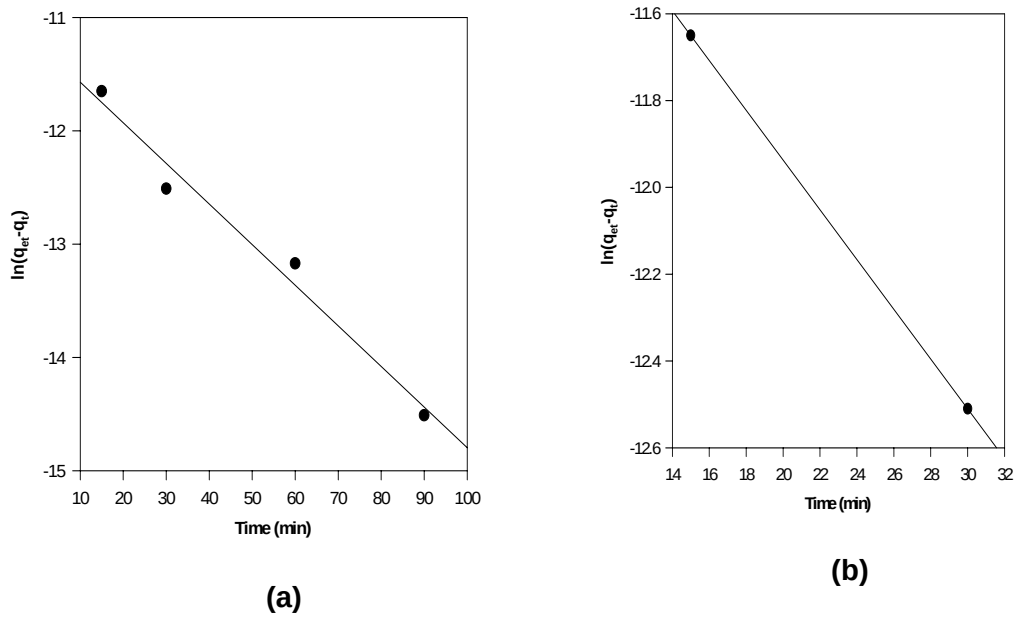

Figure 3.2.3.2: Pseudo first order kinetics for OG adsorption onto nano mixed oxide **(a)** entire process **(b)** first 30 min

Table 3.2.3.4: Comparison of the first and second order constants and calculated and experimental q_{et} values for MB and OG adsorption process onto nano mixed (Fe-Ni-Si) oxide.

Parameter→ Dye ↓	Experimental $\times 10^5$ q_{et} (mol g^{-1})	Pseudo-first-order kinetic model (Calculated)			Pseudo-second-order kinetic model (Calculated)		
		$k_1 \times 10^2$	$q_{et} \times 10^5$ (mol g^{-1})	r^2	$k_2 \times 10^2$	$q_{et} \times 10^5$ (mol g^{-1})	r^2
MB	4.77	4.5	1.48	0.95	30.9	4.9	0.99
OG	2.06	3.0	1.35	0.96	8.0	2.27	0.99

Pseudo-second-order equation

The adsorption kinetic may be described by the pseudo-second-order model [10]. The equation is generally given as follows:

$$\frac{t}{q_t} = \frac{1}{kq^2{}_e} + \frac{1}{q_e}t \qquad (2)$$

Where, k_2 [g (mol min)$^{-1}$] is the pseudo-second-order rate constant of adsorption.

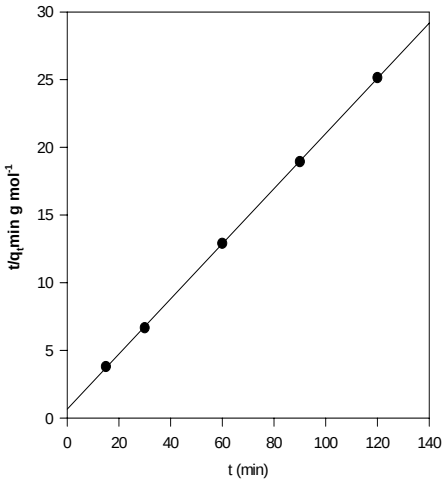

Figure 3.2.3.3: A plot of pseudo-second- order- Kinetics of MB adsorption

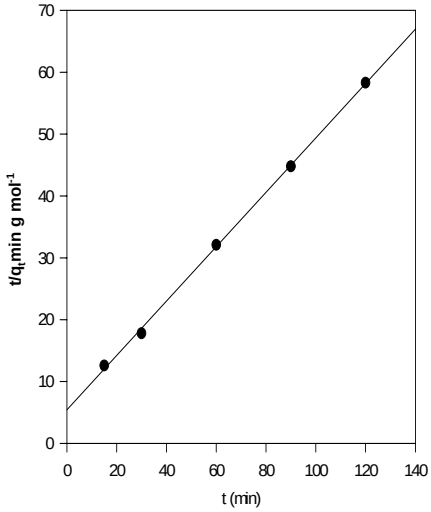

Figure 3.2.3.4: A plot of pseudo-second- order- Kinetics of OG adsorption

If the pseudo-second-order kinetics [42] is applicable, then the plot of t/q_t versus t should show a linear relationship values of k_2 and equilibrium adsorption capacity q_{et} were calculated from the intercept and slope of the plots of q_t versus t (Figure 3.2.3.3-4). The linear plots of t/q_t versus t show good agreement between experimental and calculated q_{et} values at MB and OG adsorption onto Mixed (Fi-Ni-Si) oxide. The correlation coefficient for the pseudo-second-order kinetic model are very close to 1 that is 0.999 which led to believe that the pseudo-second-order kinetic model provided good

correlation for the adsorption of MB and OG onto nano mixed (Fe-Ni-Si) oxide.

The Intra-particle diffusion model

The adsorbate species are most probably transported from the bulk of the solution into the solid phase through intraparticle diffusion or transport process [64], which is often the rate limiting step in many adsorption processes, especially in a rapidly stirred batch reactor. Since the dyes are probably transported from its aqueous solution to the nano mixed (Fe-Ni-Si) oxide by intraparticle diffusion, so the intraparticle diffusion is another kinetic model should be used to study the rate of dye adsorption onto mixed (Fe-Ni-Si) oxide. The possibility of intraparticle diffusion was explored by using the intraparticle diffusion model, which is commonly expressed by the following equation:

$$q_t = k_{id}\ t^{1/2} + C \qquad (3)$$

Where, C (mol g^{-1}) is the intercept and k_{diff} rate constant (mol $g^{-1}min^{1/2}$).

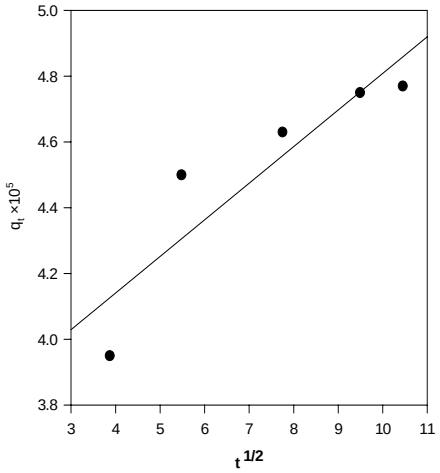

Figure 3.2.3.5: A plot of intraparticle diffusion model for MB

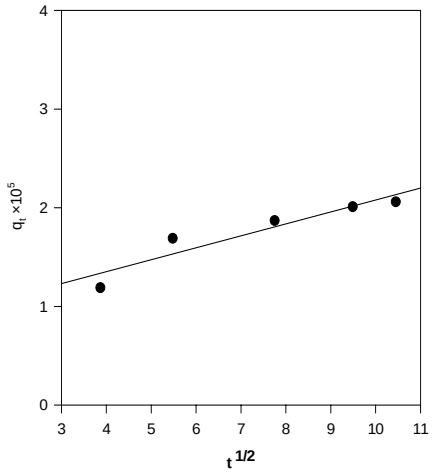

Figure 3.2.3.6: A plot of intraparticle diffusion model for OG

Table 3.2.3.5: The parameter obtained from intraparticle diffusion mode for MB and OG.

Dye	Parameter of intraparticle diffusion		
	k_{diff} (mol $g^{-1}min^{1/2}$)	C (mol g^{-1})	r^2
MB	1.11	3.70	0.87
OG	1.20	8.67	0.90

The values of q_t were found to be linearly correlated with values of $t^{1/2}$ and rate constant k_{diff} directly evaluated from the slope of the regression line (Figure 3.2.3.5-6). The values of intercept C (Figure 3.2.3.5-6) provide information about thickness of the boundary layer, the resistance to the external mass transfer increase as the intercept increase. The r^2 values given in Table 3.2.3.5 are close to unity (0.87 and 0.9) indicating the application of this model. This may confirm that the rate limiting step may thebe intraparticle diffusion process [38]. The linearity of the plots demonstrated the intraparticle diffusion played a significant role is the uptake of the adsorbent by adsorbent.

3.2.4 Effect of temperature and Thermodynamic study

Table 3.2.4.1: Data for the contact time on adsorption behavior of MB by nano mixed (Fe-Ni-Si) oxide adsorbent.

Reference: Water — Amount of mixed oxide: 0.02g

λ_{max} for MB solution: 664nm — Contact time: 120 min

Volume of the solution: 50mL — pH: 6.92

Run No	Initial conc. of MB×10^5 q_0 ($molL^{-1}$)	Temp. T (K)	Abs.	Equilibrium conc. of MB ×10^5 q_e ($molL^{-1}$)	Adsorbed conc. of MB×10^5 q_m ($molL^{-1}$)	Amount Adsorbed of MB×10^5 q_m/m ($molg^{-1}$)
1	5.00	303	2.29	3.09	1.91	4.78
2	5.00	318	2.04	2.78	2.22	5.55
3	5.00	333	1.86	2.51	2.49	6.22
4	5.00	348	1.70	2.29	2.71	6.78
5	5.00	363	1.58	2.13	2.87	7.18

Based on fundamental thermodynamics concept, it is assumed that in an isolated system, energy cannot be gained or lost and entropy change is the only driving force. In environmental engineering practice, both energy and entropy factors must be considered in order to determine which process will occur spontaneously. ΔG^o, is the fundamental criterion of spontaneity. Reaction occurs spontaneously at a given temperature if ΔG^o is a negative quantity. The adsorption equilibrium partition constant k_d is calculated as follows:

$$k_d = \frac{q_m}{q_e} \qquad (1)$$

where, q_m is amount adsorbed (mol g^{-1}) of dye onto adsorbent and q_e is the equilibrium concentration (mol L^{-1}).

Table 3.2.4.2: Data for the contact time on adsorption behavior of OG by nano mixed (Fe-Ni-Si) oxide adsorbent.

Reference: Water | Amount of mixed oxide: 0.05g

λ_{max} for OG solution: 477nm | Contact time: 120 min

Volume of the solution: 50mL | pH: 6.55

Run No	Initial conc. of OG×10^{-5} q_0 ($molL^{-1}$)	Timp. (K)	Abs.	Equilibrium conc. of OG ×10^{-5} q_e ($molL^{-1}$)	Adsorbed conc. of OG ×10^{-5} q_m ($molL^{-1}$)	Amount Adsorbed of OG ×10^{-5} q_m/m ($molg^{-1}$)
1	3.00	303	0.131	0.94	2.06	2.06
2	3.00	318	0.146	1.05	1.95	1.95
3	3.00	333	0.173	1.24	1.76	1.76
4	3.00	348	0.200	1.44	1.56	1.56
5	3.00	363	0.206	1.48	1.52	1.52

The free energy of the adsorption reaction, considering the adsorption equilibrium partition constant, k_d, is given by the following equation:

$$\Delta G^o = -RT\ln k_d \qquad (2)$$

Where, ΔG^o is the standard free energy change ($Jmol^{-1}$ or $KJmol^{-1}$); R is the universal gas constant, 8.314 $JK^{-1}mol^{-1}$ and T is the absolute temperature (K).

The Gibbs free energy change, ΔG^o, can be represented as follows:

$$\Delta G^o = \Delta H^o - T\,\Delta S^o \qquad (3)$$

A plot of ΔG^o versus T will be linear. Enthalpy change ΔH^o, and entropy change, ΔS^o, were determined from the slope and intercept of plots.

Table 3.2.4.3: Derived data for various thermodynamic parameters for MB and OG onto nano mixed (Fe-Ni-Si) oxide.

Dye	Temp. T(K)	$\frac{1}{T}\times10^{-3}$	Amount Adsorbed $\times10^{-5}$ $q_m/_m$ (molg^{-1})	Equilibrium conc. $\times10^{-5}$ q_e (molL^{-1})	k_d	lnk_d	ΔG^o (KJmol^{-1})
MB	303	3.30	4.78	3.09	1.55	0.44	-1.2
	318	3.14	5.55	2.78	1.99	0.69	-1.8
	333	3.00	6.22	2.51	2.47	0.90	-2.5
	348	2.87	6.78	2.29	2.96	1.09	-3.1
	363	2.75	7.18	2.13	3.37	1.21	-3.7
OG	303	3.30	2.06	0.94	2.19	0.78	-1.96
	318	3.14	1.95	1.05	1.86	0.62	-1.63
	333	3.00	1.76	1.24	1.41	0.34	-0.94
	348	2.87	1.56	1.44	1.08	0.08	-0.23
	363	2.75	1.52	1.48	1.03	0.03	-0.09

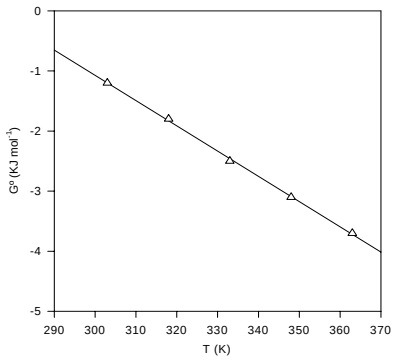

Figure 3.2.4.1: Relationship between Gibbs free energy change (ΔG^o) and temperature of adsorption of MB

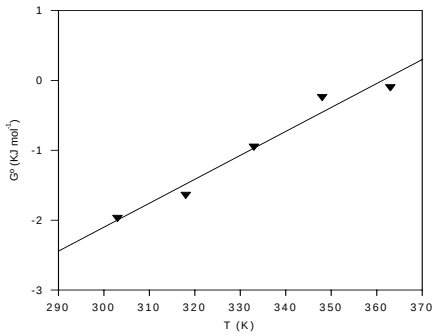

Figure 3.2.4.2: Relationship between Gibbs free energy change (ΔG^o) and temperature of adsorption of OG

Table 3.2.4.4: Obtained thermodynamic parameters from graph

Dye	ΔH^o (kJ mol^{-1})	ΔS^o (J $mol^{-1}K^{-1}$)	r^2
MB	11.26	-0.042	0.99
OG	-12.38	0.034	0.97

Thermodynamic discussion of MB

Thermodynamic parameter s for MB adsorption the values for the adsorption equilibrium constant, k_a, increased with increasing temperature. The thermodynamic parameter Gibbs free energy change, ΔG^o, confirms the feasibility of the process and spontaneous nature of the adsorption of MB. The value ΔH^o and ΔS^o are 11.255 kJ mol^{-1} and -0.042J$mol^{-1}K^{-1}$. The positive value of ΔH^o confirms that the adsorption process is endothermic in nature. The adsorption energy lies well within the range of 8-16 kJ mol^{-1} which is the adsorption energy for ion exchange process [10]. The negative values of ΔS^o reflect the affinity of the adsorbent towards MB which increase the order of the adsorbate after adsorption [50].

Thermodynamic discussion of OG

The values for the adsorption equilibrium constant, K_a, decreased with increasing temperature. The thermodynamic parameter Gibbs free energy change, ΔG^o, for the adsorption processes are shown in Table 3.2.4.3. The negative values of ΔG^o confirm the feasibility of the process and the spontaneous nature of the adsorption. The values of ΔG^o were found to decrease from -1.96 to -0.09 kJ mol^{-1}as the temperature increases from 303 to 363 K and the low values for ΔG^o indicate that a spontaneous physisorption process occurred [10]. Some researchers have also obtained similar results for ΔG^o in the adsorption of anionic dyes on other adsorbents. For example, the sorption of Acid Orange 7 onto spent brewery grains had ΔG^o =-22.8 kJ mol^{-1} [50] and sorption of Acid Blue 193 onto Naebentonite

had ΔG^{o} =-0.36 kJ mol^{-1}[119]. The values of ΔH^{o} and ΔS^{o} calculated from the plot of Gibbs free energy change, ΔG^{o}, versus absolute temperature (Figure 3.2.4.2) are given as -12.38 kJ mol^{-1} and -0.034 J $mol^{-1}K^{-1}$, respectively. The enthalpy change is negative implying that the sorption process is exothermic. Enthalpy change due to chemisorptions takes value between 40-120 kJ/mol, which is larger than that due to physiadsorption [120]. Therefore, the adsorption of the anionic dye under examination onto palm kernel fiber is likely due to physiadsorption. This result shows that the interaction between the anionic dye and the mixed oxide is mainly electrostatic. The heat of physiadsorption involves only relatively weak electrostatic interactions [121]. Generally, adsorption of dye is currently described as an exothermic process [122].

3.2.5 Effect of concentration of dye and isotherm study

Table 3.2.5.1: Data for the concentration of dye on adsorption behavior of MB by nano mixed (Fe-Ni-Si) oxide adsorbent.

Reference: Water | Amount of mixed oxide: 0.01g

λ_{max} for MB solution: 664nm | Contact time: 120 min

Volume of the solution: 50mL | pH: 6.92

Run No	Initial conc. of MB×10^6 q_0(molL^{-1})	Abs.	Equilibrium conc. of MB ×10^6 q_e (molL^{-1})	Adsorbed conc. of MB×10^6 q_m (molL^{-1})	Amount Adsorbed of MB×10^5 q_m/m (molg^{-1})
1	10.00	0.111	1.50	8.50	42.50
2	12.00	0.178	2.40	9.60	48.50
3	14.00	0.193	2.90	11.10	55.50
4	16.00	0.267	3.60	13.40	67.00
5	18.00	0.297	4.00	14.00	70.00
6	20.00	0.349	4.70	15.30	76.50
7	22.00	0.453	6.10	15.90	79.50
8	24.00	0.587	7.90	16.10	80.50
9	26.00	0.731	9.85	16.15	80.750

Isotherm data analysis

The parameters obtained from the different models provide important information on the adsorption mechanism and the surface properties and affinities of the adsorbent. The most widely accepted surface adsorption models for single solute systems are the Langmuir and Freundlich models. The correlation with the amount of adsorption and the liquid-phase concentration was tested with the Langmuir, Freundlich isotherm equations. Linear regression is frequently used to determine the best-fitting isotherm, and the applicability of isotherm equations is compared by judging the correlation coefficients.

Langmuir isotherm

The theoretical Langmuir isotherm is valid for adsorption of a solute from a liquid solution as monolayer adsorption on a surface containing a finite number of identical sites. Langmuir isotherm model assumes uniform energies of adsorption onto the surface without transmigration of adsorbate in the plane of surface [123]. Therefore, the Langmuir isotherm model was chosen for estimation of the maximum adsorption capacity corresponding to complete monolayer coverage on the adsorbent surface. The linear form of Langmuir equation is commonly expressed as followed:

$$\frac{q_e}{q_{m/m}} = \frac{1}{k_a} \times \frac{1}{Q_m} + \frac{1}{Q_m} \times q_e \qquad (1)$$

In equation (1), q_e is the equilibrium concentration (molLl^{-1}); q_m /m is the Amount adsorbed (mol g^{-1}); Q_m is a constant and reflects a complete monolayer (mol g^{-1}), k_a is a adsorption equilibrium constant (L mol^{-1}) that is related to the apparent energy of adsorption. A plot of $\frac{q_e}{q_m}$ versus q_e should indicate a straight line slope of $\frac{1}{Q_m}$ and intercept $\frac{1}{k_a} \times \frac{1}{Q_m}$.

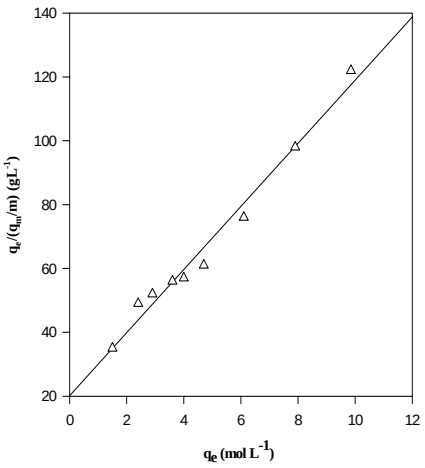

Figure 3.2.5.1: Langmuir plot of $q_e/(q_m/m)$ vs q_e

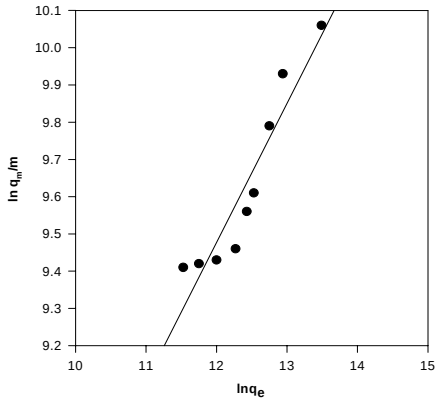

Figure 3.2.5.2: Freundlich isotherm for the adsorption MB by mixed (Fe-Ni-Si) oxide

The results obtained from the Langmuir model for the removal of MB onto nano mixed (Fe-Ni-Si) oxide are shown in Table 3.2.5.2. The correlation coefficients reported in Table 3.2.5.2 showed strong positive evidence on the adsorption of dyes onto nano mixed (Fe-Ni-Si) oxide follows the Langmuir isotherm. The applicability of the linear form of Langmuir model to nano mixed (Fe-Ni-Si) oxide was proved by the high correlation coefficients r^2 = 0.98. This suggests that the Langmuir isotherm provides a good model of the adsorption system. The maximum monolayer capacity Q_m obtained from the Langmuir is 1×10^{-4} mol g^{-1} for MB.

Table 3.2.5.2: Comparison of the coefficients isotherm parameters for MB adsorption onto nano mixed (Fe-Ni-Si) oxide

Langmuir isotherm model			Freundlich isotherm model		
Q_m	k_a	r^2	n	k_F	r^2
(mol g^{-1})	(Lmol^{-1})			(mol g^{-1})	
1×10^{-4}	4.9×10^{5}	0.98	0.373	1.61	0.88

The Freundlich isotherm

The Freundlich isotherm model [124] is the earliest known equation describing the adsorption process. It is an empirical equation and can be used for non-ideal sorption that involves heterogeneous adsorption. The Freundlich isotherm can be derived assuming a logarithmic decrease in the enthalpy of adsorption with the increase in the fraction of occupied sites and is commonly given by the following linear equation:

$$\ln \frac{q_m}{m} = \ln k_F + \frac{1}{n} \ln q_e \qquad (2)$$

where, K_F is a constant for the system, related to the bonding energy. K_F can be defined as the adsorption or distribution coefficient and represents the quantity of dye adsorbed onto adsorbent for unit equilibrium concentration.

1/*n* is indicating the adsorption intensity of dye onto the adsorbent or surface heterogeneity, becoming more heterogeneous as its value gets closer to zero. A value for 1/*n* below 1 indicates a normal Langmuir isotherm while 1/*n* above 1 is indicative of cooperative adsorption.

The applicability of the Freundlich adsorption isotherm was also analyzed, using the same set of experimental data, by plotting $\ln(q_m/m)$ versus $\log(q_e)$. The data obtained from linear Freundlich isotherm plot for the adsorption of the MB, onto nano mixed (Fe-Ni-Si) oxide is presented in Table 3.2.5.2. The correlation coefficients (r^2=0.88) showed that the Freundlich model is comparable to the Langmuir model. The 1/*n* is lower than 1.0, indicating that MB is favorably adsorbed by nano mixed (Fe-Ni-Si) oxide.

3.2.6 Effect of adsorption dose

Table 3.2.6.1: Data for the effect of adsorbent dose on adsorption behavior of MB by nano mixed (Fe-Ni-Si) oxide adsorbent.

Reference: Water — Time: 15 min

λ_{max} for MB solution: 664nm — Temperature: 31°C

Volume of the solution: 50mL — pH: 6.92

Run No	Initial conc. of MB×10^5 q_0 ($molL^{-1}$)	Dose (g)	Abs.	Equilibrium conc. of MB ×10^5 q_m($molL^{-1}$)	Adsorbed conc. of MB×10^5 (q_0- q_m) ($molL^{-1}$)	Amount Adsorbed of MB×10^5 q_m /m ($molg^{-1}$)	% of MB removal
1	4.50	0.05	0.518	0.70	3.80	3.80	84.40
2	4.50	0.10	0.307	0.41	4.09	2.05	90.90
3	4.50	0.15	0.236	0.32	4.18	1.39	92.90
4	4.50	0.20	0.208	0.28	4.22	1.06	93.80
5	4.50	0.25	0.192	0.26	4.24	0.85	94.20

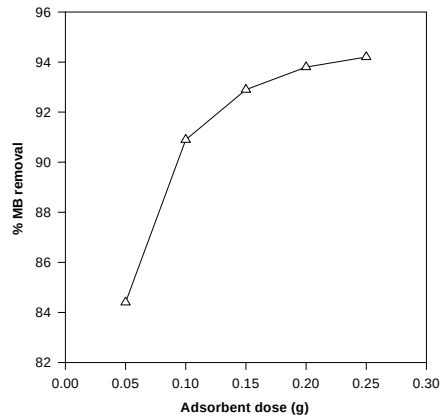

Figure 3.2.6.1: Effect of adsorbent dose on % of MB removal

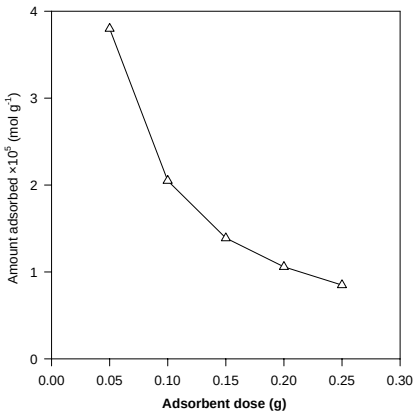

Figure 3.2.6.2: A plot for amount adsorbed per gram versus adsorbent dose

Table 3.2.6.2: Data for the effect of adsorbent dose on adsorption behavior of OG by nano mixed (Fe-Ni-Si) oxide adsorbent.

Reference: Water | Time: 15 min

λ_{max} for OG solution: 477nm | Temperature: 31°C

Volume of the solution: 50mL | pH: 6.55

Run No	Initial conc. of OG×10^5 q_0 ($molL^{-1}$)	Dose (g)	Abs.	Equilibrium conc. of OG ×10^5 q_e ($molL^{-1}$)	Adsorbed conc. of OG ×10^5 q_m ($molL^{-1}$)	Amount adsorbed of OG ×10^5 q_m/m ($molg^{-1}$)	% of OG removal
1	5.00	0.05	0.531	3.81	1.19	1.19	23.80
2	5.00	0.10	0.381	2.74	2.26	1.13	45.20
3	5.00	0.15	0.346	2.48	2.52	0.84	49.60
4	5.00	0.20	0.321	2.31	2.69	0.67	53.80
5	5.00	0.25	0.310	2.23	2.73	0.55	54.60

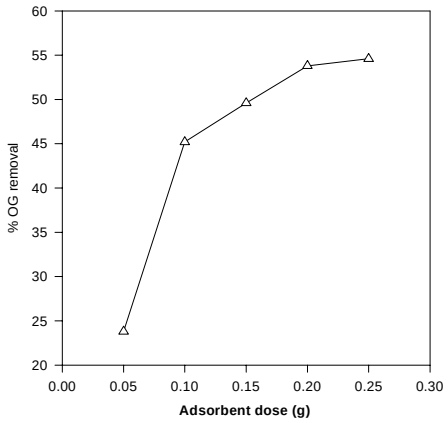

Figure 3.2.6.3: Effect of adsorbent dose on % of OG removal

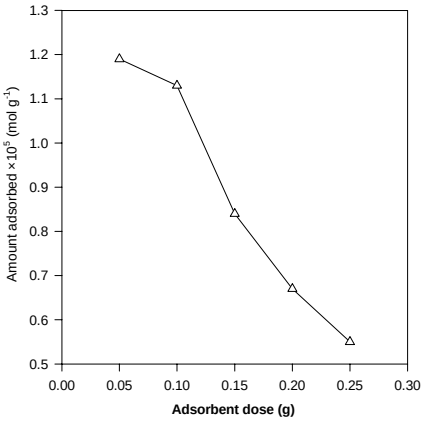

Figure 3.2.6.4: A plot for amount adsorbed per gram versus adsorbent dose

The dependence of MB and OG adsorption on adsorbent dose with varying amounts of nano mixed (Fe-Ni-Si) oxide has been examined and details are presented in Figure 4.2.6.14. It is found that (Figure 4.2.6.1 and 4.2.6.3) both MB and OG removal by adsorbents depends strongly on the adsorbent dose, indicating that adsorption is dependent on the availability of the bonding sites [125].When the adsorbent dose of adsorbents was increased from 0.05 to 0.25 g/50mL the MB and OG binding capacity was increased dramatically. The capacity was further increased, but the magnitude of the increase is proportionally less significant with each successive increase. It is postulated that at low adsorbent doses all types of sites are entirely exposed for adsorption, and the surface may become saturated faster; whereas at higher adsorbent dosages the availability of higher energy sites may decrease [126]. However, when increase the amount of dose percent of removal of MB and OG increased but amount adsorbed per gram dye onto nano mixed (Fe-Ni-Si) oxide is decreased (Figure 4.2.6.2 and 4.2.6.4) which indicate optimization of adsorbent dose is necessary before adsorption because of effective use of synthesized nano particles.

3.2.7: Photodegradation Studies

Semiconductor mediated photodegradation is one of the efficient methods for the treatment of toxic and biologically persistent compounds [51-53] and another aim to use the prepared materials as photocatalysts. In some cases irradiated light can not degrade or remove the toxic substances directly. Photodegradation will be easier in the presence of photocatalyst. Recently metal oxide and mixed oxides have been used as catalysts for photolysis widely [54]. Nano mixed (Fe-Ni-Si) oxide has been used to remove dyes from solution. Experimental setup for photodegradation was described in section 2.5. The photodegradation of MB and OG solution in the presence of mano mixed (Fe-Ni-Si) oxide suspension has been studies below.

Table 3.2.7.1: Data for photodegradation of MB in the presence nano mixed (Fe-Ni-Si) oxide suspension at different time intervals with irradiation of UV light.

Reference: Water — Amount of mixed oxide: 0.05g

λ_{max} for MB solution: 664nm — pH: 6.92

Volume of the solution: 50mL — Light source: UV

Run No	Initial conc. of MB×10^{-5} q_0 ($molL^{-1}$)	Time (min)	Abs.	Equilibrium conc. of MB ×10^{-5} q_m ($molL^{-1}$)	Adsorbed conc. of MB×10^{-5} (q_0- q_m) ($molL^{-1}$)	% of MB Removal
1	5.00	15	0.575	0.77	4.23	84.60
2	5.00	30	0.347	0.46	4.54	90.80
3	5.00	60	0.255	0.34	4.66	93.20
4	5.00	90	0.139	0.19	4.81	96.20
5	5.00	120	0.123	0.17	4.83	96.60

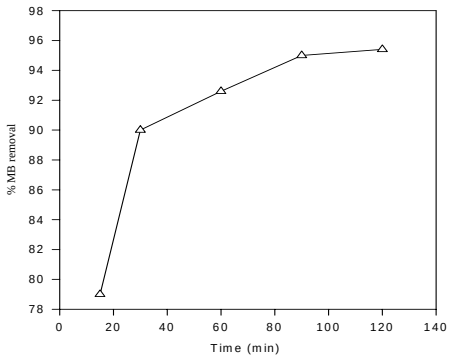

Figure 3.2.7.1: Photodegradation of MB on nano mixed (Fe-Ni-Si) oxide suspension at different time interval

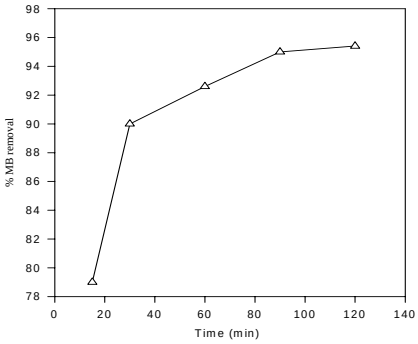

Figure 3.2.7.2: Removal of MB in the presence of nano mixed (Fe-Ni-Si) oxide suspension at different time interval without irradiation of light

Table 3.2.7.2: Data for removal of MB in the presence nano mixed (Fe-Ni-Si) oxide suspension at different time intervals without irradiation of light

Reference: Water

Amount of mixed oxide: 0.05g

λ_{max} for MB solution: 664nm

Temperature: 31°C

Volume of the solution: 50mL

pH: 6.92

Run No	Initial conc. of MB×10^{-5} q_0 ($molL^{-1}$)	Time (min)	Abs.	Equilibrium conc. of MB ×10^{-5} q_e ($molL^{-1}$)	Adsorbed conc. of MB×10^{-5} q_m ($molL^{-1}$)	% of MB removal
1	5.00	15	0.784	1.05	3.95	79.00
2	5.00	30	0.373	0.50	4.50	90.00
3	5.00	60	0.273	0.37	4.63	92.60
4	5.00	90	0.182	0.25	4.75	95.00
5	5.00	120	0.180	0.23	4.77	95.40

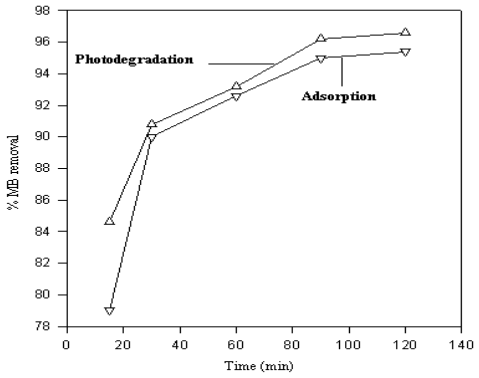

Figure 3.2.7.3: Comparison of adsorption and photodegradation for the removal of MB in the presence of mixed oxide suspension at pH 6.92

Table 3.2.7.3: Data for photodegradation of OG in the presence nano mixed (Fe-Ni-Si) oxide suspension at different time intervals with irradiation of UV light.

Reference: Water

Amount of mixed oxide: 0.05g

λ_{max} for MB solution: 477nm

Light source: UV

Volume of the solution: 50mL

pH: 6.55

Run No	Initial conc. of OG×10^5 q_0 ($molL^{-1}$)	Time (min)	Abs.	Equilibrium conc. of OG ×10^5 q_e ($molL^{-1}$)	Adsorbed conc. of OG×10^5 q_m ($molL^{-1}$)	% of OG Removal
1	5.00	15	0.478	3.43	1.57	31.40
2	5.00	30	0.432	3.10	1.90	38.00
3	5.00	60	0.405	2.91	2.09	41.80
4	5.00	90	0.382	2.74	2.26	45.20
5	5.00	120	0.379	2.72	2.28	45.60

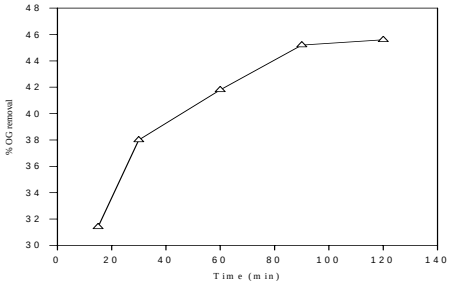

Figure 3.2.7.4: Photodegradation of OG on nano mixed (Fe-Ni-Si) oxide suspension at different time interval

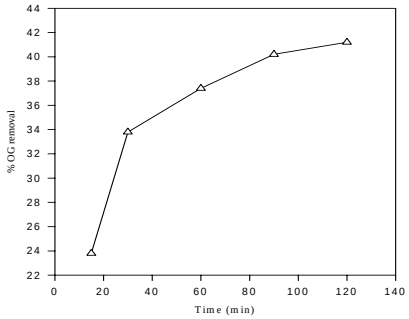

Figure 3.2.7.5: Removal of OG in the presence of nano mixed (Fe-Ni-Si) oxide suspension at different time interval without irradiation of light.

Table 3.2.7.4: Data for removal of OG in the presence of nano mixed (Fe-Ni-Si) oxide suspension at different time intervals without irradiation of light

Amount of mixed oxide: 0.05g Temperature: 31°C

Volume of the solution: 50mL pH: 6.55

Run No	Initial conc. of OG×10^{-5} q_0 ($molL^{-1}$)	Time (min)	Abs.	Equilibrium conc. of OG ×10^{-5} q_e ($molL^{-1}$)	Adsorbed conc. of OG×10^{-5} q_m ($molL^{-1}$)	% of OG removal
1	5.00	15	0.531	3.81	1.19	23.80
2	5.00	30	0.461	3.31	1.69	33.80
3	5.00	60	0.431	3.13	1.87	37.40
4	5.00	90	0.415	2.99	2.01	40.20
5	5.00	120	0.410	2.94	2.06	41.20

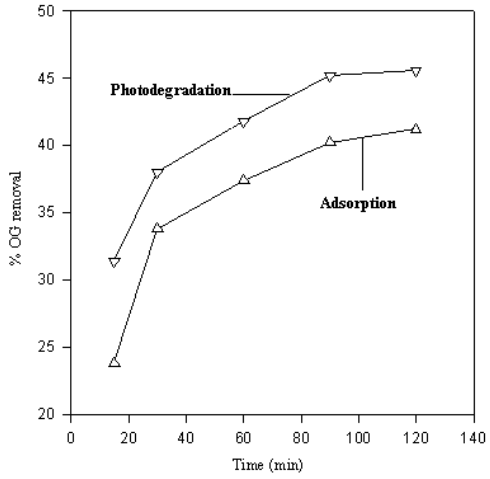

Figure 3.2.7.6: Comparison of adsorption and photodegradation for the removal of OG in the presence of mixed oxide suspension at pH 6.55

Chapter 4

CONCLUSION

5.0 Conclusion

Metal oxide nanoparticles constitute an outstanding class of functional materials with potential applications in all most all fields of technology. In the present study, iron-nickel-silicon mixed oxide nano surface was synthesized by sol-gel method. This method was used effectively to incorporate iron and nickel oxides into a silica gel network. Synthesized materials were characterized by Energy-dispersive X-ray spectroscopy (EDX), Scanning electron microscopy (SEM), and X-ray diffraction (XRD). EDX provided the information about chemical composition. The chemical composition obtained from EDX spectrum, it can be calculated that the prepared nano mixed (Fe-Ni-Si) oxide is $Fe_{0.78}$ $Ni_{0.76}$ $Si_{0.46}O_3$ and no other phases are present. In XRD analysis, the crystallite structure and particle size were found. The Miller Indice (h, k, l) lattice planes of iron, nickel and silicon oxide are present in mixed oxide with partial deviation of 2θ angle of the plane. The obtained average crystallite size of iron-nickel-silica mixed oxide is 18 nanometers. The particles were observed to be highly crystallite according to XRD analysis but from the SEM images a thin amorphous layer surroundings each particle was pragmatic.

Our synthesized multi-component (Fe-Ni-Si) nano oxides prepared via a sol-gel method exhibit high surface areas (78.30 m^2g^{-1}) with pHpzc (9.8) and hence have an advantage over conventional materials for potential application as adsorbent and catalyst. It is effective for both anionic and cataonic organic dyes. In this research work, it has been observed that multi-component (Fe-Ni-Si) oxide nanoparticle were showed higher removal capacity both cationic (MB) and anionic (OG) dyes from its single oxide. The details adsorption properties of multi-component (Fe-Ni-Si) oxide nanoparticle would be successfully characterized in this research work. Batch experiments experimented to remove organic anionic (OG) and cationic (MB) dyes from aqueous solution taking various parameters such as effect of pH, contact time, initial dye concentration, temperature and adsorbent dose.

Batch experiment study showed that adsorption of OG and MB was highly pH dependent. The maximum removal was observed of MB and OG around at pH 7. Batch kinetic studies were also performed to investigate the rate limiting of adsorption process. Results obtained revealed that adsorption of both OG and MB was rapid at the beginning approached equilibrium slowly. Experimental data can be modeled using pseudo-second-order kinetic model as first order kinetic model does not represent the whole range of adsorption process. Other than that, intraparticle diffusion was found to be prominent at a certain stage of adsorption but it would not be the only limiting step that controlled the adsorption dynamic.

The free energy, $\Delta G°$, was negative which proves that the adsorption was spontaneous. The enthalpy change, $\Delta H°$ was positive for MB and negative for OG which indicates that adsorption processes were endothermic and exothermic in nature respectively. Batch equilibrium (MB) data also had a good agreement with the Langmuir, Freundlich isotherm models with correlation coefficients > 0.9. Overall, the Langmuir isotherm showed the best fit for all adsorbents under investigation in terms of correlation coefficient as well as error analysis of the results. For all the systems in this study, the analysis of isotherm shape factor showed that adsorption was favorable. With the increase of adsorbent dose the percentage of dye removal was increased but amount adsorbed per gram was decreased. The catalytic activity of this mixed oxide was examined by photo degradation of MB and OG.

REFERENCE

References

1. Brinker, C.J. and Scherer, G.W., “Sol-Gel Science: The Physics and Chemistry of Sol-Gel Processing”, Academic, San Diego, 1990.

2. Maxim, N., Overweg, A., Kooyman, P.J., Van Wolput, J.H.M.C., Hanssen, R.W.J.M., Van Santen, R.A. and Abbenhuis, H.C.L., “Synthesis and Characterization of Microporous Fe−Si−O Materials with Tailored Iron Content from Silsesquioxane Precursors”, *J. Phys. Chem. B*., 2002, **106 (9)**, 2203.

3. Fabrizioli, P., Burgi, T. and Baiker, A., “Environmental Catalysis on Iron Oxide–Silica Aerogels: Selective Oxidation of NH_3 and Reduction of NO by NH_3”, *J. Catal*., 2002, **206**, 143.

4. http://en.wikipedia.org/wiki/Mixed_oxide

5. Pramanik, P., “Synthesis of Nano Particle of Inorganic Oxides by Polymer Matrix”, *J. Bull. Mater. Sci.,* 1995, **18(6)**, 819.

6. Bagheri-Mohagheghi, M.M., Shahtahmasebi, Mozafari, E. and Shokooh-Saremi, M., “Effect of the Synthesis Route on the Structural Properties and Shape of the Indium Oxide (In_2O_3) Nano-particles”, In Press, *J. Physica E.,* 2009.

7. Jayalakshmi, M., Venugopal, N., Raja, K.P. and Rao, M.M., “Nano SnO_2–Al_2O_3 Mixed Oxide and SnO_2–Al_2O_3–Carbon Composite Oxides as New and Novel Electrodes for Supercapacitor Applications”, *J. Power Sources*, 2006, **158**, 1538–1543.

8. El-Shobaky, H.G., “Surface and Calalytic Properties of Co, Ni and Cu Binary Oxide System”, *Appl. Catal., A*., 2004, **278(1),** 1-9.

9. Babu, K.S., Singh, D.and Srivastava, O.N., “Investigations on the Mixed Oxide Material TiO_2-In_2O_3 in Regard to Photocatalytic Hydrogen Production”, *Semicond. Sci. Technol.*, 1990, **5**, 364.

10. Chung, K. and Stevens, S., “Degradation of Azo Dyes by Environmental Microorganism and Helminthes”, *J. Environ. Toxicol. Chem.*, 1993, **54,** 435.

11. Chowdhury, A.-N., Rahim A., Ferdousi, Y.J., Azam, M.S. and Hossain, M.M., “Cobalt-Nickel Mixed Oxide Surface: A Promising Adsorbent for the Removal of PR Dye from Water”, *Appl. Surf. Sci.*, 2010, **256,** 3718-3724.

12. Nakamura, M., Saitoh, H., Maejima,Y., Yamagiwa,S. and Kaneko,S, *Fresenius Z Anal Chem,* 1989, **335**, 573 – 575.

13. Smart, L and Moore, E., *Solid State Chemistry*, Chapman and Hall, 1992, **126**, 53-54.

14. Samsonov, G. V., *The Oxide Handbook,* , Ed.; IFI / Plenum, New York,1982, **23**, 84-87.

15. Grant, F. A., *Riv. Modern Phys.*, 1959, **31**, 646.

16. Cronemeyer, D.C., *Phys. Rev.,* 1952, **87**, 876.

17. Bickley, R. I., *Chem. Phys. of Solids and Their Surface, 1978,* **7**, 118.

18. Salvador, P., *Solar Energy Matter*, 1982, **6**, 241.

19. Fahlman, B. D., *J. Materials Chemistry*, 2007, **1,** 282-283.

20. Okuhara, T., and Misono, M., *Oxide catalyst in Solid state Chemistry*, 1995, 2889-2902.

21. Greenwood, Norman N.; Earnshaw, A., *Chemistry of the Elements*, Oxford: Pergamon, 1984, 1336–37, ISBN 0-08-022057-6.

22. Lascelles, K., Morgan, L.G., Nicholls, D. and Beyersmann, D., *Nickel Compounds, Ullmann's Encyclopedia of Industrial Chemistry,* Wiley-VCH, Weinheim, 2005.

23. Pradyot, P., *Handbook of Inorganic Chemicals*, McGraw-Hill Publications, 2002, 183-185.

24. Greedon, J.E., *Magnetic oxides in Encyclopedia of Inorganic chemistry,* Ed. R. Bruce King, John Wiley & Sons, 1994, ISBN 0471936200

25. http://en.wikipedia.org/wiki/Iron(III)_oxide

26. Iler, R.K., *The Chemistry of Silica*, Plenum Press., 1979, ISBN 047102404X.

27. White, L. T., "Eilmer of Malmesbury, an Eleventh Century Aviator: A Case Study of Technological Innovation, Its Context and Tradition", *Technology and Culture* (Society for the History of Technology), 1961, **2 (2),** 97–111.

28. Wang, L. D., Major, P., Paga, P., Zhang, D., Norton, M.G. and McIlroy,D. N., "High yield synthesis and lithography of silica-based nanospring mats", *Nanotechnology,* 2006, **17**, 298–303.

29. Anderson, R. B., Dawson, P.T., *Experimental Methods in Catalytic Research*, Academic Press, New York, 1976, **2**, 215-219.

30. King, D. S., Nix, R. M., “Thermal Stability and Reducibility of ZnO and Cu/ZnO Catalysts”, *J., Catal.,* 1996, **76,** 160.

31. Iwasawa, Y., Ito, N., Ishii, H., Koruda, H., *J. Chem Soc.*, 1985, 828.

32. Toshio, O., & Makato M., Oxide catalyst in Solid state Chemistry, 1987, 2889

33. David, K., Ward and Edmond, I. K. “Preparing Catalytic Materials by the Sol-Gel Method”, *Ind. Eng. Chem. Res.,* 1995, **34(2),** 421-432.

34. Azam, M. S., “Synthesis of Catalytically Important Manganese Oxide Nano-particles and Their Dispersion into a Polymeric Matrix” Department of Chemistry, BUET, Dhaka, Bangladesh, 2008, 4.

35. Agam, M. A. and Q. Guo, “ElectronBeam Modification of Polymer nanospheres” *J. Nanosci. Nanotech.*, 2007, **7**, 3615-3619.

36. Choy, J. H., Jang, E. S., Won, J. H., Chung, J. H., Jang, D.J. and Kim, Y.W., “ Hydrothermal Route to ZnO nanocoral reefs and nanofibers” *Appl. Phys. Lett.*, 2004, **84**,287.

37. Yugang, S. and Youman, *Xia Science*, 2002, **298**, 2176.

38. Catherine, M., *Science*, 2002, **298**, 2176.

39. Aziz, M.A. “A Text Book of Water Supply Engineering”, Hafij book centre,

Dhaka, 1994, 178-182.

40. Mohan, N., Balasubramanian, N., Ahmed Basha, C. “Electrochemical Oxidation of Textile Wastewater and Its Reuse”, *J. of Hazourdous Materials.,* 2007**, 147***,* 644.

41. Cameselle, C., Pazos, M., Sanroman, M.A. “Selection of an Electrolyte to Enhance the Electrochemical Decolourization of Indigo Optimization and Scale-up”, *Chemosphere.,* 2005, **60**, 1080.

42. Caner, N., Kiran, I., Ilhan, S. and Iscen, C.F. “Isotherm and Kinetic Studies of Burazol Blue ED Dye Biosorption by Dried Anaerobic Sludge”, *Journal of Hazourdous Materials.,* 2009, **165**, 279.

43. Zhao, W., Chen, C., Li, X., Jhao, J., Hidaka, H. and Serpone, N. “Photodegradation of Sulforhodamine-B Dye in Platinized Titania Dispersions under Visible Light Irradiation: Influence of Platinum as a Functional Co-catalyst”, *J. Phys. Chem. B.,* 2002**, 106***,* 5022.

44. Tao, X., Su, J. and Chen, J.F. “Photooxidative Degradation of Dye Pollutants Accumulated in Self-Assembled Natural Polyelectrolyte Microshells under Visible Radiation” *J. Chem. Eur.,* 2006, **12**, 4164.

45. Akbal, F., “Photocatalytic Degradation of Organic Dyes in the Presence of Titanium Dioxide under UV and Solar Light: Effect of Operational Parameters”, *Environmental Progress*., 2005, **24(3)***,* 317-322.

46. Amin, N.K., “Removal of direct blue-106 dye from aqueous solution using new Activated carbons developed from pomegranate peel: Adsorption equilibrium and Kinetics”, *Journal of Hazardous Materials,* 2009, **165***,* 52.

47. Ranghu, S. and Ahmed, B. C., “Dye Destruction and Simultaneous Genaration of Sodium Hydroxided Using a Divided Electrochemical Reactor” *Ind. Eng. Chem. Res.*, 2008, **47**, 5277.

48. Wellington, S., Pereira, S., Renato, S. and Freire, S., “Azo Dye Degradation by Recycled Waste Zero-Valent Iron Powder” *J. Braz. Chem. Soc*. 2006, **17***,* 832.

49. Chen, C.C., Chaudhary, A.J. and Grimes, S.M., “Photodegradation of Acid Blue 29 and Ethyl Violet in the Presence/Absence of Sodium Hydroxide and Aluminium Ions” *Environmental Information Archives.*, 2005, **3***,* 111.

50. Sanjay, S., Vaghel, A., Ashok, D., Jethv, A., Bhavesh, B., Meth, A., Sunil, P., Dave, Adimurthy, S. and Ramachandraiah, G.., “Laboratory Studies of Electrochemical Treatment of Industrial Azo Dye Effluent”, *Environ. Sci. Technol.,* 2005, **39***,* 2848.

51. Fu, H., Pan, C., Yao, W. and Zhu, Y., “Visible-Light-Induced Degradation of Rhodamine B by Nanosized Bi_2WO_6” *J. Phys. Chem. B.,* 2005, **109**, 22432-22439.

52. Malpass, G.R.P., Miwa, D.W., Machado, S.A.S. and Motheo, A.J., “Decolourization of Real Textile Waste Using Electrochemical Techniques: Effect of Electrode Composition” *J. of Hazourdous Materils.,* 2008, **156,** 170.

53. Hasnat, M.A., Siddiquey, I.A., & Nuruddin, A., “Comparative photocatalytic studies of degradation of a cationic and an anionic dye” *Dyes and Pigments.,* 2005. **66***,* 185–188.

54. Zhou, S., Ray, A.K., “Kinetic Studies for Photocatalytic Degradation of Eosin B on a Thin Film of Titanium Dioxide”, *Ind. Eng. Chem. Res.,* 2003**, 42***,* 6020-6033.

55. Saekung, C., Pungwiwat, N., Laosooksathit, S.,“Using Porphyrin and Eosin Y as Electron Donor in Dye Sensitized Solar Cells”, *Technical Digest of the International PVSEC-14,* Bangkok, Thailand*.* 2004, LP1-024.

56. Yang, J., Chen, C., Ji, H., Ma, H., Zhao, J., “Mechanism of TiO_2-Assisted Photocatalytic Degradation of Dyes under Visible light Irradiation: Photocatalytic Study by TiO_2-Film Electrodes”, *J. Phys. Chem. B.,* 2005, **109,** 21900.

57. Deng, J., Chen, M., Gu, G.. and Wu, L. A., “Facile Method to Fabricate ZnO Hollow Spheres and Their Photocatalytic Property”, *J. Phys. Chem. B.,* 2008,**112***,* 16.

58. Wu, T., Liu, G., Zhao, J., Hidaka, H., Serpone, N., “Photoassisted Degradation of Dye Pollutants Self-Photosensitized Oxidative Transformation of Rhodamine B under Visible Light Irradiation in Aqueous TiO_2 Dispersions” , *J. Phys. Chem. B.* 1998, **102***,* 5845-5846.

59. Akbal, F., “Photocatalytic Degradation of Organic Dyes in the Presence of Titanium Dioxide under UV and Solar Light: Effect of Operational

Parameters", *Environmental Progress.,* 2005, **24(3),** 317-320.

60. Wu, T., Liu,G., Zhao, J., Hidaka, H., Serpone, N., "Evidence for H_2O_2 Generation during the TiO_2-Assisted Photodegradation of Dyes in Aqueous Dispersions under Visible Light Illumination", *J. Phys. Chem. B.,* 1999, **103***,* 4862-4863.

61. Wellington, S., Pereira, S., Renato, S. and Freire, S., "Azo Dye Degradation by Recycled Waste Zero-Valent Iron Powder", *J. Braz. Chem. Soc.,* 2006, **17**, 834.

62. Pavia, D.L., Lampman, G.M. and Kriz, G.S., "Introduction to Spectroscopy". 3rd edition. Thomson Lerning, 2001, 377.

63. Al-Ghouti, M.A., Khraisheh, M.A.M., Ahmad, M.N.M. and Allen, S., "Adsorption behavior of methylene blue onto Jordanian diatomite: A kinetic study" *J. of Hazardous Materials.,* 2009, **165**, 591.

64. Uddin, M.T., Islam, M.A., Mahmud, S. and Rukanuzzaman, M., "Adsorptive removal of methylene blue by tea waste" *J. of Hazardous Materials.,* 2009, **164***,* 58.

65. Bouras, P. and Lianos, P., "Photodegradation of Dyes in Aqueous Solutions Catalyzed by Highly Efficient Nanocrystalline Titania Films" *J. of Applied Electrochemistry.,* 2005, **35***,* 833-834.

66. Kothari, S., Ameta, P. and Ameta, S., "Photocatalytic Bleaching of Evans Blue over Zinc Oxide Particulate System" *Indian J. of Chemistry.,* 2007, **46***,* 432-433.

67. Kansal, S.K., Kaur, N. and Singh, S., "Photocatalytic Degradation of two Commercial Dyes in Aqueous Phase Using Nanophotocatalyst" *Nanoscale Res Lett*., 2009, **4***,* 709, 712-713.

68. Pauporte, T., and Rathousky, J., "Electrodeposited Mesoporous ZnO Thin Films as Efficient Photocatalysts for the Degradation of Dye Pollutants" *J. Phys. Chem.,* 2007, **111***,* 7643.

69. IUPAC Recommendations, *Pure Appl. Chem.*, 1994, **66,** 1739.

70. Atkins, P.W, Physical Chemistry, Oxford University Press, sixth edition, 1998, 857.

71. Atkins, P.W, Physical Chemistry, Oxford University Press, sixth edition,

1998, 866-867.

72. Atkins, P.W, Physical Chemistry, Oxford University Press, sixth edition, 1998, 852-857.

73. Islam, A.M., “Adsorption and Photocatalytic Degradation Studies of Methylene Blue and Eosin Y Using Semiconductor Oxides”, *Indian J. of Chemistry.,* 2007, **47***,* 132-133.

74. Ferdosi, Y. J., “Preperation of Mixed Oxide Surface and its Characteristics toward Adsorption of Textile Dyes”, Department of Chemistry, BUET, Bangladesh, 2009.

75. Cullity B.D., “Elements of X-ray diffraction”, Weseley publishing Inc.,Phillipines, 1978.

76. Scott, A. B., “Catalyst Manufacture”, Ellis Horwood, Chichester, 1993, 254.

77. Chang, R., Chemistry, McGraw-Hill Inc., fifth edition, International edition, 1994, 817-819.

78. Courty, P., Ajot, H., Marcilly, C., *B. Powder Tech.,* **7**, 1993, 21.

79. Santamarina, J. C., Klein, K.A., Wang, Y.H. and Prencke, E., “Specific Surface: Determination and Relevance”, *J., Can. Goetech.*, **39**, 2002, 233-241.

80. Schreier, M., “A Theoritical Study on CO_2 Solubility in Water as a function of pH”, *J., Can. Goetech.*, 2006, **12,** 14-17.

81. Park, J., John R.,“A Simple Accurate Determination of Oxide PZC and the Strong Buffering effect of Oxide Buffering effect of Oxide and Interface Science”, 2005.

82. Park, J., “The pH Buffering and Charging Behavior of Oxides in Aqueous Solution”, Hechman Binary Inc., Chicago, 1998.

83. Chip, A., Lenaq, Ma, R., Rhue,D., Elizabeth, Kennelly, Geoderma, *Elsevier.com***,** 2003, **113,** 77-93.

84. Preocanin, T., and Kally, N., “Application of Mass Titration to Determination of surface charge of Metal Oxides”, **71(4),** 1998, 1117-1125.

85. Marguev, D., *J. Phys. Chem*, 1998, **102,** 10778-10791.

86. Scott, A. B., “Catalyst Manufacture”, Ellis Horwood, Chichester, 1993,

254.

87. Singal, R. L., “Solid State Physics”, Kedar Nath Ram Nath & Co., Meerut, sixth edition, 1998, 304.

88. Michael J. H., and James A., J, Materials Chemistry, **6**, 1996, 89-95.

89. Maria, F. T., MRS Bulletin, November 2001.

90. Park, J., and John, R., “A Simple Accurate determination of Oxide PZC and the Strong Buffering Effect of Oxide Surfaces at Incipient Wetness”, *J. Colloid and Interface Science*, 1995.

91. Appel, C., Ma, L., Rhue, D., Elizabeth, K., and Geoderma, *Elsevier.com,* 2003, **113**, 77-93.

92. Parker, J.C., Zelazny, L.W., Samprath, S. and Harris, W.G., “A critical Evolution of the Extension of Zero Point of Charge (ZPC) Theory to Soil System”, *Soil Sci. Soc. Am,* 1991, **43**, 668-674.

93. Non, J.S., and Schwarz, J.A., *J. Colloid Interface Sci.,* 2003, **140**, 157-164.

94. Zalzc and Kallay N., *J, Colloid Interface Sci.*, 2002, **149**, 233-240.

95. Preocanin, T., and Kally, N., Crawatica Chemica Acta, 1998, **71(4)**, 117-1125.

96. Kosmulski., Advance in Colloid and Interface Science, 2002, **99**, 255-264.

97. Slejko, F. L., “Adsorption Technology”, Marcel Dekker, New York, 1985, 212-238.

98. Suzuki, M., “Adsorption Engineering”, Elsevier, Amsterdam, 1990, 135-137.

99. Ismail, A. A., El-Midany A. A., Ibrahim, I. A. and Matsunaga H., "Heavy Metal Removal Using SiO_2 -TiO_2 Binary Oxide", *Adsorption*, 2008, **14**, 21-29.

100. Raghavacharya, C., "Colour Removal from Industrial Effluent", *Chem. Engg. World*, 1997, **32**, 53-58.

101. Khan, A. R., Al-Bahri, T. A. and Al-Haddad, A., "Adsorption of Phenol Based Organic Pollutants On Activated Carbon From Multicomponent Dilute Aqueous Solutions", *Wat. Res*., **31**, 2102-2112, (1997).

102. Crittenden, J. C. and Weber, W. J., "Model for Design of Multicomponent Adsorption System", *J. Environm. Engg. Div*., 1978, **104**, 1175-1193.

103. Khenifi, A., Bouberka, Z., Kameche, M. and Derriche, Z., "Adsorption Study of an Industrial Dye by an Organic Clay", *Adsorption,* 2007, **13**, 149-158.

104. Oke, I. A., Olarinoye, N. O. and Adewusi, S. R. A., "Adsorption Kinetics for Arsenic Removal from Aqueous Solutions by Untreated Powdered Eggshell", *Adsorption*, 2008, **14**, 73-83.

105. L. Roth, *Phys. Rev,* 1956, **110,** 1333.

106. M. Tachiki, *J. Phys. Soc. Japan, 1964,* **19**, 454.

107. Kobayashi, T., Haruta, M., Sano, H. and Delmon,B., *Proceding of the third International Meeting on Chemica sensors,* Cleveland, 1990, 318.

108. Maruyama, S. T. and Arai, S., *J. Electrochem. Soc.*, 1996, **143,** 1383.

109. Svegl, F., Orel, B., Hutchins, M. G. and Kalcher, K., *J. Electrochem,* 1996, **143,** 1532.

110. Ting, Y. U. and Zexaing, S., *J. Mater. Sci. Technol.*, 2008, **24(4),** 597-602.

111. Azurdia, J. A., Mccrum, A. and Laine, R. M., *J. of material chemistry,* 2008, **18**, 3249-3258.

112. Perry, C. C., Li, X. and Waters, D. N., *Spectrochem. Acta*, 1991, **47A**, 1874.

113. Harrison, P. G., Perry, C. C., Creaser, D. A., Li, X., *In Vilminol, Nass, Schmidt (Eds.), Eurogel*,1992, **91***,*175.

114. Lopez, T., Asomoza, M. and Gomez, R., *J. Non-Cryst. Solids,* 1992, **147 & 148**, 769.

115. Atkins, P.W, “Physical Chemistry”, Oxford University Press, sixth edition, 1998, 619-633.

116. http://en.wikipedia.org/wiki/EDX

117. Pike, J., Hanson, J., Zhang, L.and chan, S. W., *Chem. Mater.*, 2007, **19**, 5609-5616.

118. Abdelwahab,E. O, EI-Sikaily, A. and Khaled, A., “Removal of Direct Blue-86 from Aqueous Solution by New Activated Carbon Developed from Orange Peel”, *J. Hazard. Mater,* 2009, **161(1)**, 102–110.

119. Anuirudh T. S. and Sreedhar, M. K. “Mercury (II) adsorption of desorption characteristics of coconut husk based carbon- Kinetics and self diffusion”, *Indian. J. Environ. Protect.*, 1999, **19**, 8.

120. Aravind, K. S. and Prem, N.T., “Removal Basic Dye from Industrial Wastewater by Adsorbent”, *Indian. J. Chem. Technol.*, 2003, **10**, 215.

121. Senthikumar, S., Varatharajan, P.R., Porkodi, K. and Subburaam, C. V., “Adsorption of Methylene Blue Carbon onto Jute Fibre Carbon”, *Colloid.Interface Sci*., 2005, **284**, 79.

122. Vadivelan, V. and Vasanthkumar, “Equilibrium, Kinetics, Mechanism and Process Design for the Sorption of Methylene Blue onto Rice Husk”, *J. Colloid. Interface Sci.,* 2005, **286**, 91.

123. Renmin, G., Yingzhi, S., Jian, C., Huijun, L., and Chao, Y “Effect of Chemical Modification on Dye Adsorption Capacity of Peaunut Hull”, *Dyes and Pigments.,* 2005, **67**, 179.

124. Catena, G.C., Bright, F.V., “Effect of Temperature on the Adsorption of Dyes” *Anal. Chem.*, 1999, **61**, 905.

125. Krishna, D.G. and Bhattacharyyya, G. “Adsorption of Methylene Blue on Kaolinite, *Appl. Clay Sci.,* 2002, **20**, 295

126. Namasivayam, C. and Yamuna, R.T.,“Adsorption of Direct Red by Biogas Residual Slurry”, *Environ. Pollut*, 1995, **89**, 1.

APPENDIX

Appendix

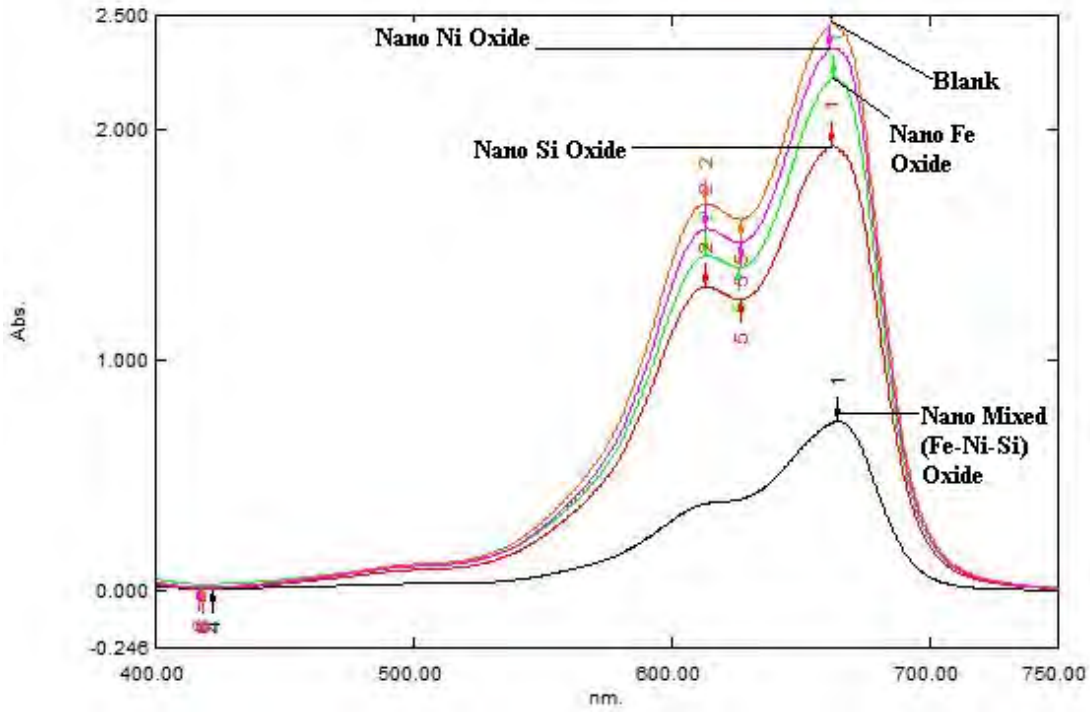

Figure 5.1: UV spectrum of comparative adsorption of MB dye onto different nano oxide.

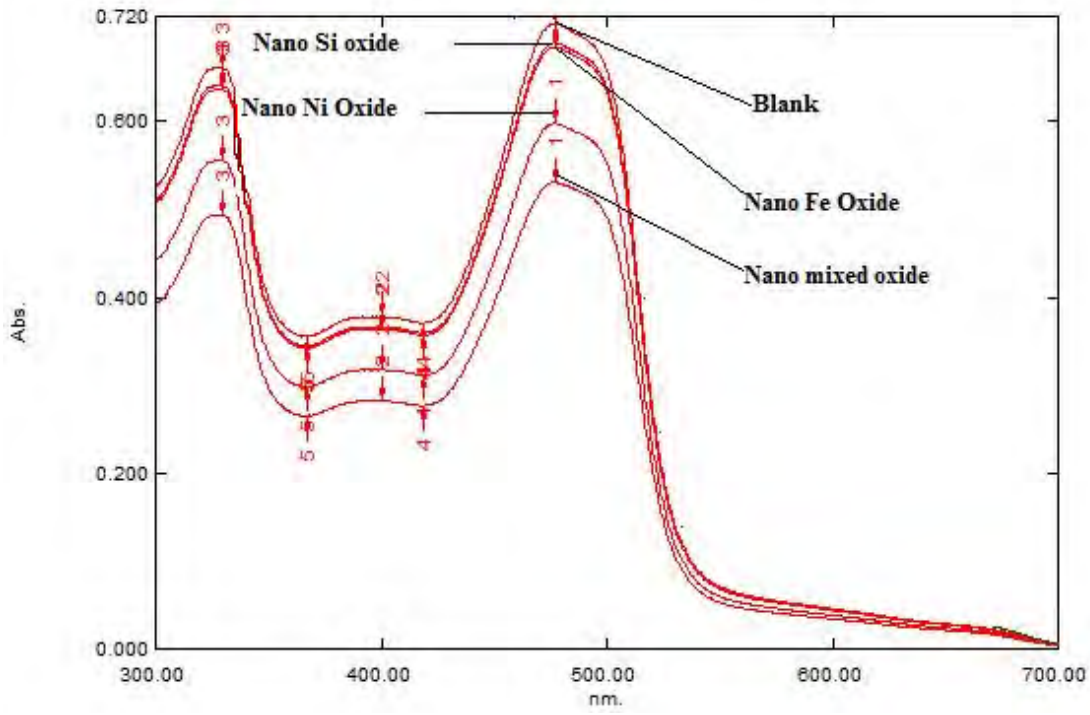

Figure 5.2: UV spectrum of comparative adsorption of OG dye onto different nano oxide.

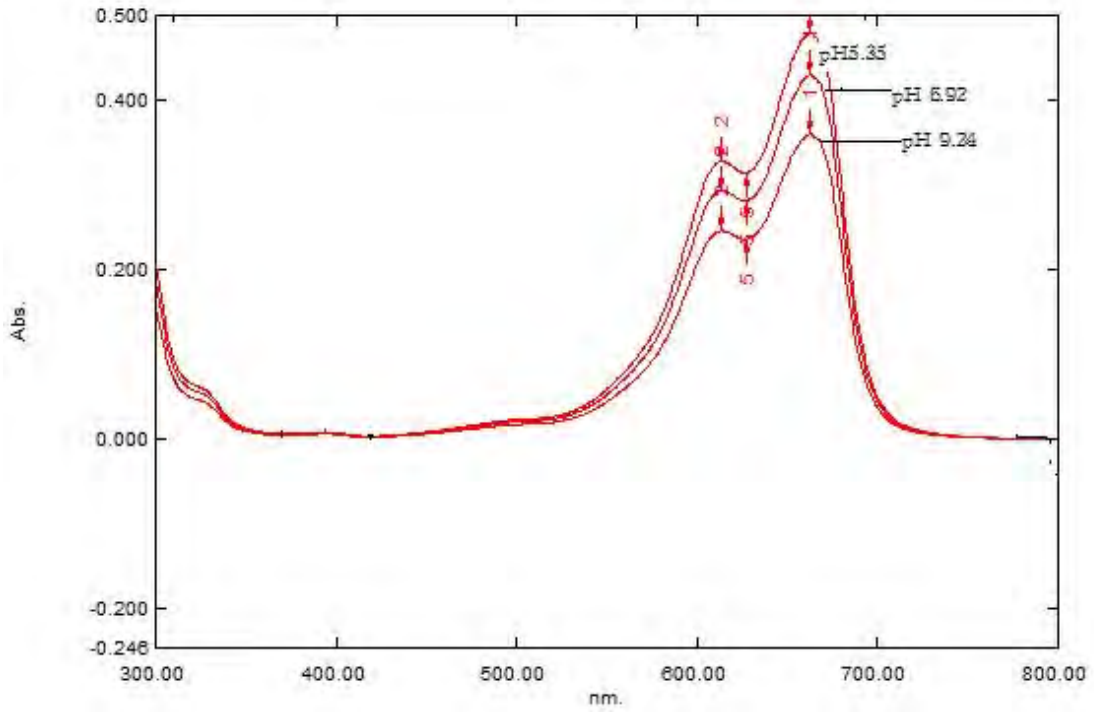

Figure 5.3: UV spectrum of pH effect of adsorption of MB onto nano mixed oxide

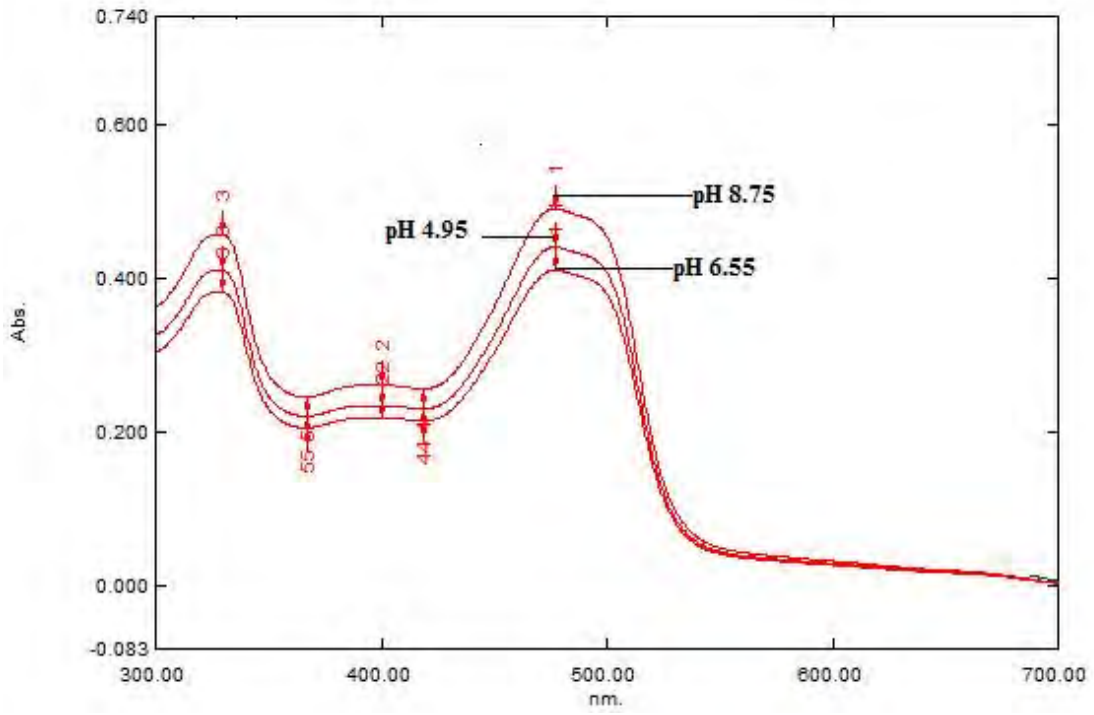

Figure 5.4: UV spectrum of pH effect of adsorption of OG onto nano mixed oxide

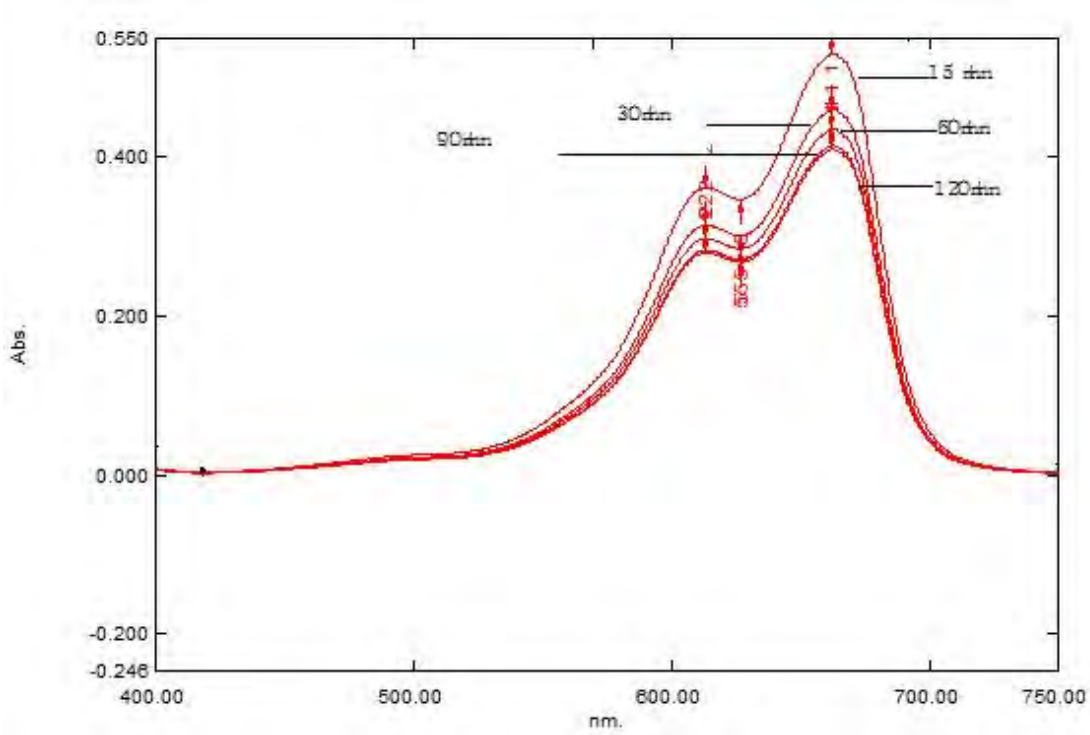

Figure 5.5: UV spectrum of effect of contact time of adsorption of MB onto nano mixed oxide

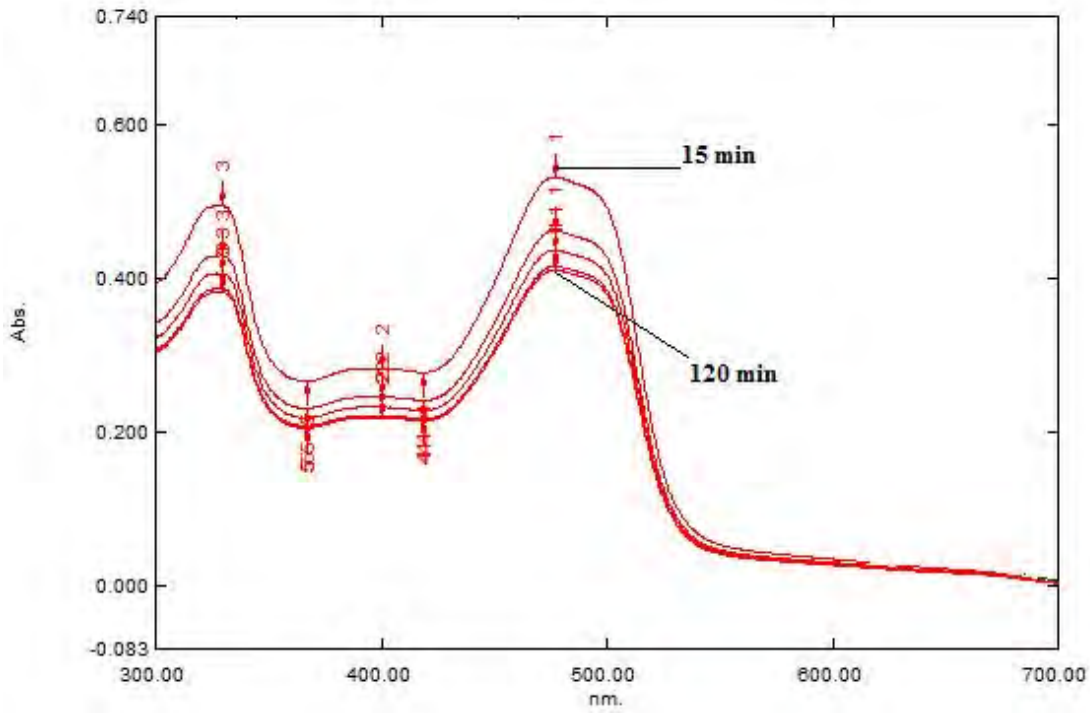

Figure 5.6: UV spectrum of effect of contact time of adsorption of OG onto nano mixed oxide

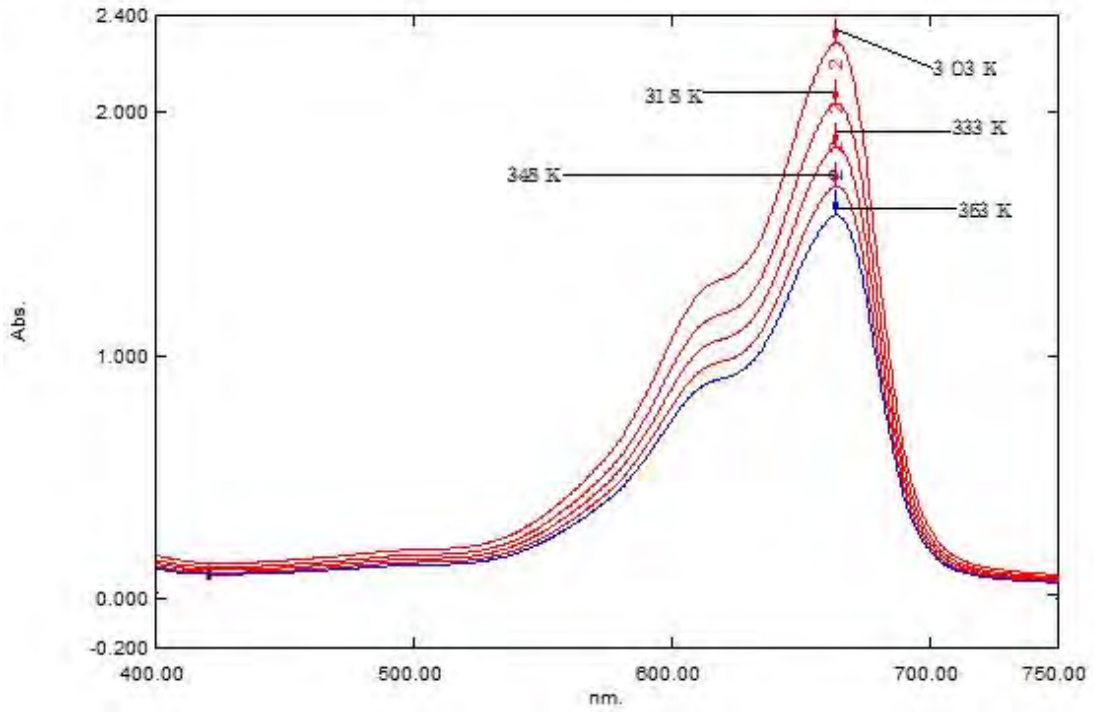

Figure 5.7: UV spectrum of effect of temperature of adsorption of MB onto nano mixed oxide

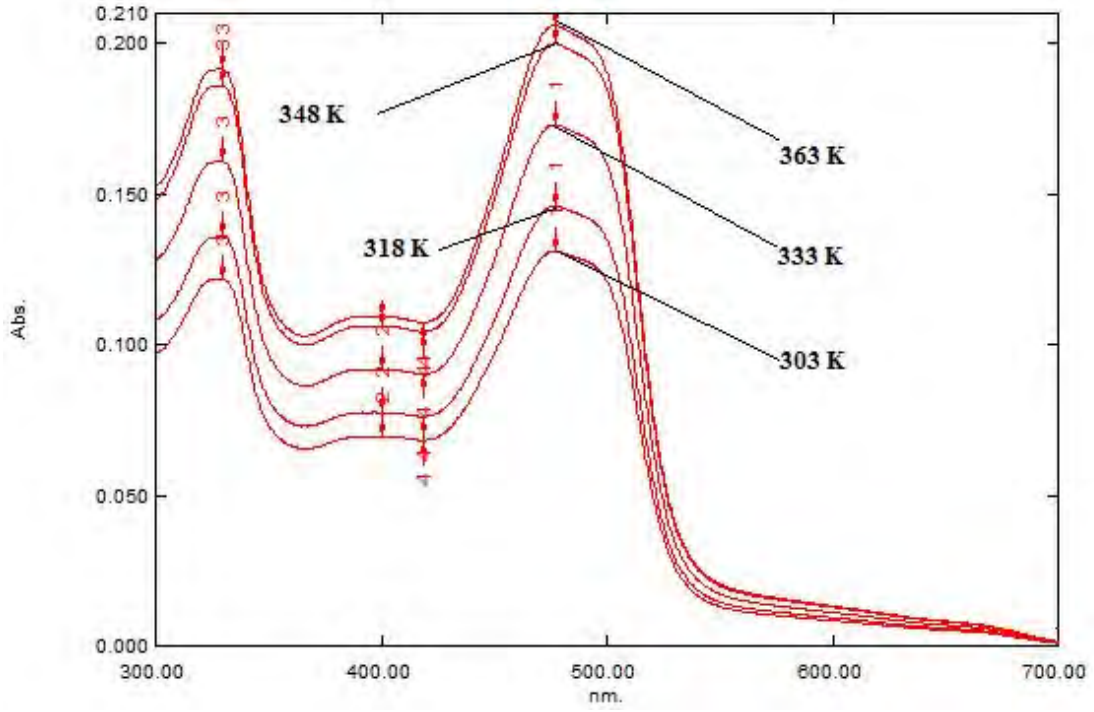

Figure 5.8: UV spectrum of effect of temperature of adsorption of OG onto nano mixed oxide

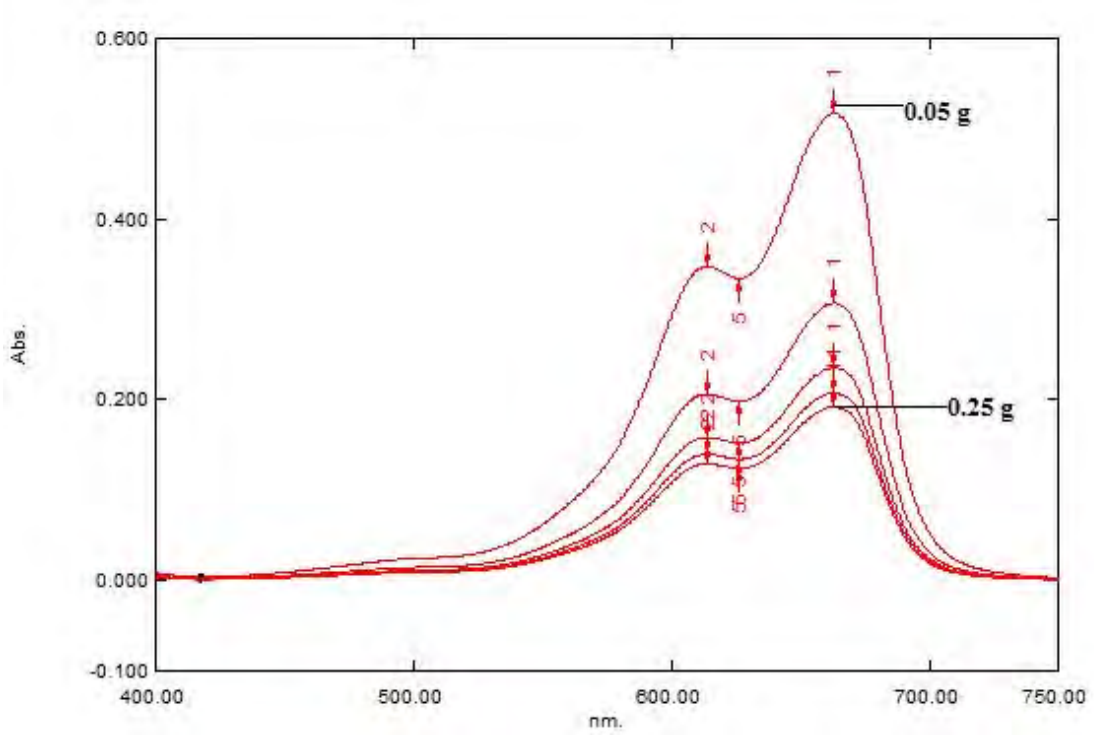

Figure 5.9: UV Spectrum of effect adsorbent dose of adsorption of MB onto nano mixed oxide

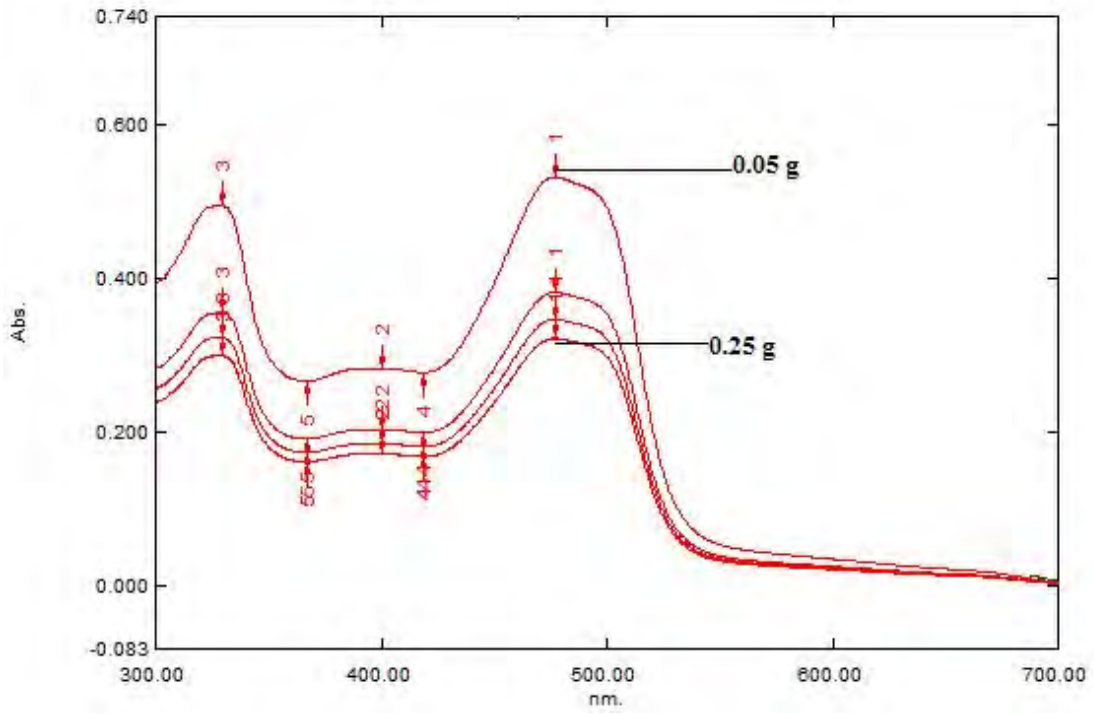

Figure 5.10: UV spectrum of effect of adsorbent dose of adsorption of OG onto nano mixed oxide

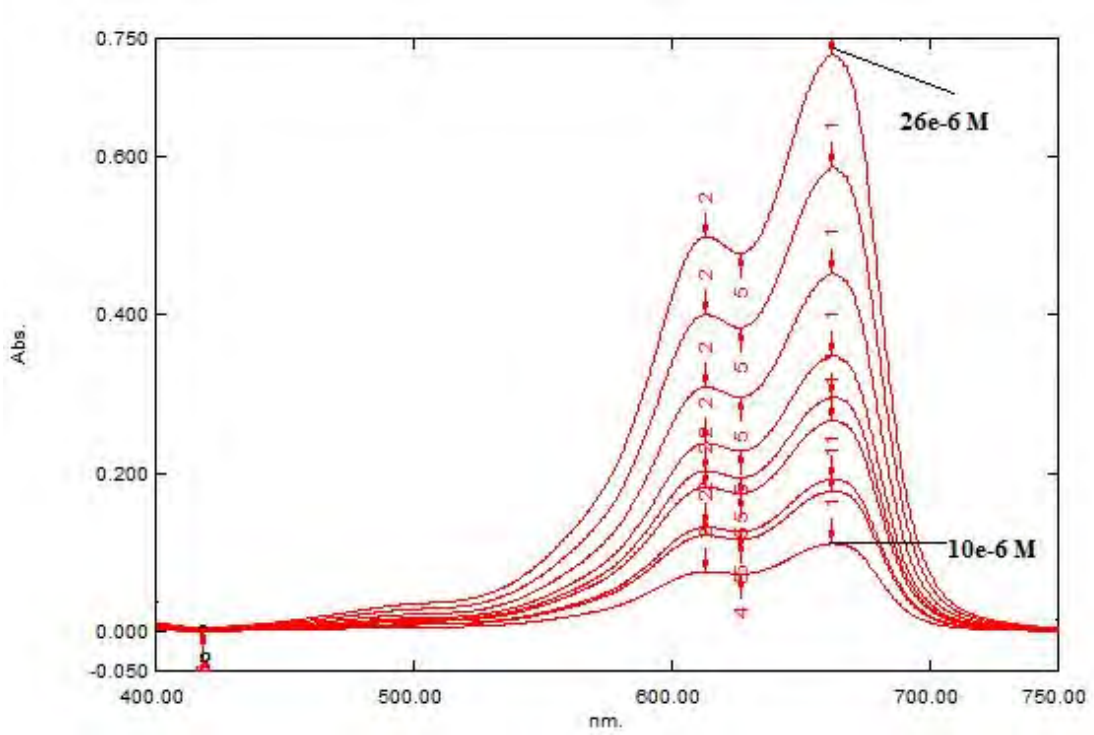

Figure 5.11: UV spectrum of effect concentration of dye of adsorption of OG onto nano mixed oxide